

**FIELD-INDUCED TRANSPORT OF FERROFLUID  
DROPLETS ON A MULTITASKING SURFACE  
MICROFLUIDIC PLATFORM**

**PhD Thesis**

**Submitted by**

**Debiprasad Chakrabarty  
Doctor of Philosophy (Engineering)**

*Faculty of Engineering and Technology  
Department of Power Engineering  
Jadavpur University  
Kolkata, India  
Year 2023*

# JADAVPUR UNIVERSITY

KOLKATA – 700032, INDIA

INDEX NO. : 24/16/E

1. **Title of the thesis:** Field-Induced Transport of Ferrofluid Droplets on A Multitasking Surface Microfluidic Platform.
  
2. **Name, Designation & Institution of the Supervisor:**
  1. Prof. Niladri Chakraborty  
Professor, Department of Power Engineering  
Jadavpur University  
Salt Lake Campus,  
Kolkata – 700098  
West Bengal, India
  
  2. Prof. Ranjan Ganguly  
Professor, Department of Power Engineering  
Jadavpur University  
Salt Lake Campus,  
Kolkata – 700098  
West Bengal, India

### 3. List of Publications:

1. Debiprasad Chakrabarty, Susovan Dutta, Niladri Chakraborty, Ranjan Ganguly, “Magnetically actuated transport of ferrofluid droplets over micro-coil array on a digital microfluidic platform”. Sensors and Actuators B: Chemical,  
**doi: <http://dx.doi.org/10.1016/j.snb.2016.06.001>**. Accepted, June, 2016
  
2. Debiprasad Chakrabarty, Susovan Dutta, Niladri Chakraborty, Ranjan Ganguly, “Manipulating magnetic fluid droplets on a configurable, multitasking surface microfluidic application”, Communicated.

**4. List of Patents:** Nil

**5. List of Presentations in National/International/Conferences/ Workshops:**

1. Debiprasad Chakrabarty, Susovan Dutta, Niladri Chakraborty, Ranjan Ganguly, “2-Dimensional, magnetic actuation of ferrofluid droplet on an open surface- microfluidic platform”, **9th International and 49th National Conference on Fluid Mechanics and Fluid Power (FMFP), IIT Roorkee, Roorkee-247667 Uttarakhand, India, December 14-16, 2022**

JADAVPUR UNIVERSITY  
FACULTY OF ENGINEERING AND TECHNOLOGY

"Statement of Originality"

**IDEBIPRASAD CHAKRABARTY** registered on **21.09.2016** do hereby declare that this thesis entitled "**Field-Induced Transport of Ferrofluid Droplets on a Multitasking Surface Microfluidic Platform**" contains literature survey and original research work done by the undersigned candidate as part of Doctoral studies.

All information in this thesis have been obtained and presented in accordance with existing academic rules and ethical conduct. I declare that, as required by these rules and conduct, I have fully cited and referred all materials and results that are not original to this work.

I also declare that I have checked this thesis as per the "Policy on Anti Plagiarism, Jadavpur University, 2019", and the level of similarity as checked by iThenticate software is 07 %

*Debiprasad Chakrabarty*  
(Debiprasad Chakrabarty) 04/09/23

Certified by Supervisors :

*Niladri Chakrabarty*  
1. (Prof. Niladri Chakrabarty) 4/09/23


Professor  
Dept. of Power Engineering  
Jadavpur University  
Salt Lake, 2nd Campus  
Kolkata-700 098

*Ranjan Ganguly*  
2. (Prof. Ranjan Ganguly) 04/09/23


Professor  
Dept. of Power Engineering  
Jadavpur University  
Salt Lake, 2nd Campus  
Kolkata-700 098

CERTIFICATE FROM THE SUPERVISOR(S)

This is to certify that the thesis entitled “**Field-Induced Transport Of Ferrofluid Droplets On A Multitasking Surface Microfluidic Platform**” submitted by Shri **DEBIPRASAD CHAKRABARTY**, who got his name registered on **21.09.2016** for the award of Ph. D. (Engg.) Degree of Jadavpur University is absolutely based upon his own work under the supervision of the undersigned persons and that neither his thesis nor any part of the thesis has been submitted for any degree/diploma or any other academic award anywhere before.

  
1. Prof. Niladri Chakraborty 04/09/23  
Professor, Department of Power Engineering  
Jadavpur University, Salt Lake Campus

Professor  
Dept. of Power Engineering  
Jadavpur University  
Salt Lake, 2nd Campus  
Kolkata-700 098

  
04/09/23  
2. Prof. Ranjan Ganguly  
Professor, Department of Power Engineering  
Jadavpur University, Salt Lake Campus

Professor  
Dept. of Power Engineering  
Jadavpur University  
Salt Lake, 2nd Campus  
Kolkata-700 098

*Dedicated*

*to*

*Mother, Father,  
Wife and Daughter*

# ACKNOWLEDGMENT

I would like to express my sincerest gratitude to my supervisor Prof. Niladri Chakraborty and Prof. Ranjan Ganguly for their valuable guidance and generous assistance throughout the course of my research work. They have always encouraged me to go forward with my research work and brought out the best in me related to my PhD work. I am also thankful for their valuable suggestions regarding my articles and precise revision of my thesis.

I do remain grateful to my mother Mrs. Jharna Chakraborty and my wife Mrs. Tuktuki Chakraborty for their endless love, untiring support, and encouragement in every sphere of my life. I owe this success of completing my PhD to my wife who was the main source of inspiration for me pursuing this degree.

I acknowledge the support provided by the Head of the Department, of Power Engineering as and when required. The other faculty members have been equally supportive throughout the time of my research and I am really grateful for the nice bonding that I have grown with the entire department. Thanks are also due to the members of my Individual Research Committee for their valuable suggestions throughout my research activity in the Power Engineering Department.


I would also like to show my humble thankfulness to Jadavpur University Administration which has provided me an opportunity to perform my research work leading to my PhD successfully. I remain indebted to the staff of the department who have provided me with the necessary help.

I want to thank all my friends and all the other research scholars of the department with whom I have spent fun moments during the course of my PhD work. This group of people has helped me enjoy an extended college life full of fun and activities. The love and support that they have shown towards me are really praiseworthy.

Last but most importantly, I am grateful to the almighty God for keeping me in good physical and mental health throughout the course of this research work.

I may have been not able to mention individually the names of all the persons who have provided their full-fledged support during this entire duration of PhD research work but I am indebted to each and every one. I want to thank all my well-wishers once again from the bottom of my heart.

September 2023

  
Debiprasad Chakraborty  
Department of Power Engineering  
Jadavpur University, Salt Lake Campus

# CONTENTS

<b>Subject</b>	<b>Page No.</b>
<b>Abstract</b>	viii
<b>Overview of Chapters</b>	x
<b>Chapter 1 Introduction</b>	1
1.1. Overview of Digital Microfluidics (DMF)	1
1.2. Mechanisms of droplet manipulation in closed channel DMF	4
1.3. Mechanisms of droplet manipulations in Open surface DMF (ODMF) platforms	9
1.3.1. Passive manipulation strategies on ODMF	9
1.3.2. Active manipulation strategies on ODMF	12
1.4. Different attributes of droplet transports in open and closed channel DMFs	14
1.4.1. Droplet sorting	14
1.4.2. Droplet merging	20
1.5. Applications of DMF	21
1.6. Overview of salient surface phenomenon for open surface DMF	24
1.6.1. Fundamentals of droplet manipulation on solid Substrates	25
1.6.1.1. Contact Angle Hysteresis (CAH)	26
1.6.1.2. Effect of contact angle hysteresis on droplet manipulation	27
1.6.1.3. Effect of Substrate wettability on droplet manipulation	28



<b>Subject</b>	<b>Page No.</b>	
1.7	Magnetic Digital Microfluidics (MDMF)	29
1.7.1	Open Surface Magnetic Digital Microfluidics (OMDMF)	30
1.7.2	Electromagnets and their configuration	36
1.7.3	Magnetic force-based droplet manipulation in host fluid film	36
1.7.4	Magnetic force-based droplet manipulation on solid substrate	37
1.8	Research gaps	37
1.9	Intent and objective of present work	38
1.10	Exclusiveness and novelty of the work	41
<b>Chapter 2</b>	<b>Theoretical Formulation</b>	43
2.1	Specification of planar coils and coil array	43
2.2	Magnetic field due to planar micro-coil	49
2.2.1	Computation of magnetic field due to current through a loop	50
2.3	Magnetic force due to current carrying planar microcoil	50
2.4	Droplet transport model on open surface microfluidic Platform	52
2.4.1	Droplet transport model within liquid film	52
2.4.2	Droplet transport model on solid surface	55

<b>Subject</b>	<b>Page No.</b>
<b>Chapter 3 Results and Discussion</b>	<b>60</b>
3.1 Description of magnetic field plot for different coil structures	60
3.2 Motion of ferrofluid droplets stably floating on the aqueous Film	61
3.2.1 Validation of the droplet transport model	62
3.2.2 Ferrofluid droplet trajectory using sequentially switchable array of microcoils	63
3.2.3 Effect of variation of field current	66
3.2.4 Effect of variation of host fluid viscosity	69
3.2.5 Effect of ferrofluid droplet size	70
3.2.6 Scaling argument	72
3.3 Motion of a spherical cap ferrofluid droplet on solid surface	74
3.3.1 Validation of the droplet transport model	75
3.3.2 Spherical cap ferrofluid droplet trajectory using two-tier array of electromagnet coils	78
3.3.3 Spherical cap ferrofluid manipulation using array of single layer electromagnetic micro-coils arranged in a five stranded row	82
3.3.3.1 Time evolution of different forces on the spherical cap volume ferrofluid droplet	84
3.3.3.2 Effect of variation of field current	85
3.3.3.3 Effect of variation of droplet base diameter	87
3.3.4 Droplet multiplexing and complex transport	88
3.3.4.1 Targeted delivery of multiple monodisperse droplets	89

<b>Subject</b>	<b>Page No.</b>	
3.3.4.2	Spatiotemporal separation of multiple polydisperse droplets	92
3.3.4.3	Multiple droplets merging and pooling	95
3.4	Closing remark	97
<b>Chapter 4</b>	<b>Conclusions and Scope of future work</b>	98
4.1	<b>Conclusions</b>	98
4.2	<b>Future Scopes of work</b>	100
<b>Appendix</b>		102
A1	Volume of asymmetrical spherical cap ferrofluid droplet sliding on a solid substrate due to an external force	102
A2	Derivation of the equation to determine thickness or height of the droplet to find resistive frictional drag on the spherical cap ferrofluid droplet	104
<b>Reference</b>		107

<b>List of Figures</b>	<b>Page No.</b>
<b>Chapter 1</b>	
Figure 1.1 Schematics of different active droplet manipulation in closed DMF platforms	8
Figure 1.2 A few salient mechanisms of passive droplet manipulation on open surface microfluidic (ODMF) platforms	11
Figure 1.3 A few salient mechanisms of active droplet manipulation on open surface microfluidic (ODMF) platforms	13
Figure 1.4 A few salient mechanisms of active droplet sorting	18
Figure 1.5 A few means of magnetic droplet sorting	19
Figure 1.6 A few salient schemes of droplet merging	21
Figure 1.7 A few salient schemes of Applications of DMF	24
Figure 1.8 Schematics of contact angle and CAH	26
Figure 1.9 A few relevant schemes of open Surface Magnetic Digital Microfluidics	35
<b>Chapter 2</b>	
Figure 2.1 Arrangements of planar square coil (First transport model):	45
Figure 2.2 Arrangements of planar square coil (Second transport model)	47
Figure 2.3 Arrangements of planar square coil (Third transport model)	49
Figure 2.4 Geometrical configuration for calculation of the magnetic field due to a current carrying segment of conductor.	51
Figure 2.5 Forces on a ferrofluid droplet (FF), half-immersed at the surface of water	53
Figure 2.6 Forces model of a spherical cap ferrofluid droplets on a solid hydrophobic surface over planar electromagnet coil	58
<b>Chapter 3</b>	
Figure 3.1 Magnetic field plot of square coils	61
Figure 3.2 Validation of droplet transport model	63

<b>List of Figures</b>		<b>Page No.</b>
Figure 3.3	Ferrofluid droplet trajectory and corresponding coil switching	64
Figure 3.4	Droplet trajectories for different values of current in the coil and force plot	68
Figure 3.5	Droplet trajectories for different values of host fluid viscosity and corresponding time of flight plot	70
Figure 3.6	Droplet trajectories for different values of radius $R_{FF}$ of the droplet and corresponding time of flight plot	71
Figure 3.7	Combined plots of droplet transport time as function of the group-variable	73
Figure 3.8	Validation of the droplet transport model on solid surface	77
Figure 3.9	Magnetic field (Tesla) plot computed on the hydrophobic surface (i.e., at $z = 2$ mm) with respect to coil switching and force plot	80
Figure 3.10	Complete droplet trajectory and respective coil switching pulse	81
Figure 3.11	Spherical cap ferrofluid droplet trajectory and corresponding force plot	85
Figure 3.12	Variation of droplet trajectories and time of flight with respect to field current and droplet base diameter	87
Figure 3.13	Monodisperse droplet trajectories and corresponding coil switching pulses	91
Figure 3.14	Polydisperse droplet trajectories and corresponding coil switching pulses	94
Figure 3.15	Multiple droplets merging and pooling trajectories and corresponding coil switching pulses	96
<b>Appendix</b>		
Figure A1	Schematic of a spherical cap droplet and its sliding profile with nomenclature with two-circle method:	102
Figure A2	The schematic diagram of extended sphere profile of cap volume droplet at equilibrium position	104

---

<b>List of Tables</b>	<b>Page No.</b>
Table 1.1 Comparison of EWOD and magnetic manipulation of discrete droplets	32
Table 3.1 Set of coils to be energized to transport a specific droplet to a pre-designated location on the substrate.	90

## Abstract

Droplet based Digital Microfluidics (DMF) has emerged as a promising enabling technology for a wide range of applications in the areas of low-cost biosensors and molecular diagnostics. In an Open-surface Magnetic Digital Microfluidics (OMDMF) nano-liter to micro-liter sized, magnetically responsive droplets, containing samples and reagents can be manipulated on a liquid-film coated or a hydrophobic surface, executing key tasks of a micro-total analysis system ( $\mu$ -TAS). An OMDMF platform uses magnetic forces to transport droplets, presenting a few exclusive benefits over the conventional digital microfluidic platform. Effective deployment of such OMDMF would warrant precise manipulation of the magnetically responsive droplets – usually a stable suspension of magnetic nanoparticles dispersed in a nonmagnetic liquid – using chip-embedded miniaturized magnetic coils that are electrically insulated from the liquid medium. The driving magnetic force should, in one hand be strong enough to overcome the capillary pinning and viscous forces, while on the other hand it has to be spatially and temporally resolved with sufficient accuracy to engender directional transport; such action-at-a-distance is challenging and requires delicate combination of operating parameters, e.g., magnetizing current and timing of switching of the chip-embedded coils, fluid viscosity, droplet size, etc. Unlike microchannel-based fluidics, in magnetic OMDMF system, multiple droplets can be steered concurrently using sequentially switched array of chip-embedded micro-coils; at the same time strategic manipulation of droplets can be attained using such design. Here, two magnetic force-based droplet manipulation strategies have been proposed where an array of planar electromagnetic micro-coils embedded in a substrate provides the motive force. In the first scheme a numerical analysis is performed where the manipulation of an immiscible, microliter-scale ferrofluid droplet over a thin aqueous film on a solid substrate, using embedded micro-electromagnet coils, is performed. The numerical model is first validated against an experimentally observed droplet trajectory in a simple, single-coil configuration. Subsequently, simulation of the ferrofluid droplets transport on a liquid film is carried out under a magnetic field that is produced by a sequentially-switched array of square-spiral micro electromagnets. Guided

transport of the droplet in predefined meandering path over an active substrate area is achieved through precisely tuning the operating parameters. The droplets clearly display two distinct regimes of transport – one dominated by viscosity and the other by inertia. In the viscous-regime, the time-of-flight of a given ferrofluid droplet over the magnetic actuator section is found to scale with a generalized group-variable involving the operating parameters, viz., the field current, droplet size, and the viscosities of the magnetic fluid and the film-liquid. The second strategy demonstrates two distinct transport models of a spherical-cap ferrofluid droplet that is manipulated on solid surface. The first transport model proposed a microliter-volume droplet manipulation in a sequence of rectilinear paths using an array of double-layer electromagnetic micro-coils embedded in the substrate. Appropriate sequence of coil energization for attaining the desired trajectory of the droplet is described. The study paves the foundation of developing an OMDMF platform for more complex digital microfluidic manipulations that are pertinent to different bio-microfluidic applications. The second transport model proposes a concept of several two-dimensional multi-droplet manipulations, such as multiple droplets sorting, sequential merging as well as pooling on a solid hydrophobic surface by the sequentially switched array of electromagnetic micro-coils. By applying appropriate sequences of micro-coil switching multiple droplets can be manipulated simultaneously and various droplet operations can be attained. Results of the study lead to the formulation of design bases for magnetically manipulated, configurable, multi-tasking open-surfaced, digital microfluidic platforms.



## Overview of Chapters

This thesis describes series of study that that I have completed during my Ph.D. at Department of Power Engineering, Jadavpur University, Kolkata, India. My thesis on “**Field-Induced Transport of Ferrofluid Droplets on a Multitasking Surface Microfluidic Platform**” illustrates concept of a multi-tasking, magnetic force-based droplet manipulation strategy using an array of planar electromagnetic microcoils embedded in a substrate. This thesis consists of four distinct chapters which provide the pertinent background of the work, identify the gap area, delineate the objectives, provide the theoretical formulation and solution strategy, discuss the results and finally, draw out the salient conclusions and suggest the future course of research that the current study may engender.

**Chapter One** provides the background literature review on Open-surface Magnetic Digital Microfluidics (OMDMF) with specific importance on its attributes studied in the thesis. This chapter describes an overview of Digital Microfluidics (DMF) along with its importance, applications and current challenges. Subsequently, it introduces the concept of Droplet-based Magnetic Digital Microfluidics (MDMF) along with its importance and application over other DMF. The chapter then highlights the relatively new concept of Open-surface Droplet-based magnetic Digital Mirofluidics (OMDMF) and identifies the research gaps in this field. Finally, the proposed objectives and novelties of this study are mentioned.

**Chapter Two** portrays the theoretical formulation involved in this study. The salient forces at play in determining the transport of a magnetically actuated ferrofluid droplet are taken into consideration. The chapter deduces the governing equations of droplet transport from the first-principle and presents the ensuing transport models in an OMDMF platform. The design of planar coil and coil array, along with the rationale of the magnetic field computation due to current through the loops are explained, and calculation of the resulting magnetic force on the ferrofluid droplet is performed.

**Chapter Three** describes the results of the simulation of magnetic actuation on the OMDMF platform and discussion of different study corresponding to magnetic force-based droplet transport models. Two magnetic force-based droplet manipulation strategies have been proposed in this chapter. In the first scheme the manipulation of an immiscible, microliter-scale ferrofluid droplet over a thin aqueous film on a solid substrate, using embedded micro-electromagnet coils, is analyzed. For the second case, simulation of the ferrofluid droplets transport on a liquid film is carried out under a magnetic field that is produced by a sequentially-switched array of square-spiral micro electromagnets. Guided transport of the droplets in predefined meandering path over an active substrate area is achieved through precisely tuning the operating parameters. Time evolutions of different forces for both models have been discussed. Droplet multiplexing and complex transport on solid surface such as targeted delivery of multiple monodisperse droplets, spatiotemporal separation of multiple polydisperse droplets and multiple droplets merging and pooling are described.

**Chapter Four** summarizes key findings of this study based on flexible magnetic force-based droplet manipulation strategy using an array of planar electromagnetic micro-coils embedded in a substrate. It also draws out the salient conclusions from the previous chapters and discusses the potential areas of improvement of OMDMF and highlights the future scopes of work for the study.

**Appendix** includes supporting information relevant to this study such as calculation of the deformed spherical cap volume of a sessile droplet, as well as the computation of the viscous drag of spherical cap ferrofluid droplet sliding over a solid substrate. This chapter also includes theoretical determination of Contact Angle Hysteresis (CAH) on droplet manipulations.

# Chapter 1: Introduction

Microfluidics is an emerging technology of handling fluid flow in diminutive amounts, either in the form of flow through microfluidic channels or in the form of discrete droplets from nanoliter to microliter, in micro total analysis systems ( $\mu$ -TAS). These devices can perform varied bioanalytical tasks, which are normally carried out in a lab, like sample preparation, purification, separation, reaction, transport, immobilization, labelling, biosensing and detection on a chip [1, 2]. Microfluidics offer salient advantages over the conventional bioanalytical protocol through reduced biochemical reaction time, enhanced efficiency and mobility and reduced sample and reagent consumption. Small reactor volumes are also favored where the analyzed sample is available in extremely small amount, e.g., in case of forensic detection. The key generic steps in any MEMS (Microelectromechanical Systems)-based bioanalytical device (e.g., a biosensor) involves sample handling for mixing, reaction and separation. Therefore, development in each of these attributes of microfluidic transport serves as the key enabler for the development of miniature biosensors for healthcare, food, agriculture, low-cost biomedical diagnostic devices, and platforms for drug development or unraveling new biological phenomena [3, 4, 5].

## 1.1. Overview of Digital Microfluidics (DMF)

There has been a recent shift of sample handling strategy from the continuous-flow to the droplet-based digital microfluidics (DMF) system, which focuses on generation and manipulation of discrete nanoliter to microliter droplets in microfluidic environment. DMF can be used to manipulate reagents and biochemical entities like DNA, proteins, or cells in very small liquid volumes using lesser quantities of costly reagents with better biochemical reaction efficiency within shorter operating times. Due to handling of individual droplets each reagent can be addressed individually with no need for complex networks and the sample volume is further reduced to nano-liter or pico-liter which implies to get faster result as lower the reagent volume. The scaling of volumes used also reduces the device size thus creating several opportunities for portable devices which can be easily used. DMF is relatively free from the common problems of flow-through microfluidics like sample

dilution and cross-contamination [6,7]. Several useful applications of droplet-based microfluidics, e.g., protein purification [8], biosensor [9], immunoassays [10], DNA-replication [11, 12], cell-based assays [13], bio-molecular extraction [14], point of care diagnostics [15] etc. have underscored the importance of on-chip droplet manipulation [16,17]. In droplet-based digital microfluidics, isolated liquid droplets are generated and transported in an immiscible liquid medium, either in a closed, flow-through microchannel configuration [18,19,20], or in an open environment, e.g., atop an open liquid film or a solid surface [21]. In closed-channel confinement cross-contamination and evaporation of the droplets are minimized, ensuring their integrity and stability throughout the process of manipulation. One of the significant advantages of DMF is the ability to achieve complex biochemical reactions on a small scale with high accuracy and control. It also allows for the execution of multi-step processes and on-demand droplet manipulation. DMF can handle very small volumes of fluid, typically in the range of microliters to nanoliters, which is convenient for reducing rare or expensive sample and reagent consumption. DMF can also be programmed, which reduces manual involvement and increases the reproducibility and accuracy of experiments. DMF has many potential applications in fields such as biotechnology, diagnostics, and drug discovery, where it can be used to perform a wide range of assays and reactions with high efficiency and accuracy. DMF can also be combined with other technologies, such as sensors and microcontrollers, enabling the creation of complex, multifunctional systems. It enables the integration of multiple assay steps into a single device, which can simplify experimental workflows and reduce the risk of cross-contamination between samples. Droplet-based compartmentalization can be implemented in DMF to increase the sensitivity and specificity of assays. However, DMF also faces several challenges that limit its widespread adoption and scalability. In DMF the stability of droplets can be affected by factors such as surface tension, contact angle hysteresis, and electrostatic effects. The number of droplets manipulated at once is often limited in high-throughput applications. Increasing the number of droplets that can be manipulated requires complex designs and fabrication processes, which can be costly and time-consuming. DMF devices can encounter compatibility issues when working with biological samples due to factors such as surface tension, cell adhesion, and surface chemistry. These compatibility issues can limit the range of applications for DMF in

biology and biomedicine. The fabrication of DMF devices can be challenging and expensive, requiring specialized equipment and materials. The complexity of the designs and the need for high precision can also make fabrication time-consuming and error prone. While DMF can be integrated with other technologies, such as sensors and microcontrollers, there are still challenges to achieving seamless integration. The compatibility of different technologies, the need for specialized interfaces, and the complexity of the overall system can limit integration and increase costs.

In digital microfluidics discrete droplet can be manipulated in both close and open environment. Both open and closed digital microfluidic systems extend benefits in terms of reducing reagent consumption and increasing automation, allowing parallel processing and decreasing the time needed for completing the requisite protocol. In a closed channel environment, droplets are contained within microchannels or chambers, reducing the risk of evaporation and contamination. However, droplet insertion, access and dispensing can be arduous due to the confinement and may often require significant off-chip infrastructure (e.g., the need for a syringe pump to flow the host fluid through the microchannel). Fabricating microchannels and enclosed structures can also pose complexity as it requires specialized microfabrication techniques. On the contrary, open surface systems are more versatile and can accommodate a wider range of applications and offer easy access for droplet dispensing and manipulation, and allow easy detection (e.g., colorimetric detection using a simple image analysis). Open surface setups can be simpler to fabricate. Due to the direct access to droplets, open surface microfluidics is also easier to integrate with interfacing devices.

Generation of discrete droplets in an immiscible host fluid is a prerequisite in digital microfluidics [22, 23]. In a typical DMF platform, droplets are generated in-situ using a competition between surface tension and another force, e.g., viscous [24, 25], electric [26, 27] or magnetic force [28, 29, 30]. In a typical closed-channel microfluidic platform, droplets are generated using flow-focusing in a coaxial-flow [31] or parallel-flow [32] arrangement, and Y- shaped [33], T-shaped [34,35,36] or cross-type [37, 38] flow focusing junctions. Once these droplets are generated, the next task is to manipulate these droplets as per the required protocol of the micrototal analytical system supported on the DMF

platform. The following sub-sections discuss different mechanisms of droplet manipulation in closed channel and open-surface DMF platforms, and the salient attributes of droplet transports on DMF platforms.

## **1.2.Mechanisms of droplet manipulation in closed channel DMF**

Active droplet manipulation in closed channel may be achieved by electrostatic force [39,40,41], dielectric force [42], electrowetting on dielectric[43], magnetic force [44, 45, 46, 47, 33], shear gradients [48], thermal actuation [49, 50], surface acoustic waves (SAW) [51,52,53, 54], sequential modulation of hydrodynamic resistance [55], laser-induced actuation [56], or under competitive influences of surface free energy-based confining force and the hydrodynamic force [57, 58]. The following section summarizes the salient traits of droplet manipulation in a closed DMF platform.

***Dielectrophoresis: (DEP):*** Dielectrophoresis (DEP) is the method which drives a polarizable object under a non-uniform AC electric field [59]. For small droplets DEP leverages the charge distribution within the droplet and generates a net force based on the charge and the electric field gradient. Wu et al. [60] proposed a low-voltage electrostatic droplet manipulation technique where a dielectric droplet of silicon oil moved between two ITO (Indium Tin oxide) electrodes (see Figure 1.1(a)) which further demonstrated experimentally [61]. In another technique silicone oil droplets and dielectric organic solvent droplets along with decane and hexadecane was successfully manipulated in parallel-plate devices by DEP [62]. Different droplet operation such as generation, transportation, splitting and merging could be performed simultaneously on a single plate by Liquid Dielectrophoresis (L-DEP) for both nonconductive (dielectric) and conductive (DI water with/without surfactant) fluids in an open environment [63]. In this device fringing electric field generated by interdigitated electrodes which penetrate the dielectric liquid and the corresponding L-DEP force changes the wetting property of liquid on a single substrate. The contact angle of dielectric liquid varies upon the applied voltage and performs the various fundamental operations in digital microfluidic circuit. EWOD is another very popular droplet manipulation techniques which is more flexible and versatile and faster response compared to DEP.

***Electro Wetting on Dielectric (EWOD):*** Electro Wetting on Dielectric (EWOD) has been by far the most widely deployed means of digital microfluidics. EWOD leverages the change of local surface energy of a droplet with the DC electric potential applied to the underlying substrate. When a droplet sits atop a pair of electrically insulated surfaces (electrodes) at two different potentials, a net unbalanced driving force emerges due to asymmetric contact angles subtended by the droplet on the electrodes. Thus, directed motion of the droplets on an array of sequentially energized electrodes is realized in EWOD (see Figure 1.1(b):(i) and (ii)) [64, 65, 66]. Fan et al. [67] advanced the technique to manipulate multiple droplets by cross-reference driving concept with EWOD-based digital microfluidic circuits, performing essential fluidic functions such as creation, cutting, merging, and mixing of droplets. Widespread use of EWOD has also elicited detailed work to resolve the dynamics of flow in EWOD, through several numerical and experimental works [68, 69]. Despite the maturity of EWOD technology, the method suffers from a few salient drawback. Firstly, the elaborate arrangement of electrodes drives up the cost of the device. Also, studies have indicated anomalies in the EWOD transports, such as instabilities at higher voltage and fluids with higher dielectric constants. Often a high applied voltage large force may generate large enough force leading to droplet breakup [68].

***Surface Acoustic Waves (SAW):*** Surface Acoustic Waves (SAW) is another very popular droplet manipulation techniques which does not require any external voltage source and surface treatment for droplet manipulation. Moreover this method is more energy efficient, faster and has a higher range of operation compared to EWOD. Droplet manipulation using surface acoustic wave was successfully employed in digital microfluidics. The benefits of this actuation technique are simple fabrication, compact, high biocompatibility, fast fluid actuation, contact-free particle manipulation, high energy density and compatibility with other microfluidic components. A SAW device consists of a piezoelectric substrate and at least one set of metallic interdigital transducers (IDTs) to generate SAWs to the piezoelectric material [70]. When SAW input wave increased beyond a critical value then the pressure gradient inside the droplet to be larger than the surface tension which in turn drives the droplet along the wave propagation direction. This device requires higher power to drive droplet as the piezoelectric ceramics' substrate is naturally hydrophilic and therefore surface treatment technique is required to improve the droplet actuation

performance by adding different materials [71, 72]. Cecchini et al. proposed a microchannel-based, SAW-driven device where SAW-aided coalescence is able to lead to liquid counterflow with respect to the SAW propagation direction. This process produces effective water injection into the microchannels at a convenient rate (see Figure 1.1(c)) [73]. Thalhammer et al. [74] reported SAW controlled droplet actuation technique to perform serial DNA- isolation, amplification, and array detection on a modified chip surface. In SAW-based systems, acoustic radiation may cause unnecessary disruptions to nearby components or samples. Thermocapillary actuation can be an alternative approach here as this method does not generate acoustic waves, mitigating this concern.

***Thermocapillary actuation:*** Thermocapillary actuation is another important droplet manipulation technique in microfluidics. It refers to the manipulation of a liquid droplet within a channel using temperature gradients. This method provides a way to manipulate droplets without direct physical contact and external pumps, which can be advantageous in certain microfluidic applications. Tafti et al. proposed a droplet manipulation method on a free surface of immiscible liquid then droplet can move in either direction from warm to cold region or vice-versa depending on the shape of the droplet [75]. In this scheme the liquid droplets manipulate on a free surface of a chemically inert and thermally stable liquid carrier platform using thermal gradient. Droplets which maintain spherical are propelled from cold to warm region and the others break up into a sessile lens move in the opposite direction. Droplets are not experienced heating directly as these are not in direct contact with solid substrates and this free surface droplet transports are achieved much higher speeds (~4 mm/s) using least thermal fluctuation (<5°C). The speed of the binary drop is linearly proportional to its diameter and the imposed temperature gradient, with an offset accounting for the hysteresis force. The different techniques of droplet actuation normally used in recent microfluidic device already been discussed in previous sections. Jiao et al. proposed a channel-based thermocapillary droplet actuation method where droplets were driven in a closed loop using various heating schemes of the heaters were located at the channel sides(see Figure 1.1(d)) [76].

***Magnetic actuation:*** Magnetic actuation in closed channel involves manipulating droplets using magnetic forces in a closed microfluidic channel system Its contactless nature, precise control, and ability to handle multiple droplets simultaneously make it a valuable tool for a



wide range of applications, from biology and chemistry to material science and diagnostics. Teste et al. proposed a droplet manipulation technique using miniaturized magnetic rails. This proposed digital microfluidic device able to implement sorting, trapping and merging operations by combination of magnetic rails network and trapping structures employed at the end of each rail [77]. Zhang et al. demonstrated a microfluidic chip-based superparamagnetic droplets manipulation technique into the designated sub microchannels by changing the position of the external magnetic field [45]. Chiou et al. proposed automated electromagnetic droplet manipulation platform to actuate magnetic particles by magnetic field gradients using electromagnetic coil array and topographical barriers. This automated magnetic droplet-based system is capable of whole blood genetic testing, nucleic acid extraction, amplification, and real time fluorescence detection (see Figure 1.1(e)) [78].

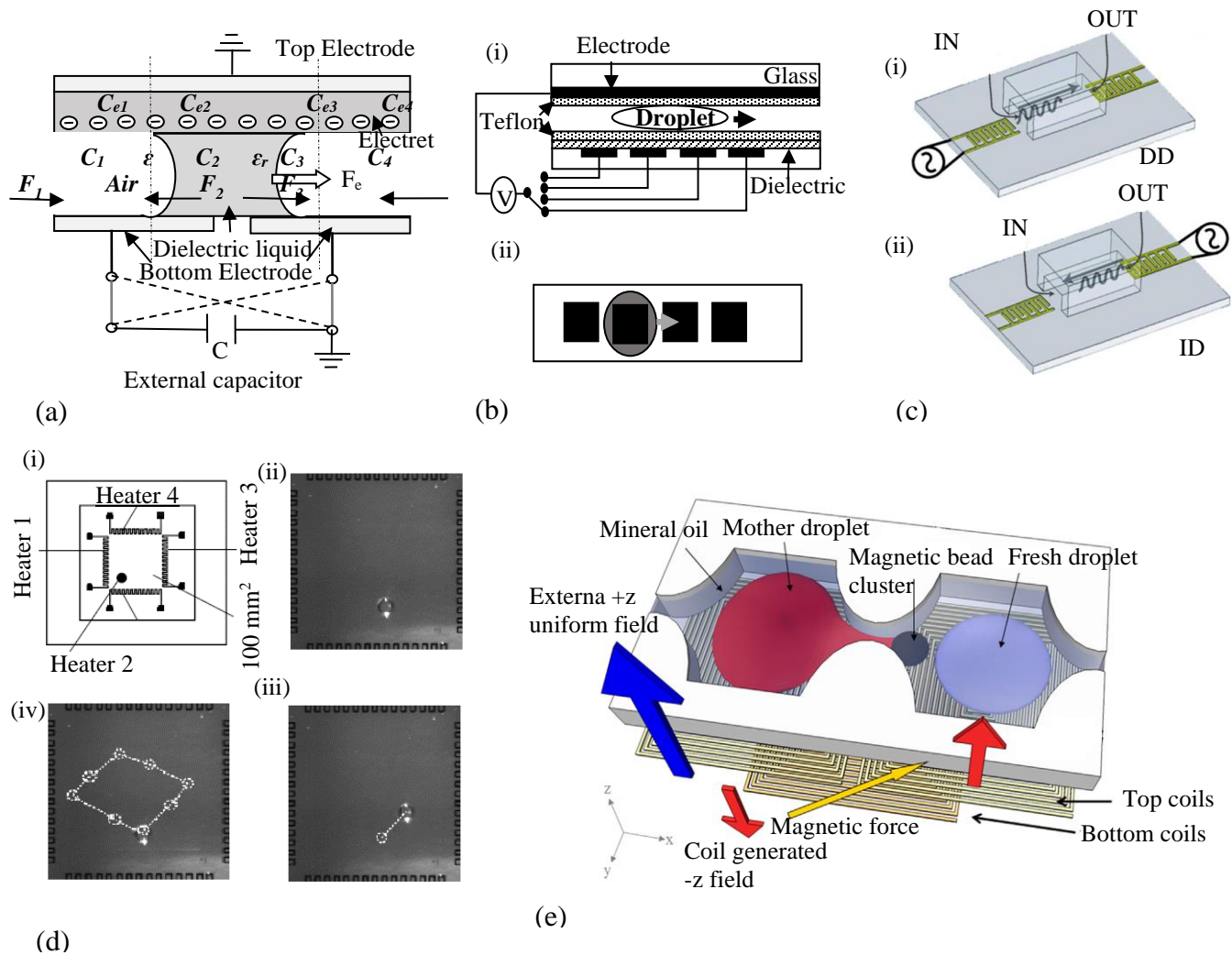


Figure 1.1: Schematics of different active droplet manipulation in closed DMF platforms (a) Liquid DEP on electret (L-DEPOE) [61] (b): (i) EWOD-based droplet manipulating device Cross-sectional view [66] (ii) Top view (c): (i) IDT at the channel entrance is used to generate SAWs toward its outlet (Direct Drive (DD)) (ii) Other IDT at the channel outlet is used to spread SAWs toward its inlet (Inverted Drive (ID)) [73] (d): (i) schematic of Experimental setup with 4 heater coil.(ii) – (iv) Image of droplet motion under periodic heating scheme[76] (e) Topography-assisted droplet splitting where magnetic particle cluster is squeeze out from the mother droplet [78]. Inset figures reproduced from (a) Ref. [61] with permission from the Royal Society of Chemistry, (b) Ref. [66] with permission from IEEE (c) Ref. [73] with permission from AIP Publishing and (d) Ref. [76] with permission from Institute of Physics Publishing (e) Ref.[78] with permission from Elsevier

### **1.3. Mechanisms of droplet manipulations in open surface DMF (ODMF) platforms**

In spite of higher- stability and controllability, closed channel droplet actuation technique restricts droplet manipulation flexibility and entail large pressure drops [79]. Establishing complicated channel networks with precise dimensions increases overall fabrication and operational cost. Moreover, narrow channels in such systems are more liable to clogging. To circumvent these difficulties, flexible and wide-range, two-dimensional droplet manipulation on open surface may be adopted. Open-surface droplet-based digital microfluidics (ODMF) is more accessible to fabrication by simple surface modifications or coatings. Droplet manipulation in such system, including reagent mixing, droplet splitting, merging, sorting had been demonstrated with a large variety of active and passive techniques [80]. Direct accessibility of droplets on open surface facilitates the integration of external components, such as sensors, electrodes, magnet, electromagnetic coil which can otherwise be challenging in closed-channel systems. Open surface DMF requires reduced sample volumes compared to closed channel systems and hence has decreased risk of cross-contamination between droplets because each droplet dwells on a distinct location on the surface. Like the closed channel counterpart, droplet manipulation on open surfaces has also attracted intense research effort where active and passive manipulations strategies have been put forth [ 81].

#### **1.3.1. Passive manipulation strategies on ODMF**

Passive manipulation of discrete droplets on ODMF platform requires no external energy, but they harness the capillary force generated by substrate wettability patterning in terms of surface energy gradient [82, 83,84, 85] surface roughness heterogeneity [86, 87, 88, 89, 90] and a combination of both [91]. Surface energy gradient may be created appropriate wettability patterning, where selected areas of the substrate are coated with low surface-energy substances like Teflon [92] and fluoroalkyl silanes [93]. Surface roughness also plays a role in determining the apparent surface energy density, and creation of micro- nano- roughness through a combination of micromachining, etching and nanocomposite-deposition can lead to spatial heterogeneity in surface wettability [94, 95]. Such spatial heterogeneity in wettability lead to unbalanced capillary force on a liquid droplet on a wettability-engineered surface, which in turn moves the droplet. While most

of the works on capillary-driven passive manipulation of droplets have demonstrated relatively simpler modes of transport (e.g., linear movement of droplet over the surface), few works have shown effective manipulation and complicated droplet-transport, e.g., metering, merging and splitting [96,97]. Figure 1.2 shows a few salient mechanisms of passive droplet manipulation strategies on ODMF platforms. Figure (a) shows a separation device to achieve multilevel separation and create additional split droplets. This device contains a small reservoir connected with four first-level branched reservoirs which farther connect to another level of reservoirs. Droplets dispensed in the first small reservoir were continuously carried to the two-level reservoirs in sequence and divided into eight separated droplets of nearly equal-volume [90]. Figure (b) exemplifies a multi-inlet, single-outlet model on the micropatterned superhydrophobic textiles platform employing the independent interfacial transportation concept [84]. Figure (c) shows photographs of liquid accumulation on a polyethylene terephthalate (PET) film substrate on the track when the device pumped for 1, 4, 7 and 10 non-stop cycles. The drained liquid rests on the track indicating a expand morphology, with the liquid attached on the wettability contrast track along the margin of the larger track (see Fig. (c.b3) and (c.b4)) [96]. Fig. (d) demonstrates a two-dimensional wettability gradient surface from superhydrophobic to common hydrophobic along the  $x$  direction and from hydrophobic to hydrophilic along the  $y$  direction. The consecutive images in Fig. d(i)–d(i) represent the self-transport of an individual droplet on the gradient surface.

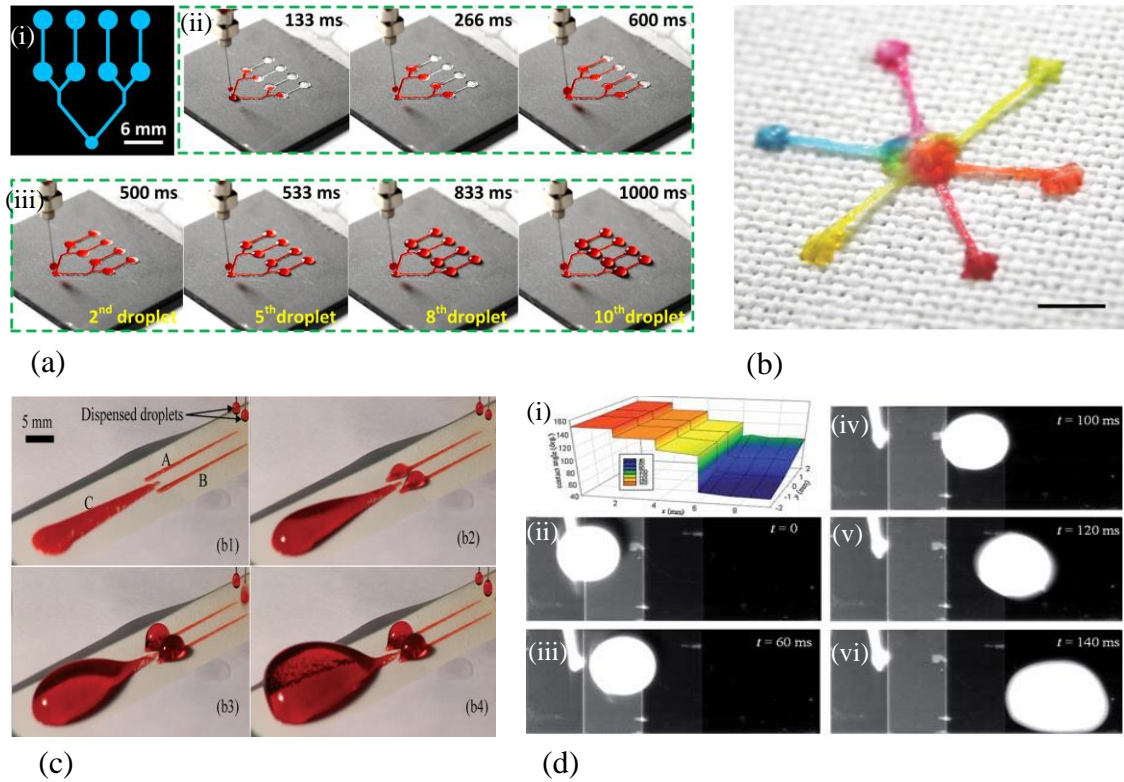


Figure 1.2: A few salient mechanisms of passive droplet manipulation on open surface microfluidic (ODMF) platforms (a): (i) Top view of a multilevel separation device (ii) Time-span image indicating separation method while first droplet was dispensed in the middle reservoir (iii) Digital image of the equilibrium state after the second, fifth, eighth and tenth droplet was separated.[90] (b) A multi-inlet–single-outlet strategy on the Micropatterned Superhydrophobic Textiles platform employing the autonomous interfacial transport concept [84] (c) Collection of liquid on the bridge circuit on a horizontal polyethyl-terephthalate (PET) film substrate after pumping for (b1) 1 cycle ( $\sim 56 \mu\text{L}$ ), (b2) 4 cycles ( $\sim 226 \mu\text{L}$ ), (b3) 7 cycles ( $\sim 395 \mu\text{L}$ ), and (b4) 10 cycles ( $\sim 564 \mu\text{L}$ ) [96] (d) (i) The static contact angle of the double-direction wettability gradient surface; (ii)–(vi) motion of a droplet on the double-direction wettability gradient surface [89] Inset images reproduced from (a) Ref. [90] with permission from Springer Nature, (b) Ref. [84], (c) Ref. [96] (d) Ref.[89] with permission from Royal Society of Chemistry

### 1.3.2. Active manipulation strategies on ODMF

On the contrary, active droplet sorting, which requires external force and/or energy input for droplet manipulation, has greater controllability over the passive modes. Like the closed-channel DMF, active droplet manipulation on open surfaces is also based on different external forces, such as electrostatic [98, 99], electrowetting [100], magnetic [101,102], thermal [103, 104], surface acoustic wave [105, 106], pneumatic [107, 108], triboelectric [109], etc. Figure 1.3 shows a few examples of active droplet manipulation strategies on ODMF platform. Figure 1.3 (a) describes an ODMF platform that leverages pneumatic suction force to actuate droplet on Polydimethylsiloxane (PDMS) substrates which was rendered superhydrophobic using an air-cushion to float the droplets, and suction-induced drag to pull them at the same time, the technique achieved simultaneous and precise droplet positioning on-chip [108]. Du et al. proposed an SAW based droplet actuation schemes where ZnO film on silicon substrate used to manipulate a droplet of 10 $\mu$ L (see Figure 1.3 (b)) [105]. Zhang et al. presented a scheme of generating serial dilutions in the form of droplet on an open surface platform through surface energy traps-assisted magnetic droplet manipulation (see Figure 1.3(c)) [110]. A two-dimensional open surface droplet manipulation technique proposed by Yang et al. (see Figure 1.3(d)) [102], accommodates a superhydrophobic magnetic film (SHMF) and an electromagnetic pillar array (EMPA) to frame the active surface of droplet manipulation with conjunction of gravity.

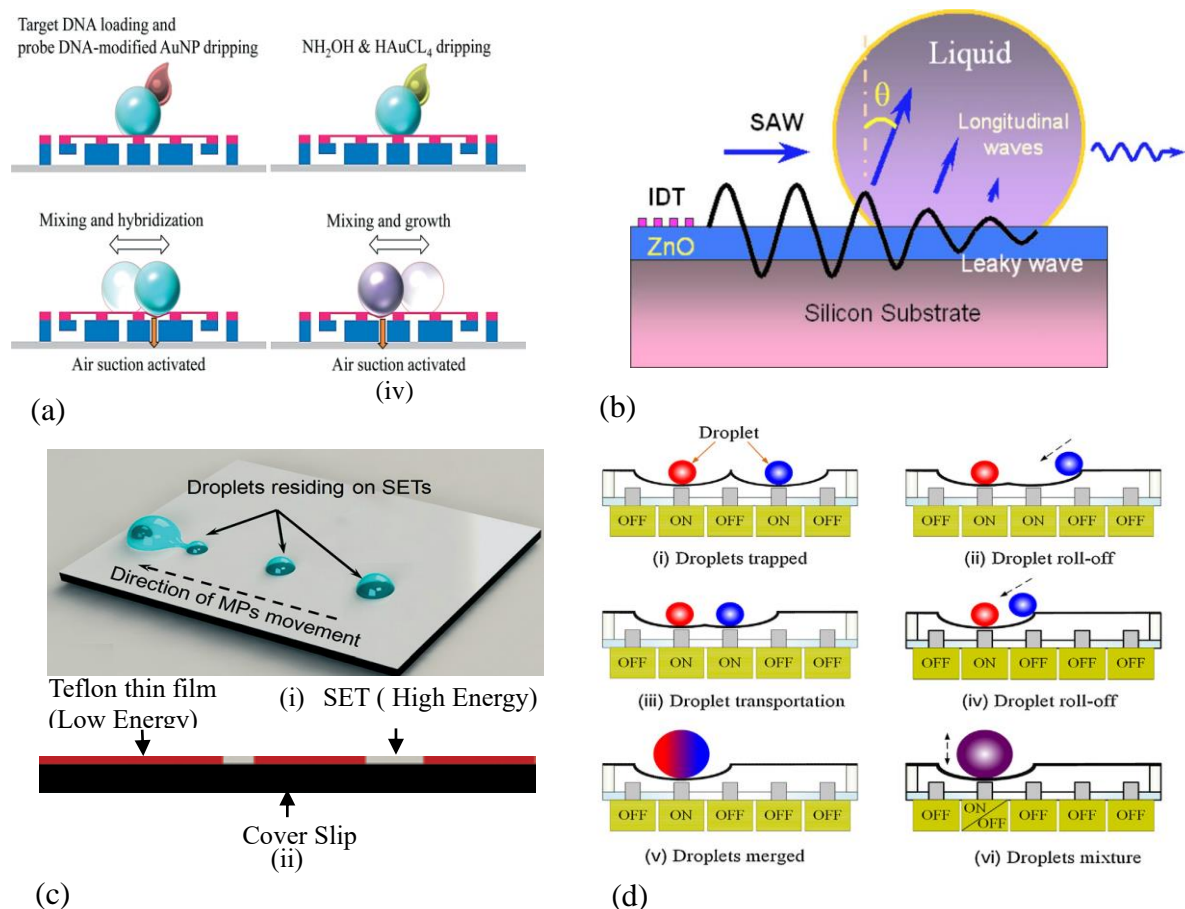


Figure 1.3: A few salient mechanisms of active droplet manipulation on open surface microfluidic (ODMF) platforms (a) Schematic illustration of the colorimetric detection for rapid identification of multi-nucleotide polymorphisms based on the hybridization-mediated growth AuNP probe [108] (b) Schematic drawing of interaction between Surface Acoustic Wave (SAW) and a liquid droplet and defining the Rayleigh angle [105] (c) (i) Illustration of droplet operations on SETs enabled open-surface platform (ii) Side view of a SETs device [110] (d) Schematic illustration of the principle for programmable droplet manipulation with the electromagnetic pillar array [102] Inset figures reproduced from (a) Ref.[108] and (c) Ref.[110] with permission from Royal Society of Chemistry (b) Ref. [105] with permission from AIP Publishing (d) Ref. [102] with permission from Elsevier

#### **1.4. Different attributes of droplet transports in open and closed channel DMFs:**

Salient attributes of droplet transport in open and closed-channel droplet-based digital microfluidic platform include operations like droplet sorting, merging and pooling. The following subsections discuss the salient attributes of these transports.

##### **1.4.1. Droplet sorting**

Varieties of chemical and biological applications are there in digital microfluidics which demand different size of droplets for specific applications. To fulfil this objective, droplet sorting is a very important issue in digital microfluidics. There are two types of droplets sorting such as passive droplet sorting and active droplet sorting depending on the requirement of external force. Passive droplet sorting requires no external force, only internal hydrodynamic force based on fluid property, flow condition and channel geometry actuate the droplets position. Pinched flow fractionation technique [111] is an example of passive droplet sorting micro scale hydrodynamics. Another very important size based passive droplet sorting method is deterministic lateral displacement (DLD) [112]. Though this droplet sorting scheme is very simple in fabrication but unable to sort droplets in same size if required. On the other way active droplet sorting is more beneficial over passive droplet sorting which requires external force for manipulation the droplet position. This category includes droplet sorting based on different external forces such as electric, SAW, thermal, pneumatic and magnetic forces.

**Sorting by electric force:** This method of droplet sorting is useful regarding on demand control with higher preciseness using rapid electric detection. Electric force is used to actuate droplets with presence of free charges in liquid droplet using interfacial stresses on the droplets. This method is categorised into two types, such as direct current control and alternating current control. Link et al. [40] demonstrated a droplet sorting method using direct current into a T-Junction bifurcation where droplets enter in selected channels as per direction of electric field applied. Droplets can be charged by exposing it to an energised electrode before going to the bifurcation channel as demonstrated by Niu et al. [113]. Ahn et al. [114] demonstrated a microfluidic device for high-speed sorting of water drops using dielectrophoresis. The dielectrophoretic force characterize by measuring the dependence of



the drop velocity on the drop size and the applied voltage. In a symmetric Y junction channel in the absence of electric field all the drops flow along the shorter channel with lower hydrodynamic resistance but with an electric field applied through electrode at other channel drops are attracted toward the energized electrode and flow into the second channel of Y junction. Individual water-in-oil droplets can generate charge and sort one by one in a controlled fashion. In this system researchers showed triple sorting of positively charged, negatively charged, and uncharged droplets without cell encapsulation with sorting rates as high as 600 droplets/s. In another precharging scheme by the same researchers (See Figure 1.4 (a)) [39].

**Sorting by SAW:** Droplet sorting using Surface Acoustic Wave (SAW) is another reliable technique. AC electric field is used to excite Interdigitated Transducer (IDT) to generate SAW, travelling on the surface of a piezoelectric substrate in Microfluidic channels [115]. The IDT consists of two microfabricated electrodes on a piezoelectric substrate. SAW can be controlled in two manner, Travelling SAW (TSAW) and Standing SAW (SSAW). Figure 1.4 (b) illustrates the droplet sorter setup (top view). A is the Inlet channel, B and C are the top and bottom focusing channels which focus the droplets on the way to the center of the channel to direct the droplets into the lower default outlet. Now when a surface acoustic wave (SAW) is applied via path F, droplets were directed upwards into the upper outlet H [53]. Franke et al. [51] Proposed a TSAW based droplet sorting method using a Y junction PDMS microchannel where droplets flow towards the upper branch of Y junction microchannel having a lower flow resistance when IDT is switched off, but later droplets deflect toward the lower channel when the IDT is excited. This concept further developed to fluorescence activated droplet sorting system by same researchers [52] where droplets are sorted in different channel depending on their fluorescence intensity using tapered IDTs. Standing SAW (SSAW) field can be generated using two IDTs excited with the same AC signal.

**Thermal sorting:** Thermal control droplet sorting can be performed by utilizing the thermocapillary effect on a very small scale. This thermocapillary force can be generated by both resistive heating and focused laser beam. Microheater and temperature sensor are required for resistive heating for precise alignment at a specific location [49,116]. Additional resistive elements can be linked to resistive heating to provide in site localized

temperature readings. On the contrary laser beam extends the resilience to transport droplets to several locations as required. Thermal sorting method commonly limited to specific applications as excessive temperature rise can vaporised the droplets or can damage the chemical or biological reagents. First thermally controlled droplet sorting scheme [50] presented in a T-junction bifurcation channel where a mother droplet splits up and a greater segment of it is taken into the lower branch due to its high temperature gradient at the lower channel as shown in figure 1.4 (c). Figure 1.4 (d) represents a suction-based droplet sorting logic with two W/O emulsions by asymmetric hydrodynamic resistances. After being slowed down by the two bypasses, the red droplets were subjected to the suction force and sorted into the collection channel, while other droplets continued to flow into the waste chamber [117].

***Magnetic sorting:*** Droplet sorting using magnetic force is used to separate droplets containing magnetic particles based on their physical and magnetic properties. The basic principle behind this technique is that droplets containing magnetic particles experience a magnetic force when placed in a magnetic field. The magnitude and direction of the magnetic force depend on the size and magnetic properties of the particles, as well as the strength and direction of the magnetic field. By adjusting the strengths and directions of the external magnetic fields, the droplets can be separated into different chambers based on their magnetic properties [118]. One common method for droplet sorting using magnetic force is to use a microfluidic chip that contains a series of channels and chambers. Another method involves the use of a magnetophoretic cell sorting system, which uses a combination of magnetic fields and hydrodynamic forces to sort droplets containing magnetic particles [119]. This technique is particularly useful in biological and biomedical applications, such as cell sorting and drug screening. The advantages of droplet sorting using magnetic force include high sorting efficiency, low sample consumption, and the ability to sort droplets containing a wide range of magnetic particles. Additionally, the technique is relatively simple to implement and does not require complex microfabrication processes. Figure 1.5 shows some prominent ways of active droplet sorting using magnetic force. Zhang et al. present a microfluidic chip-based CMDM (Continuous Magnetic Droplet Manipulation) approach to direct superparamagnetic droplets into the specified submicrochannels. An external magnetic field was applied perpendicular to the main-

microchannel (see Fig. 1.5 (a)) to deflect droplets into two different submicrochannels (2 and 3). Droplets deflection was controlled by the magnetic nanoparticle concentration, the magnetic field gradient and the position of the magnet [45]. Hetlani et al proposed a ferrofluid sorting method by employing a permanent magnet positioned beneath a microfluidic channel where the droplets would be deflected with respect to the size of the magnet [120]. Figure 1.5 displays the sketch of microfluidic chip in which external magnetic field gradient accessed by employing the main-channel close to the chip edge (see Figure 1.5 c. (i)). This microfluidic device was capable to implement precise dispensation of single droplet and any numbers of droplets into the specified sub-channels 2 and 3. Zhang et al. proposed another ferrofluid droplet sorting scheme based on flow speed or droplet size (see Figure 1.5 d).

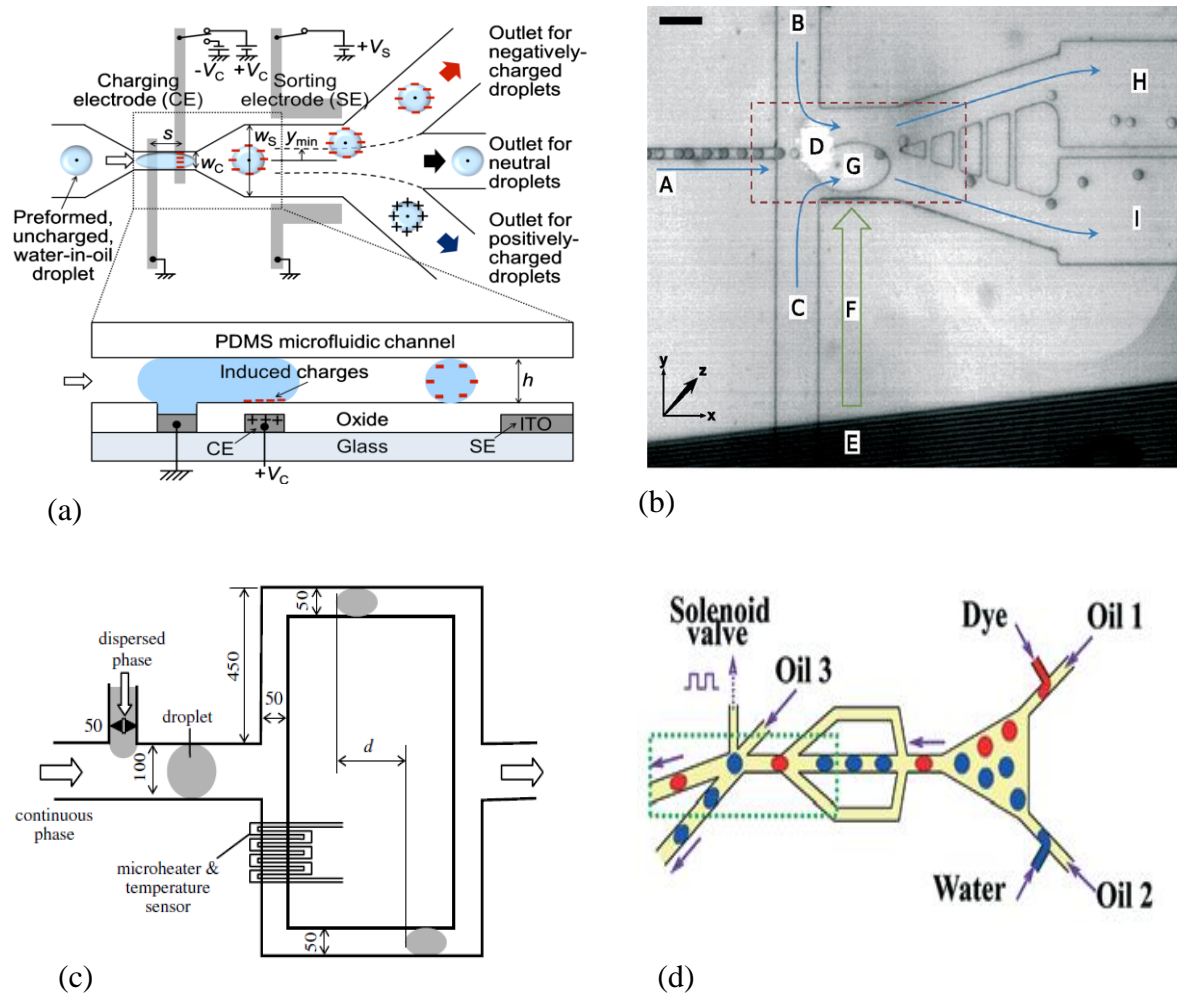


Figure 1.4: A few salient mechanisms of active droplet sorting: (a) Schematic diagram of the on-demand electrostatic droplet charging and sorting device [39] (b) SAW based Droplet sorter setup (top view) [52] (c) A microheater reduces the flow resistance on the lower branch and droplets are sorted to the lower branch [50] (d) Suction-based droplet sorting logic with two W/O emulsions by asymmetric hydrodynamic resistances [117] Inset figures reproduced from (a) Ref. [39] with permission from Biomicrofluidics, (b) Ref. [52] and (d) Ref.[117] with permission from Royal Society of Chemistry, (c) Ref. [50] with permission from IOP Publishing

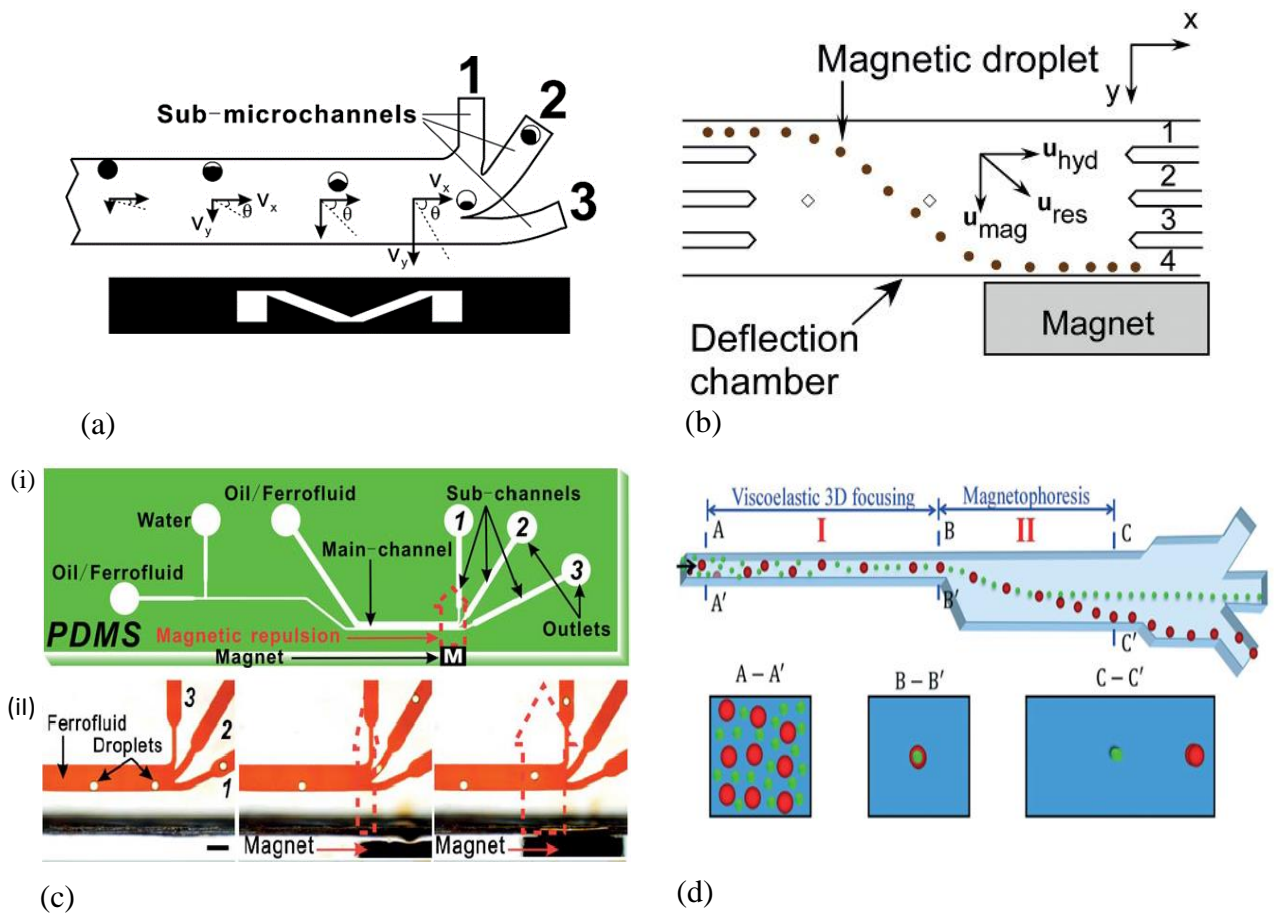


Figure 1.5: A few means of magnetic droplet sorting: (a) Schematic diagram of superparamagnetic droplets pulled into the sub-microchannel 2 or 3 depending on magnetic nanoparticle concentration, magnetic field gradient and the position of the magnet [45] (b) Deflection of the magnetic droplets in the  $y$ -direction across the chamber in presence of the magnetic field [120] (c): (i) Schematic diagram of microfluidic device containing the place and direction of applied magnetic repulsion (ii) Droplets contained in ferrofluid are selectively allotted into sub-channels 1, 2 and 3 by translating magnet [118] (d) Magnetic sorting methods based on the difference in flow speed and droplet size [119] Inset figures reproduced from (a) Ref.[45], (c) Ref.[118] and Ref.[119] with permission from Royal Society of Chemistry, (b) Ref. [120] with permission from AIP Publishing

### 1.4.2. Droplet merging

Droplet merging is a major operation in digital microfluidics, dealing with manipulating and supervising tiny liquid droplets on a microscale. It performs an important role in several applications, ranging from chemical and biological analysis to lab-on-a-chip systems. It is utilized to merge reagents or samples in exact proportions to allow controlled chemical reactions and medical diagnostics. Truthful merging confirms accurate sample preparation, lowering experimental errors and improving the consistency of results. Droplet merging can be applied for diluting concentrated samples or reagents to specific concentrations. Several biochemical assays require various reaction steps which can be enabled by droplet merging in a sequential manner. Figure 1.6 (a) demonstrates merging of the ferrofluid droplet (FFD) in a microchannel with mineral oil as a CM (Continuous Medium)(see Figure a.(i)). Figure a.(ii) indicates simulation results of FFDs (red) in a CM (blue). It has been observed that commencement of experimental merging (10 ms) is slightly longer than that from the simulated results (6 ms). Figure a.(iii) shows generation of Rhodamine and FFDs in a double T-junction with mineral oil as a CM. Figure a.(iv) indicates complete merging of the rhodamine-FFD along the Y-direction [121]. Varma et al. reported experimental studies of two different type of uniform magnetic field-induced droplet merging (Figure 1.6 (b)). Figure b.(i) shows generation and merging of two ferrofluid droplets under an applied uniform magnetic field ( $H$ ) while Figure b.(ii) represents generation and merging of color dye and ferrofluid composite droplets [122]. Figure 1.6 (c) shows another permanent magnet-induced droplet merging technique where the droplets deflect towards the magnet on the way of its moving along the cross-shaped channel and merged into a larger droplet [123].

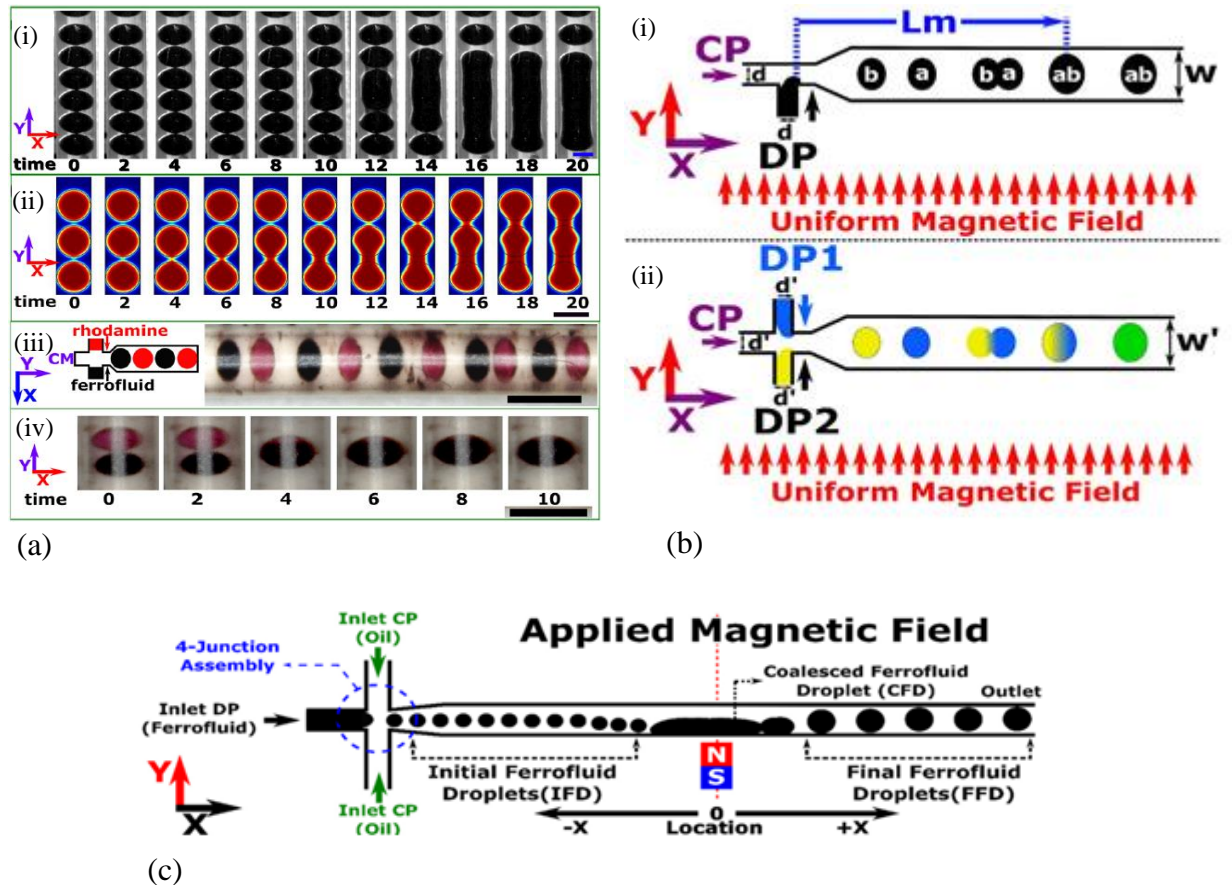


Figure 1.6: A few salient schemes of droplet merging: (a) Experimental micrographs of FFD's (black) in a transparent CM (i), simulation results of FFD's (red) in a CM (blue) (ii), an array of rhodamine (red) and FFD (black) generated by a double T-junction (iii), and experimental micrographs of rhodamine and FFD's merging with time (iv) [121] (b) Two ferrofluid droplets 'a' and 'b' with different velocity merge and formed the new droplet 'ab'(i) and the dye-ferrofluid composite droplets (ii) [122] (c) permanent magnet induced droplet merging in a cross shaped channel [123]. Reproduced (a) Ref.[121] with permission from IEEE (b) Ref.[122] (open access) and (c) Ref.[123] from Elsevier

### 1.5. Applications of DMF

As already mentioned, digital microfluidics is a very popular technology amongst all other recent microfluidic systems. It is a micro scale liquid handling technique characterizes by the manipulation of droplets with actuation of different force. Each picoliter to microliter sized droplet serves as an isolated vessel for chemical processes which can be moved, merge, split, and dispense from reservoirs. Because of its unique advantages, including simple instrumentation, flexible device geometry, and easy coupling with other

technologies, DMF is being applied to a wide range of fields. Different areas of DMF application discussed as follows.

**Chemical Application:** This platform can actuate different organic solvents including acetone, acetonitrile, ethanol, dichloromethane, and others [124]. A broad collection of micro-particles, along with semiconducting microbeads and capsules can be synthesized [125]. Dubois et al. [126] proposed a method to synthesize tetrahydroquinolines by Grieco's reaction with ionic liquid droplets as microreactors. A two-plate DMF platform for chemical synthesis was first introduced by Jebrail et al. which is convenient to control multi-step parallel functions [127]. This platform can synchronize synthesis of five peptide macrocycles from three different components. In another application a radiotracer is synthesized with reliable radio-fluorination efficiency using two-plate DMF device with four concentric heaters (see Figure 1.7 (a))[128].

**Biochemical Application:** Digital microfluidics (DMF) has discovered several applications in the field of biochemistry due to its capability to manipulate tiny droplets with accuracy and control. It is used to make the typical and cumbersome laboratory procedures easier by manipulating micro-droplets. These latest developments of DMF are used in several biochemical applications. Sista et al. proposed a technique to employ DMF platform for collection and analysis of anonymous and affected newborn dried blood spots samples to screen for Pompe and Fabry diseases [129]. The cumulative effects of these parameters' variability can be studied by applying Monte Carlo simulations [130]. In some cases analytes may exist in substantial quantities of diluted concentration, however investigation procedures require small volume. This problem can be tied out by integrating Solid-phase micro extraction (SPME) with high-performance liquid chromatography (HPLC) utilized DMF as the interface (Figure 1.7 (b)) [131]. In another application a parallel-plate DMF device utilized to synthesize a large array of Metal-Organic Frameworks (MOFs) crystals with high parallelism without any complicated and expensive equipment (Figure 1.7(b))[132]. In this method HKUST-1 [Cu<sub>3</sub> (BTC)<sub>2</sub>] crystals were printed by actuating a mother droplet of HKUST-1 precursor solution were actuated over 20 μm × 20 μm ITO coated top plate (Figure 1.7 (c)).



**Biological Application:** DMF platform also utilized for biological applications using costly or precious reagents. There are some challenges regarding sample loss or cross-contamination due to absorption of biological molecules [133]. This sticking behavior can be decreased by using an oil matrix which reduces the probability for biomolecules to encounter surfaces [134]. Samples and reagents which are incompatible with oil, can be mixed with Pluronic [135, 136] or graphene oxide [137]. Consecutive experiments can be achieved on a fresh device surface using removable hydrophobic insulators [138]. Barbulovic-Nad et al. [139] employed a toxicity assay where droplets carrying cells initially merged with droplets containing surfactant and later merged with droplets carrying viability dyes. In this method reagent consumption was reduced almost 30 times. Bogojevic et al. [13] developed an alternative method where several cell samples are exposed to varying concentrations of drug at the same time resulting in very little cell de-lamination from the surfaces. A concept of 3D cell cultures was proposed by Fiddes et al. [140] where cylindrical hydrogel discs were integrated onto DMF devices. George and Moon [141] utilized DMF into an enhanced chemical investigation system using the 3D cell culture technique. Manipulating and characterizing DNA samples are other important MFD applications. Hung et al. [142] developed a DMF-based DNA extraction protocol with a smaller number of washing cycles. Initially magnetic particles collected onto one side of the droplet and then the unbound reagents or DNA washed out from magnetic particles. Manipulating and characterizing DNA samples are other important MFD applications.

**Digital microfluidic applications in portability:** Portable DMF platform is the most important development of DMF technology [143]. This portable device can perform certain applications such as clinical diagnostics, enzymatic assays, and immunoassays but to perform the entire assay process (from sampling to sensing) is still under development. Sista et al. [144] reported an electrowetting-based digital microfluidics platform for development of immunoassays and DNA amplification with reduced time-to-result and integrated sample-to-answer functionality. Kim et al. [145] (see Figure 1.7(c)), developed a portable DMF hub using a capillary-based interface for direct sample delivery. Yafia et al. proposed another smart phone operated sample processing and detection technique by means of a colorimetric method [146].

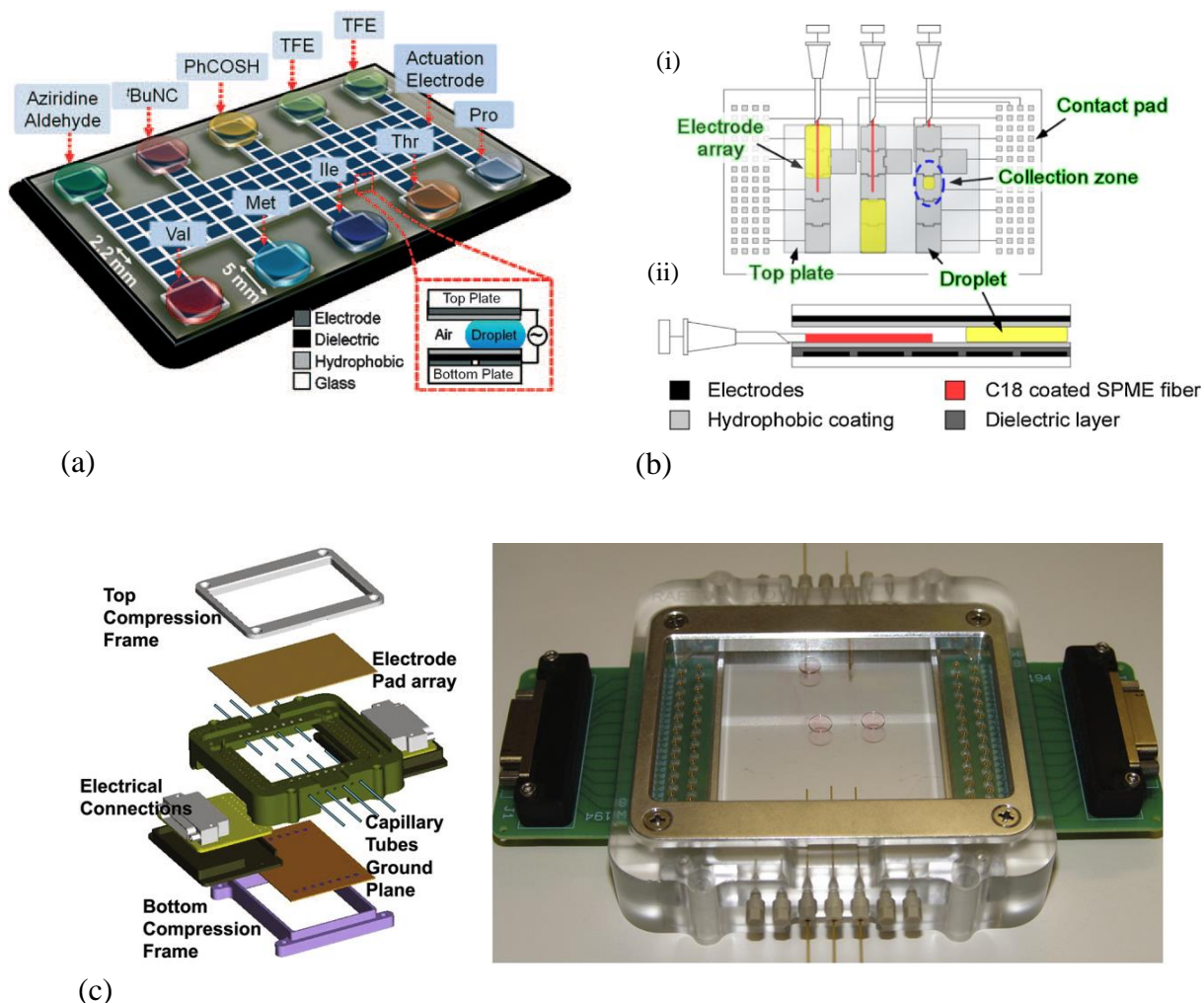


Figure 1.7: A few salient schemes of Applications of DMF: (a) Top and side views of the digital microfluidic device used for peptide-based macrocycle (PM) synthesis [127] (b) SPME-DMF Schematics and digital microfluidic chip designed for printing of MOF crystals (i) Top-view (upper) and (ii) side-view (lower) schematics of the SPME-DMF interface [131] (c) DMF hub for DNA applications with capillary-based interface for sample delivery [145]. Inset figures reproduced from (a) Ref.[127] with permission from John Wiley and Sons, (b) Ref.[131] with permission from Elsevier and (c) Ref. [145] (Open access)

### 1.6. Overview of salient surface phenomenon for open surface DMF

Characterization of surface of digital microfluidic platform is the most important task in design of digital microfluidic device. Droplet manipulation techniques and their characteristics mostly depend on the surface property of digital microfluidic platform.

Presently two types of droplet manipulation techniques are mostly adopted, droplet can be handled on digital microfluidic platform with contact under different actuation mechanism, on the other hand a host fluid liquid film on a microfluidic substrate may be used to transport droplet. Surface characteristics such as wettability gradient, contact angle hysteresis, temperature gradient influence the droplet actuation method on solid substrate, where as host fluid liquid film property such as viscosity, surface tension mostly influence the droplet manipulation velocity in case of host fluid film-based contact less droplet manipulation.

### **1.6.1. Fundamentals of droplet manipulation on solid substrates**

Droplet manipulation in Digital Microfluidic System performs various chemical or biological functions on small microchips. At initial stage microfluidic systems use microchannels for continuous fluid flow which require complicated micropumps, microvalves and voluminous peripheral apparatus to drive the liquid through the channel networks [147]. Compared to continuous flow liquid system in micro channels, the discrete microdroplet manipulation on open surface microfluidic substrate offers higher flexibility, limited sample consumption with lower cost of device fabrication. Yang et al. [147] proposed a method of droplet manipulation on a hydrophobic surface using variable Laplace pressures. Surface wettability gradients created by patterning microstructure distributions which are composed of several textured regions with gradually increased structural roughness. Laplace pressures exerted on a droplet due to variation of hydrophobicity of surfaces whereas resistance forces come from the contact-angle hysteresis. Another technique of high-speed droplet manipulation on a hydrophobic surface is displacing a permanent magnet where microliter droplets (5 – 15  $\mu\text{L}$ ) containing paramagnetic particles can be transport with a speed around 7 cm/s [148]. Different operations such as movement, coalescence and splitting of drops of water as well as drops of biological fluids can be performed using paramagnetic microparticles chains. Marston et al. [149] demonstrated an experimental analysis of liquid drop's initial dynamics onto a powder surface using high-speed photography. The qualitative features of this drop dynamics strongly depend on the bed packing fraction ( $\phi$ ), the impact Weber number ( $We$ ) and Ohnesorge number ( $Oh$ ) which characterizing the role of viscosity and the Bond number ( $Bo$ ). Yonemoto et al. [150] experimentally demonstrated the sliding behavior of

water–ethanol mixture droplets on a low surface energy solid surface inclined with constant angular velocities.

### 1.6.1.1. Contact Angle Hysteresis (CAH)

When a droplet is placed on a plane, horizontal solid surface then the contact angle defined as the angle formed by a liquid at the three-phase boundary where a solid surface, liquid, and vapor meet. The dynamic contact angle implies the measurement of the contact angle of a liquid droplet on a solid surface while the droplet is in motion, typically advancing or receding [151]. Contact angle hysteresis refers to the difference in contact angles observed when a liquid is advancing (spreading,  $\theta_A$ ) on a solid surface versus when it is receding (retracting,  $\theta_R$ ) and represented by the expression  $(\cos \theta_R - \cos \theta_A)$ .

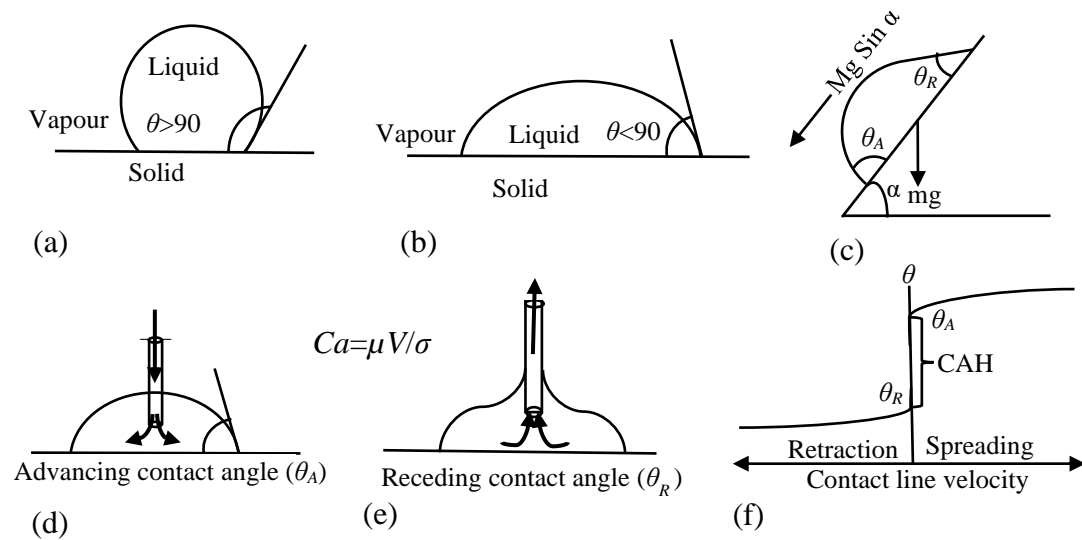


Figure 1.8: Schematics of contact angle and CAH (a) Equilibrium contact angle on a hydrophobic surface (b) Equilibrium contact angle on a hydrophilic surface. (c) Advancing and receding contact angles on a sliding droplet on an inclined plane (d) and (e)  $\theta_A$  and  $\theta_R$  measurement using goniometer. (f) Variation of  $\theta_A$  and  $\theta_R$  with contact line velocity

The interface where solid, liquid, and vapour coincide is referred to as the “three phase contact line” (see Figure 1.4 (a) and (b)). Contact angle hysteresis is defined as the difference in advancing contact angle  $\theta_A$  and the receding contact angle  $\theta_R$ . It can be understood by observing a droplet resting on an inclined substrate (Figure 1.4(c)). Here Gravity pulls ( $mg \sin \alpha$ ) acting on the droplet trying to drive it downward while CAH will hold the droplet in

place. Therefore droplets will turn distorted and will stick in place. The upper portion of the droplet becomes thin, with a reduced contact angle, while the lower part of the droplet becomes broad, with a high contact angle. Advancing and receding contact angles are typically measured by a Goniometer (see Figure 1.4 (d) and (e)). Here a needle is brought close to the substrate surface and liquid is dispensed slowly to increase the volume of the drop. As the contact line between the substrate and the drop is increasing, the advancing contact angle is measured. When the liquid is sucked slowly off the substrate and the contact line is withdrawing, the receding contact angle is measured. The relation between contact line velocity and dynamic contact angle for advancing contact line dynamics and receding contact line dynamics is shown in Figure 1.4 (f), which implies that droplet motion is impeded by contact angle hysteresis (CAH). This is further elucidated below.

#### **1.6.1.2. Effect of contact angle hysteresis on droplet manipulation**

The effect of contact angle hysteresis on droplet manipulation is an important issue in digital microfluidics. Eisherbini et al. [152] experimentally describe the geometric shapes of liquid drops at various inclination angles with eight surfaces covering a range of advancing contact angles from  $49^\circ$  to  $112^\circ$  and receding angles from  $12^\circ$  to  $78^\circ$ . The dimensionless retentive force can be related to the contact angle hysteresis by

$$F_S = k\gamma R(\cos \theta_R - \cos \theta_A) \quad (1)$$

Where  $\gamma$  denotes the liquid–vapour surface tension,  $k$  is a constant and  $R$  is the equivalent radius of the droplet footprint [153, 154]. A numerical model proposed by Annappagada et al. [155] to predict static spherical-cap droplet shapes, critical droplet motion on an inclined plane and the critical angle of inclination as a function of droplet size at which droplet about to start. Droplet profile, advancing and receding contact angles for different droplet sizes and surface inclinations also experimentally measured [156]. Deflection of droplet is a function of droplet size, droplet speed, the angle of transition, contact angle hysteresis created in the direction of droplet motion and Weber number. Change of contact angle hysteresis from a region of higher to lower results deflection of droplets towards the transition line whereas transition of contact angle hysteresis from lower to higher deflect the droplet away from the transition line. On the other hand, transition from high to low hysteresis results in some of the drop's interfacial energy converted into kinetic energy as

the deformation of the droplet is reduced. A droplet's velocity either increases or reduces in the normal to the line of transition depending on whether the drop transitions onto a surface of a higher or lower receding contact angle. Overall deflection can be decreased on the downstream with high hysteresis as it creates higher surface drag. The motion of a droplet sliding down in an inclined substrate under gravity also depends on contact angle hysteresis at different stages of motion [157]. Another simple analytical model based on Newton's second law reproduced to predict the dynamics of the sliding motion which does not depart too much from spherical cap configuration. In some cases, the forces due to hysteresis may overcome the forces present due to gravitational pull which results in the droplet sticking to the substrate. The droplet with small equilibrium contact angle form long tail when sliding down in the inclined surface, alternately the droplet likely to have shapes closer to teardrops for droplets with large equilibrium contact angle. Substrate wettability gradient can influence droplet manipulation and its speed in DMF platform.

#### **1.6.1.3. Effect of Substrate wettability on droplet manipulation**

Droplet manipulation with wettability gradient surface has attained a remarkable role in Digital Microfluidics (DMF). Various techniques have been used to fabricate desired wettability gradients, for example, using chemical patterning [158,159], physical texturing [86,160,161,87], or combination of both [162,89]. Various wettability gradient surfaces with low CAH can be fabricated where droplets can be manipulated in a pre-defined path with a minimum distance maintained between droplets. Subramanian et al. [82] reported a spherical cap droplet motion on a wettability gradient surface where the variation in droplet velocity is a consequence of change in driving force as well as the change in hydrodynamic resistance that occurs along the gradient surface. This theoretical model farther validated experimentally with tetraethylene glycol droplet in a wettability gradient present on a silicon surface [163]. Droplets of magnetic bead can be handled magnetically using wettability gradient and surface tension between different liquids without sticking the beads to the glass surface [164]. Sample bead droplets can be extracted as well as diluted and finally confirmed that beads can be effectively collected and rinsed using extraction and dilution units. Another process to generate alternating wettability is to incorporate anisotropic chemically defined linear-stripe-patterned surfaces where fluorinated self-assembled monolayer creates the hydrophobic stripes and the hydrophilic stripes generated

by SiO<sub>2</sub> substrate [165]. Gosh et al. [96] presented substrate-independent and wettability patterning method to transport a large volume of droplet (up to 350  $\mu\text{L s}^{-1}$ ) in a tapered, superhydrophilic, open microfluidic tracks overcoming viscous and other opposing forces (e.g., gravity) without power input.

### **1.7. Magnetic Digital Microfluidics (MDMF)**

Magnetic digital microfluidics (MDMF) is a technology that combines digital microfluidics and magnetic fields to manipulate small volumes of liquids, typically in the range of microliters or nanoliters [166]. This technology enables precise and automated control of droplet size, shape, movement, mixing and formation for various applications such as chemical analysis, medical diagnostics, and biotechnology [9,167,168]. A magnetic field is applied to manipulate the particles, and hence, control the movement of the liquid droplets. Droplet manipulation using magnetic force is achieved by adding magnetic nanoparticles (ferromagnetic, paramagnetic, and superparamagnetic particles) to the liquid or by using a ferrofluid, which is a liquid that contains suspended magnetic particles [169,170,171]. Ferrofluid droplets in magnetic digital microfluidics refer to tiny droplets of a liquid containing colloidal suspensions of single domain magnetic nanoparticles such as Ni, Co, Mg, or Zn compositions of ferrite (Fe<sub>2</sub>O<sub>4</sub>), magnetite (Fe<sub>3</sub>O<sub>4</sub>), or maghemite ( $\gamma$ -Fe<sub>2</sub>O<sub>3</sub>) in a nonmagnetic liquid carrier phase [172]. The droplets can be moved along pre-defined pathways, merged, or separated by changing the magnetic field strength and direction. MDMF can handle a wider range of sample types and volumes from nanoliters to microliters, compared to other digital microfluidic technologies. Magnetic particles used in MDMF can be functionalized to specifically bind to different types of molecules, including proteins, nucleic acids [173], and cells. MDMF can be easily integrated with other technologies such as optics, sensors, and electronics, making it a powerful tool for various applications. For example, MDMF can be used to perform multiplexed immunoassays [174,175] using magnetic beads as detection labels, or to perform cell sorting and manipulation using magnetic nanoparticles. This is a cost-effective and easy-to-fabricate technology. It can be fabricated using standard microfabrication techniques, and the magnetic particles used in MDMF are commercially available and relatively inexpensive. Overall, magnetic digital microfluidics has several advantages over

other digital microfluidic technologies, making it a promising tool for various applications in healthcare [176,177,178,179], environmental monitoring and biotechnology. There are mainly two type of approach in MDMF, Close channel digital microfluidics and open surface digital microfluidics. Closed channels MDMF present a controlled environment, where enclosed channels allow precise and controlled manipulation of droplet with curtailing the risk of contamination and evaporation. Most techniques are channel-based and paths of magnetic field-movement are predefined, underlining the issue of lack of controllability. Closed channel droplet actuation technique restricts droplet manipulation resiliency [79]. Constructing microchannels with the necessitated accuracy can be complicated and may include advanced microfabrication techniques. This approach can be disposed to clogging due to particulate matter or biological samples. In closed channel direct surveillance might be more challenging, possibly needing dedicated imaging techniques. Compared to closed channel MDMF, open surface has simpler fabrication processes since this approach does not require complicated microchannel designs [180,181,182]. Droplets can be more dynamically manipulated on an open surface without the restrictions of confined channels. Absenteeism of microchannels lessens the risk of clogging due to particles or debris. This systems allow for a wide range of fluidic operations, such as droplet merging, splitting, mixing, and transporting. Therefore, to achieve more precise, flexible, and wide range two-dimensional droplet manipulation, open surface microfluidic platform is preferred where micro-coil array can be an appropriate alternative to attain two-dimensional control of magnetic force [183, 184].

### **1.7.1. Open Surface Magnetic Digital Microfluidics (OMDMF)**

Out of the different droplet manipulations strategies discussed so far, magnetic force offers a viable alternative for open-surface magnetic digital microfluidic (OMDMF) platforms. In OMDMF, liquid droplets are impregnated with magnetic nano- or microparticles, which may be functionalized with reactive entities (e.g., molecules, ligands, polymers, proteins, or even cells) to perform a host of different bioanalytical tasks. For transport of non-magnetic biological samples, such as blood, saliva, or urine, such samples may be infused with the functionalized magnetic nano- or micro-particles, and liquid droplets containing the suspension may be transported using appropriately designed magnetic field gradients [185]. Thus, the droplets can serve as mobile reactors in an OMDMF. Such platform is easy



to implement in term of fabrication and integration, can actuate droplets containing minuscule volume of biological reagents and chemical samples with flexible controllability and high accuracy. The underlying substrate requires a minimal preparation, e.g., surface coating with a hydrophobic material such as Teflon AF (amorphous fluoropolymer) or coating with an immiscible liquid film, so as to minimize the undesirable droplet pinning on the surface. For effective magnetic fluid droplet manipulation in a microfluidic device the imposed magnetic field should be strong enough to overcome the viscous resistance, but at the same time should not lead to particle aggregation and droplet splitting. The requisite localized magnetic field gradients can be created by using minimized permanent magnet (see Figure 1.9 (a) and (b)) [186, 187] or electromagnetic coils [78] or by combination of both [188]. Figure 1.9(a) show a movement and merging of liquid droplets on Teflon coated glass using permanent magnet and figure 1.9(b) demonstrate another droplet manipulation technique using permanent magnet on magnetically deformable flexible substrates. Figure 1.9 (c) illustrate a concept of water droplet movement on a soot-wax coated PDMS-iron particle composite substrate using a permanent magnet with focused mild steel cone. Here the deformed surface profile (by movement of the cone) forms sufficient roll off angle for droplet movement [189].

Reckoning the current widespread relevance of EWOD in the microfluidic community, it is important to introspect the salient differences between the two techniques (see Table 1.1). There are few distinct advantages of OMDMF over the traditional DMF mode employing electrowetting on dielectric (EWOD), thermal or acoustic actuations. For example, dielectric control involves applying high potential difference ( $\sim$ kV), which often associates with the phenomenon of gas evolution due to electrolysis; it may also affect the viability of bioparticles due to Joule heating and dielectric breakdown. In thermal control, droplet sorting requires a threshold level of temperature difference which may not be viable for some reagents; additionally, generation of the requisite thermal gradient may either increase the requirement of the chip infrastructure, or the temperature range may interfere with the viability of the biological moieties. SAW-based droplet sorting requires heavy investment in terms of RF oscillating materials with high modulus of elasticity, e.g., platinum; embedding the oscillators in the chip is often cumbersome. One major shortcoming in realizing widespread OMDMF stems from the fact that the actuation is still

hardwired into the system (the substrate), and hence flexibility and versatility in droplet manipulation is missing.

**Table 1.1: Comparison of EWOD and magnetic manipulation of discrete droplets**

EWOD manipulation	Magnetic manipulation
<p>It modulates the wettability of a surface with respect to a liquid by applying an electric field to a thin dielectric layer on a hydrophobic surface. This alters the contact angle of the liquid droplet, enabling precise manipulation.</p>	<p>It uses magnetic fields to control the movement of droplets with magnetic nanoparticles within it. External magnetic fields exert forces on the droplets, directing their motion.</p>
<p>The apparent contact angle of a sessile droplet under an applied electric field is governed by an interplay of surface and electrostatic energy, as per the Lippman-Young equation [190]. Droplet motion is caused by an asymmetric change in the contact angle of a droplet when asymmetric voltage is applied through multiple electrodes.</p>	<p>The apparent contact angle of a sessile droplet under an applied magnetic field is governed by an interplay of surface and magnetostatic energy [191, 192]. Droplet motion is primarily caused by magnetic polarization force [172] under a magnetic field gradient. The role of change of apparent contact angle on droplet transport is less [191].</p>
<p>Requires high electric potential (~ kV) [193]</p>	<p>Requires spatial gradient of magnetic field [194].</p>
<p>EWOD offers precise droplet manipulation, but the transport speed is most often limited to ~3 mm/s [195].</p>	<p>Magnetic manipulation is faster (velocity ~ 11.5 cm/s) but precision is less than that of EWOD [196].</p>

EWOD manipulation	Magnetic manipulation
EWOD systems can be complex, requiring precise control of voltages and elaborate electrode assembly within the substrate [197].	Magnetic systems may have simpler setups, but incorporating magnetic components may introduce complexities [198].

Nguyen et al. [199] experimentally demonstrate the effect of magnetowetting and sliding motion of a sessile ferrofluid droplet on a planar homogeneous surface using permanent magnets of different sizes and strengths. The magnetic force should be large enough to overcome the resistive friction and the capillary force to actuate the droplet (see figure 1.9(d)). Nguyen et al. [200] reported a simple actuation system to drive ferrofluid droplet by four planar coils in combination with a pair of permanent magnets and a soft magnetic steel sheet. A closed loop two-dimensional, programmable actuation of a ferrofluid droplet using four planar micro-coils demonstrated by Ali Beyzavi et al. [194]. Magnetic beads assigned in an oil-coated aqueous droplet can be actuated by an external magnet along with different operation such as coalescence and splitting on an open hydrophobic surface (see figure 1.9(c)) [189]. Assadsangabi et al. [188] studied a new method to actuate ferrofluid droplet using micropatterned planar coils coupled with bias field of permanent magnets. Precise manipulation of large amounts of individual droplets with controlled flexible trajectory was achieved by an approach developed by Chen et al. [201]. Ganguly et al. [202] provided an insight into the transport of ferrofluid and magnetic microspheres for droplet-based microfluidics and presented a review of their applications in microscale devices. The Kelvin body force on the magnetic nanoparticles is proportional to both the gradient of the magnetic field and the field strength [172]. Thus, on a microfluidic platform, it is possible to create strong localized magnetic force-fields by deploying static or rail-mounted miniaturized permanent magnets next to the chip, or embedding miniature electromagnet coils [203, 204, 205, 206], sometimes a combination of an active electromagnet, for creating localized gradient, and a macroscale magnet for creating the magnetic bias has also been used (see Figure 1.9(e)) [207]. Deng et al. [208] employed lithographically developed

micro-electromagnets in a superposed biasing external magnetic field to realize controlled movement of superparamagnetic microbeads in a suspension. More recent applications have shown better on-chip maneuverability, lower power consumption and high throughput using sequentially switchable multiple-coils and arrays [209]. A new dynamic and compact technology by Fulcrand et al. [210] demonstrated simultaneous manipulation of microbead batches in continuous flow along controlled spatial pathways by synchronizing the injection of beads in the channel and the actuation of micro-coils. While most of these above techniques manipulated individual magnetic microbeads (micron sized polystyrene beads containing superparamagnetic nanoparticles) in a suspension, similar manipulation of ferrofluid droplets have not been undertaken widely. On-chip transport of ferrofluid droplets have initially been carried out by the group of Nguyen et al. [211], who reported a system for magnetic manipulation of ferrofluid droplets by an array of PCB-based planar coils in conjunction with permanent magnets. Probst et al. [183] developed a strategy for optimally controlled planar steering of ferrofluid droplet using four electromagnets. Studies on manipulation of magnetic particle-laden droplet on superhydrophobic substrates have provided an insight of the relevant operating regimes (see figure 1.9(b)). Nguyen et al. have investigated the fluid dynamic aspect of ferrofluid droplet manipulation on an open substrate that is covered with an immiscible liquid or a superhydrophobic coating [212]. Bijarchi et al. proposed a platform to pull a fully immersed water-based ferrofluid droplets in a pool of olive oil (carrying substrate) using switching two electromagnet in either direction [213] see (Figure 1.9(f)). While these works have nicely portrayed the controllability of the ferrofluid droplets in one or two dimensions on the substrates through controlling the excitations in the field-producing coils, ferrofluid transport behaviors using multiple-coil arrays have not yet been studied.

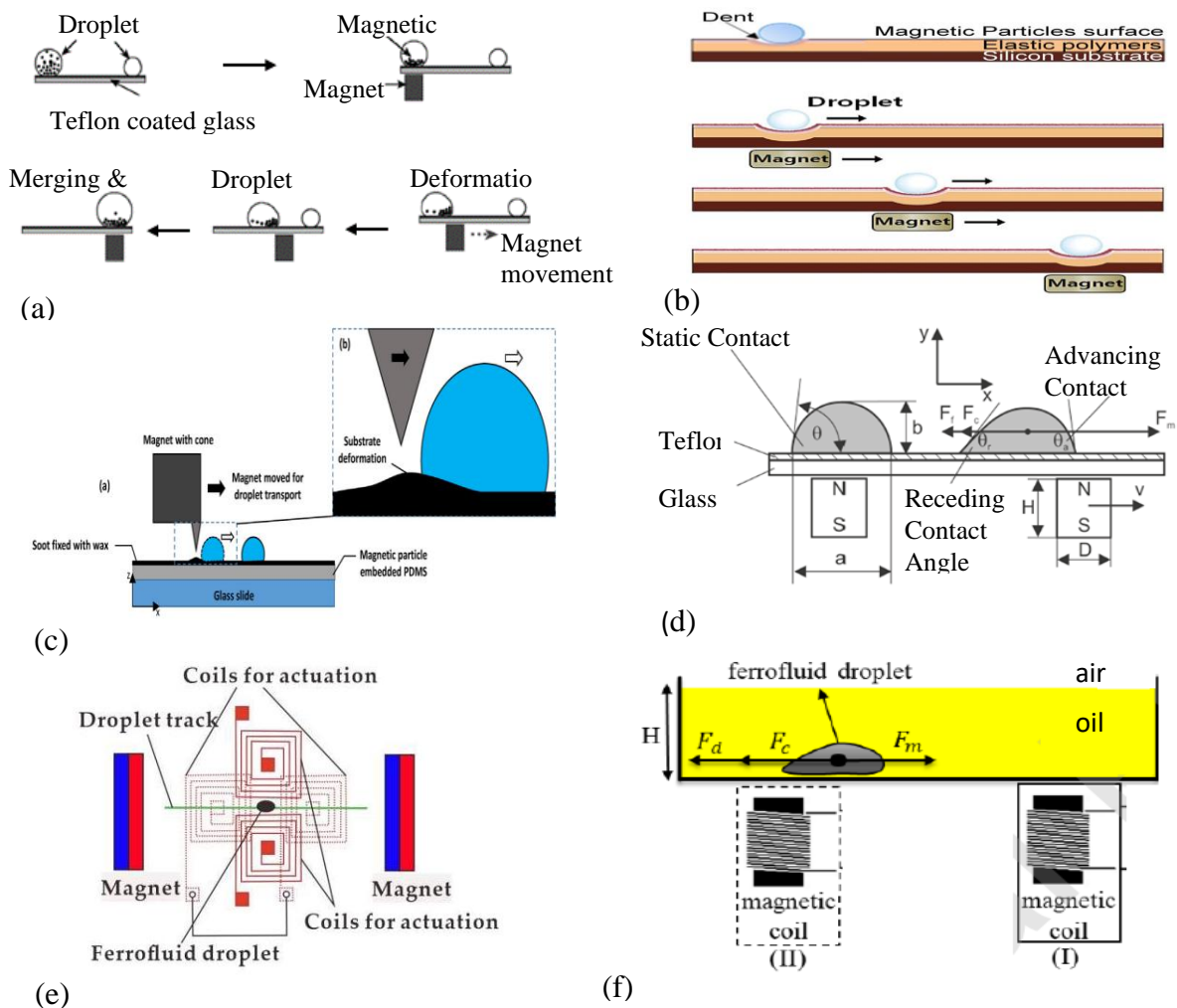


Figure 1.9: A few relevant scheme of open Surface Magnetic Digital Microfluidics: (a) Movement and merging of droplets containing magnetic particles by permanent magnet beneath a Teflon coated glass [186] (b) Droplet actuation approach on a magnetically deformable flexible substrate using permanent magnet [187] (c) Droplet movement on a (magnetic nanoparticles) MNP-embedded PDMS chip using a permanent magnet [189] (d) Schematics of experimental setup of a static and sliding water based ferrofluid droplet on a Teflon coated glass substrate [199] (e) Actuation of ferrofluid droplets using combination of permanent and electromagnetic fields [207] (f) Schematics of a fully immersed water-based ferrofluid droplet pull [213] Inset figures reproduced (a)[186] with permission from IOP Publishing (b) [187] and (d) [199] with permission from Elsevier (c) [189] with permission from Langmuir (e) [207] with permission from Royal Society of Chemistry (f) [213] with permission from Wiley and Sons

### **1.7.2. Electromagnets and their configuration**

Electromagnets are commonly used in digital microfluidics to manipulate and control the movement of droplets or particles within a microfluidic system. The configuration of the electromagnet can be either planar or vertical. In planar electromagnets, the coil is laid flat on a substrate, while in vertical electromagnets, the coil is wound around a vertical axis. Planar electromagnets are commonly used in digital microfluidics because they can be integrated with other components on a single substrate, which simplifies the fabrication process and reduces the overall cost. In digital microfluidics, the droplets are typically manipulated by changing the magnetic field around them. This can be accomplished by controlling the current flowing through the coil, which in turn changes the magnetic field strength and direction. By changing the magnetic field, it is possible to attract, repel, and move droplets along specific paths, enabling precise control over their movement. The configuration of the electromagnet used in digital microfluidics depends on the specific application and design requirements. Planar and vertical configurations both have their advantages and disadvantages, and the choice depends on factors such as the size of the droplets, the complexity of the device, and the required precision of the manipulation. In open surface Magnetic force-based droplet manipulation technique droplets can be conducted in a host fluid film or can be actuated on solid surface. In both techniques droplets are manipulated under the influence of external magnetic field.

### **1.7.3. Magnetic force-based droplet manipulation in host fluid film**

Magnetic force-based droplet manipulation in a host fluid film is a technique that implies the manipulation of small droplets of one liquid suspended in a thin film of another liquid using magnetic fields. The film of the host fluid is spread over a surface, and droplets containing magnetic nanoparticles are deposited on the film. The suspended droplets can be manipulated by applying an external magnetic field to the surface. The magnetic nanoparticles in the droplet align with the field, creating a magnetic moment in the droplet. This magnetic moment interacts with the external magnetic field and generates a force on the droplet, allowing it to be moved or positioned as desired. Confined droplets in a thin film limit its drive in the vertical direction and allows more precise control over the droplet's position and movement. Additionally, the host fluid film can be planned to have

specific properties, such as viscosity or surface tension, which can be used to control the droplet's behavior. It provides a versatile and powerful tool for manipulating small droplets in a controlled and precise manner. This technique has applications in microfluidics, lab-on-a-chip systems, and biomedical engineering. This provides a more flexible and versatile approach to droplet manipulation and enables the creation of complex droplet patterns.

#### **1.7.4. Magnetic force-based droplet manipulation on solid substrate**

This technique is used to manipulate and control the movement of droplets on a surface using magnetic fields. This method is particularly useful in microfluidic systems and lab-on-a-chip devices, where precise control over droplet position and movement is critical. Here droplets can be functionalized with magnetic nanoparticles, which can be manipulated using external magnetic fields. By controlling the direction and strength of the magnetic field generated by an electromagnet or a permanent magnet, the droplets can be controlled to direct at specific locations on the substrate, merged, or split into smaller droplets. The advantages of magnetic force-based droplet manipulation on a solid substrate include high precision and repeatability, as well as the ability to manipulate droplets non-invasively without the need for direct contact with the droplets or substrate. Additionally, the technique is relatively simple to implement and does not require complex microfabrication processes.

#### **1.8. Research gaps**

Magnetic digital microfluidics is a relatively new and emerging field that combines digital microfluidics and magnetic actuation to control the movement of droplets in small volumes. It is a promising technology for various applications, including lab-on-a-chip devices, point-of-care diagnostics and drug discovery. While there has been some notable prior work around contact-less manipulation of magnetically polarizable liquids on open-surface microfluidic platform, the state-of-art is still far from the stage of commercial implementation, and there are definite gaps that need to be addressed for its continued development and field-deployment of the technology. Identified gaps are as follows:-

1. One of the major gap is that relatively simple mode of droplet manipulation that is achieved. For example, the works reported in Ref [186,187,199,211] have primarily

demonstrated field-induced droplet movement on open surface platforms along a straight line only.

2. There are again very few reports [78,207] where droplets are manipulated along a more complicated, predesignated path.

3. The chip real estate and magnetic circuitry deployed for most of the existing magnetic micro-manipulators are custom designed for only one specific purpose. For widespread practical usage, it is imperative that the chip design has high operational flexibility.

4. It is necessary for MDMF to manage the expanding complication of bioassays where multiple reactions can be carried out in parallel for high-throughput analysis. Therefore, multiple droplets must be manipulated simultaneously.

5. Although some earlier works demonstrated parallel magnetic droplet manipulation where droplets move along a single path. [214, 215] those did not strive to tackle more complex manipulation like multiplexing, merging, and sorting of discrete droplets.

6. Another major gap in the existing on-chip droplet manipulation strategies is the lack of configurability in terms of droplet manipulation. Existing works in literature have shown proven capabilities of dedicated transport but have not demonstrated the ability of changing the transport on-the-go, and transport reversibility. MDMF reported in the literature have shown great potential for automation, but still, it is required to improve control and accuracy for point-of-care diagnostics in low-resource settings.

## **1.9. Intent and objective of present work**

Considering the aforementioned gaps in the literature, the present study attempts to identify a versatile design of droplet actuation on surface microfluidic platform with more precise control over droplet movement and positioning. In this study, two adaptable magnetic force-based droplet manipulation strategies have been proposed using an array of planar electromagnetic micro coils embedded in a substrate. The first approach presents a proof-of-concept demonstration of transporting microliter-size, oil-based ferrofluid droplets over a thin aqueous film on a flat substrate under the spatiotemporal distribution of magnetic field produced by a substrate-embedded circular micro coil. Subsequently, a numerical model is presented to describe the directional transport of the ferrofluid droplets on the liquid film overlaying the substrate using sequentially switched double stranded array of



electromagnetic micro-coils. Influence of the salient design and operating parameters like coil current, ferrofluid droplet size and magnetizing current, fluid viscosities, etc. are also studied. Ferrofluid droplet transport time over the length of the active substrate is characterized in terms of a group variable that can serve as the basis of a general design criterion for similar ferrofluid droplet-based micro-manipulation devices.

In the second approach two distinct transport models are discussed where cap volume ferrofluid droplet manipulated on solid surface. In the first transport model an array of double layer electromagnetic micro-coils is used to actuate a cap volume ferrofluid droplet in a rectilinear path on a solid substrate. Like the previous case, a sequentially switched array of electromagnetic micro-coils is used to generate a spatio-temporal distribution of magnetic field that steers the ferrofluid droplet on the surface. A square coil with different orientation and dimension is used to get better packing density (minimizing the dead space between the neighbouring coils). The second transport model demonstrates exclusive two-dimensional droplet manipulations such as multiple droplets sorting, sequential merging as well as pooling on a solid hydrophobic surface by sequentially switched array of 31 square-shaped electromagnetic micro-coils. A numerical model is proposed to analyze controlled manipulation of spherical cap ferrofluid droplets on a solid substrate. This numerical model is used to analyze the behavior of droplets under various external factor such as magnetic field strength, surface frictional drag, droplet size and contact angle hysteresis and help to design of optimal experimental conditions for droplet manipulation. It can be used to predict the movement and positioning of the droplets and to optimize the magnetic field parameters to achieve desired droplet operations such as sorting, merging, and pooling. A concept of spherical cap ferrofluid droplet sorting on a solid hydrophobic surface actuated by sequentially switched array of electromagnetic micro-coils is demonstrated. The technique of multiple droplets sequentially merging as well as pooling on solid hydrophobic substrate is also proposed. Such a type of transport in digital microfluidics offers a versatile platform for performing a wide range of chemical and biological assays with high precision and accuracy. Sequential merging of multiple droplets increases the volume of liquid that can be manipulated on the substrate where small volumes of liquid need to be combined or diluted. It enables the mixing of their contents to initiate a chemical reaction. By pooling droplets, it is possible to create a higher concentration of a particular

sample, or to combine different samples for analysis or reaction. Such droplets essentially remain as spherical cap volumes on a solid surface, with slight to moderate deformation in shape arising of contact angle hysteresis. The study reports the influence of the operating parameters like the coil current, droplet volume and contact angle hysteresis. Various microfluidic functions require different amount of reagent and sample volumes for specific functional objectives [216,217] which can be successfully achieved and precisely controlled by the present approach of polydisperse droplet-sorting on digital microfluidic platform. In the next paragraph, an overview of Digital Microfluidics (DMF) has been discussed in detail. The predicted motion of ferrofluid droplets offers possibility of on-chip handling of biochemically functionalized droplets for different microfluidic tasks.

Specific objectives of the current work is to

1. Develop a numerical model for magnetic manipulation of a ferrofluid droplet on an open surface digital microfluidic (OMDMF) platform deploying switchable array of embedded electromagnetic micro-coils. The theoretical model is capable of resolving different forces, e.g., magnetic, viscous, surface tension (contact pinning) while describing droplet manipulation on
  - i) a liquid film atop a solid substrate, and
  - ii) a hydrophobic solid substrate
2. Validate the models against benchmark experimental results
3. Describe the transport of a spherical-cap ferrofluid droplet on a liquid film atop a substrate and characterize the transport time in terms of the salient operating parameters, e.g., coil-current, droplet size, and host-fluid viscosity.
4. Describe the droplet transport and precise positioning on a hydrophobic solid platform using sequentially switchable array.
5. Describe complex droplet manipulations, e.g., sorting, merging and pooling using a versatile, configurable magnetic micro-coil array, and characterize the requisite switching sequences of the magnetic microcoils.

## **1.10.Exclusiveness and novelty of the work**

Based on literature reviews and identified research gaps, in this study certain exclusive methods are proposed for ferrofluid droplet manipulation by planar electromagnetic micro coil in magnetic digital microfluidics system. These offers several novel features and advantages compared to traditional microfluidic systems.

1. The use of ferrofluid droplets enables the manipulation of droplets using magnetic fields, which provides highly precise means of control.
2. Magnetic fields generated by planar electromagnetic micro coil, which can manipulate the droplets in a wide range of directions with high accuracy thereby enabling non-contact manipulation of ferrofluid droplets, minimizing the risk of contamination and damage to the droplets.
3. The planar electromagnetic micro coil facilitates high-speed manipulation of ferrofluid droplets, which is essential for applications such as droplet sorting and merging.
4. The planar electromagnetic micro coils can be promptly switched on and off for speedy movement and manipulation of the droplets. The use of ferrofluid droplets and the planar electromagnetic micro coils allow for manipulation at small scales, which is particularly useful for applications in microscale manufacturing, chemical analysis, and biological assays.
5. The arrays of planar electromagnetic micro coils are designed and operated in such a way that it provides real-time control and monitors the actuation of droplets with high operational flexibility.
6. The most glaring novelty of this study is configurability of planar electromagnetic micro coils arrays in terms of droplet manipulation. By adjusting coil geometry, orientation, magnetic field strength and coil switching droplets actuation speed, direction and droplet transport route can be controlled and even reconfigured to meet specific requirements.
7. This reconfigurable design enables manipulation of multiple droplets simultaneously, which is necessary to manage the expanding complication of bioassays where multiple reactions are required to be carried out in parallel for high-throughput analysis. This is one major novel attribute of the work.

8. This feature can improve the accuracy and efficiency of droplet manipulation and reduce the amount of time and resources needed for testing.

The abovementioned attributes underscores the exclusiveness and novelty of the current work.

## **Chapter 2: Theoretical Formulation**

This chapter describes the physical arrangement of planar micro-coil array, the magnetic field produced by the coils as current flow through them, magnetic force created by the magnetic field on magnetic fluid droplets and the ensuring ferrofluid droplet transport equations that are complied. As already mentioned in the previous section the physical arrangement comprises an array of microfluidic chip embedded electromagnetic coil which are energized appropriately to produce a directional transport to individual droplets in a predetermined fashion. Configurations of the magnetic coils play an important role in creating droplet manipulation in digital microfluidic platform and thereby require special attention.

### **2.1. Specification of planar coils and coil array**

The configuration of micro coils is an important issue in magnetic digital microfluidics because it directly affects the magnetic field generated and, therefore, the ability to manipulate droplets. The strength and directionality of the magnetic field is important because it affects the force exerted on the droplets and the ability to manipulate the droplets in specific directions and patterns. Furthermore, the configuration of micro coils can also impact the uniformity of the magnetic field generated. A non-uniform magnetic field can cause droplets to move in unpredictable directions, making it difficult to accurately manipulate droplets for various assays. A planar coil is a type of electromagnetic coil that is flat and has a square or circular shape. When a current passes through the coil, it generates a magnetic field that can be used to manipulate ferrofluid droplets. The magnetic field generated by a planar coil can be described by the Biot-Savart law, which states that the magnetic field at a point due to a current element is proportional to the current and inversely proportional to the distance from the point to the current element. When a ferrofluid droplet is placed in a magnetic field generated by a planar coil, it experiences a magnetic force due to the interaction between the magnetic moment of the droplet and the magnetic field. In this study three distinct strategy have been proposed where in all approach square coils of different specifications and corresponding arrays are employed to manipulate ferrofluid droplets. Square coils are chosen over the traditional circular coils as the former provide the greater packing, allowing minimum gap between two adjacent coils. An array of

circular coils would have left empty spaces between coils that do not contribute to the magnetic field.

**1<sup>st</sup> Transport model:** Figure 2.1(a) shows the arrangement of a planar square coil of 10 mm×10 mm size in a double-stranded array. Ten coils are placed under an 18 mm×60 mm flat substrate (dimension typical of a microfluidic chip) on which a thin (2mm) film of aqueous solution renders mobility of the ferrofluid droplet. Figure 2.1 (b) shows a single square coil with detailed specifications while the inset (upper left corner) shows a cross-section view of the bottom substrate, embedded conductors under the substrate, the overlaying liquid film on top. Each square spiral consists of 6 turns of conductors at 800 μm pitch. The conductors have 800 μm × 800 μm square cross section. Each conductor of the planar coils is considered as composed of a bundle of 5×3 slender of current-carrying wires (see the inset (lower left corner) of Figure 2.1 (b)). This array of electromagnetic micro-coils is employed to manipulate ferrofluid droplets over a thin aqueous film (at AA´ plane, see figure 2.1(c)) on a flat substrate at. The micro-coils array embedded under the substrate to generate a field required to actuate droplets.

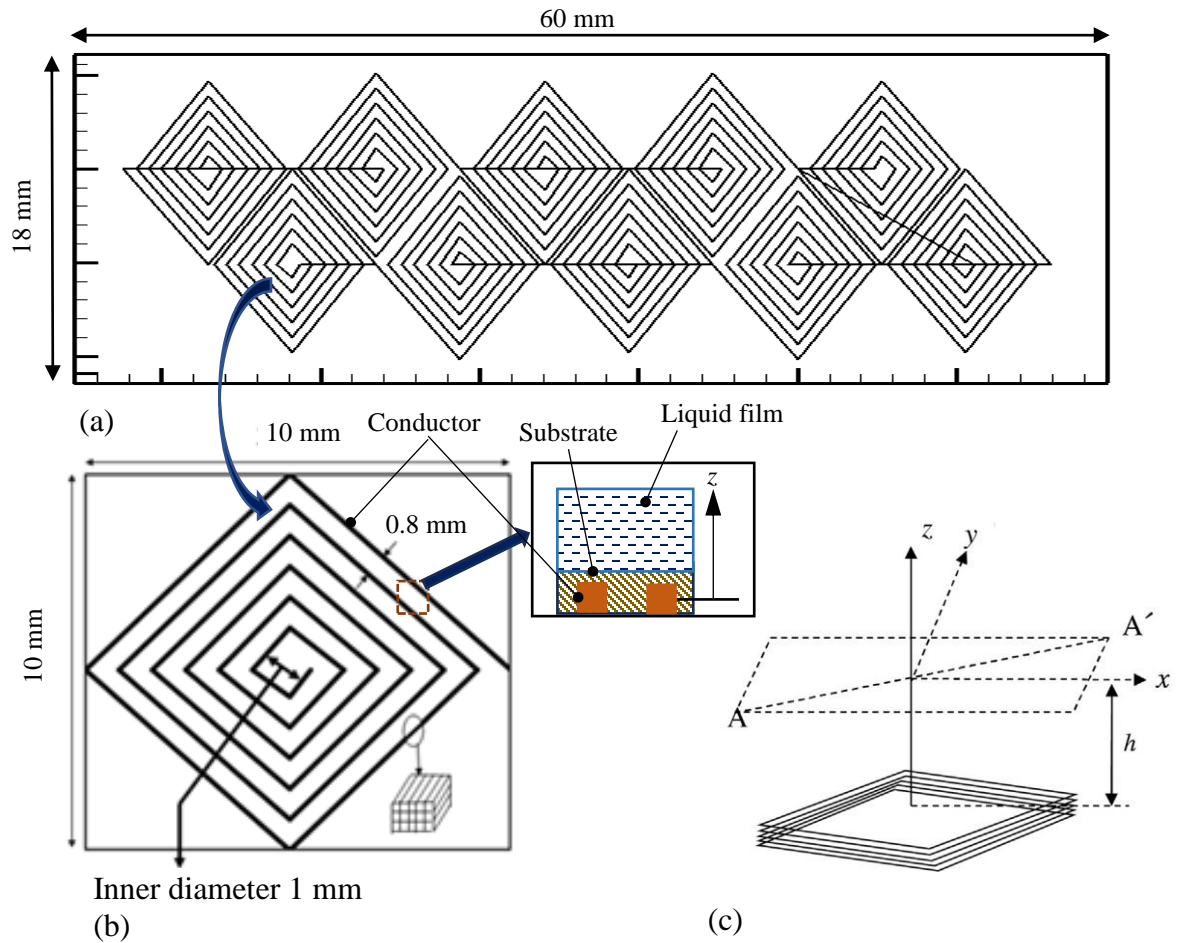


Figure 2.1: Arrangements of planar square coil (First transport model): (a) Array of the square coils arranged in double row (b) A single coil (coil subsequent array shown in Figure 2.1(a)) is shown with its specifications. (c) Schematic arrangement showing the relative positions of the coil and the AA' plane

**2<sup>nd</sup> Transport model:** Figure 2.2(a) shows the arrangement of double-layer planar square coils of two different size (six 20 mm<sup>2</sup> square coil in lower layer and six 10 mm<sup>2</sup> square coils in upper layer) in a two stranded array of 12 coils (Typical dimension of a stranded array is 40 mm × 60 mm) fabricated on a flat PDMS substrate of 50 mm × 70 mm. The smaller coils are positioned in the upper tier accurately in between two larger coils (20 mm<sup>2</sup>) which act as a booster-field to accelerate the droplets as they pass over one coil to the other. The two layers of coils are separated by an insulating layer of 350 μm thickness (see figure 2.2(d)).

The substrate can be assembled in two layers –the lower portion may be built from a soft polymeric material (e.g., a polydimethylsiloxane or PDMS) in which the millimetric-scale electromagnet coil may be set in. A thin ( $\sim 2000 \mu\text{m}$ ) layer of the identical substrate material may be placed atop the coil to provide electrical insulation. Lastly, a coating of a hydrophobic (HPB) material, such as Teflon AF or a fluoroalkylsilane, is positioned atop the upper layer. The hydrophobic coating is meant to offer nominal droplet pinning (e.g., a low contact angle hysteresis), permitting the droplet actuation with lowest restraining force. Figure 2.2 (b) and Figure 2.1 (e) show the smaller and larger square coils of with detail specification respectively. Each square spiral consists of 12 turns of conductors at  $500 \mu\text{m}$  pitch. The conductors have  $500 \mu\text{m} \times 500 \mu\text{m}$  square cross section. This array of double-layer planar square coils fabricated on a flat PDMS substrate and used for controlled manipulation of spherical cap ferrofluid droplets on a solid substrate. Figure 2.2 (c) symbolizes zoomed in image from a specific section of four conductors (two conductors from lower tire and two from upper tire as shown in in figure) from the two tire array of planar coils. Figure 2.2(d) indicates a cross-section view of the bottom substrate, embedded two tire conductors, insulating layer between two layer of array, the overlaying substrate and the HPB coating on top.



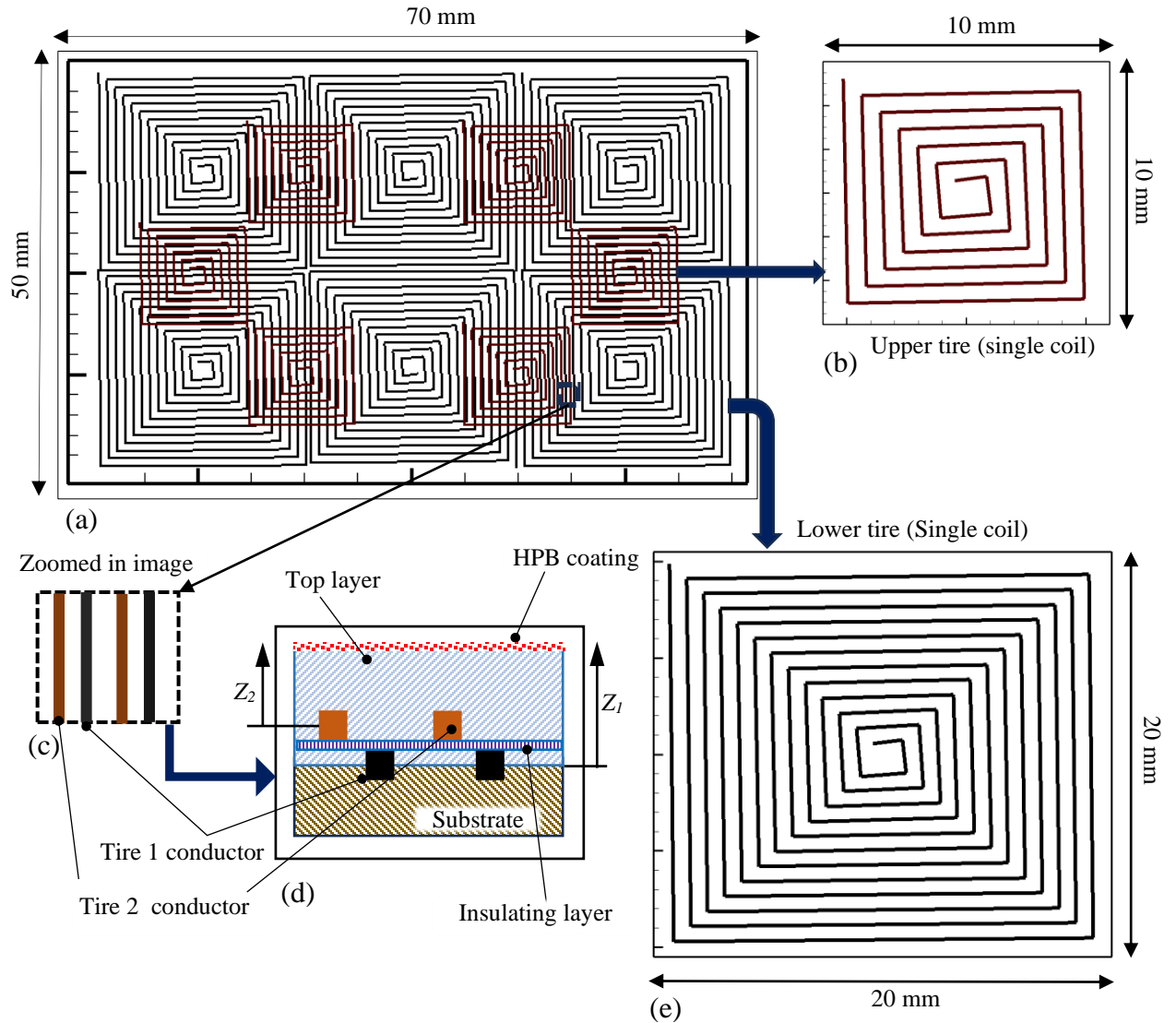


Figure 2.2: Arrangements of planar square coil (Second transport model): (a) Arrangement of double layer planar square coil (number of coils are 12) (b) and (e): Distinct coil specification of smaller coil (upper tire 10 mm×10 mm) and larger coil (lower tire 20 mm×20 mm) respectively. (c) Zoomed in image of four conductors from the two tire array of planar coils. (d) A cross-section view of the bottom substrate, embedded two tire conductors (two conductors from lower tire and two from upper tire as shown in figure (c)), insulating layer between two layer of array, the overlaying substrate and the HPB coating on top

**3<sup>rd</sup> Transport model:** Fig 2.3 (a) shows the schematic arrangement of 31 planar square coils of 15 mm×15 mm size, embedded in a 60 mm×150 mm substrate in an array of five rows – having 5, 6, 9, 6 and 5 coils, respectively. The substrate may, in reality, be fabricated in two layers – the lower section may be made from a soft polymeric material (e.g., a polydimethylsiloxane or PDMS) in which the millimetric-scale electromagnet coil may be embedded. A thin (~ 2000 μm) layer of the same substrate material may be deposited atop the coil to provide electrical insulation. Finally, a coating of a hydrophobic (HPB) material, such as Teflon AF or a fluoroalkylsilane, is laid atop the upper layer (Fig 2.3 (c) shows a 3-d rendering of the coil array embedded in the substrate). The hydrophobic coating is meant to offer minimal droplet pinning (e.g., a low contact angle hysteresis), allowing the droplet actuation with minimum restraining force. Fig 2.3 (b) shows a single square coil with detailed specification, while the inset shows a cross-section view of the bottom substrate, embedded conductors, the overlaying substrate and the HPB coating on top. Each square spiral consists of 12 turns of conductor at 500 μm pitch. The conductors have 500 μm × 500 μm square cross section.

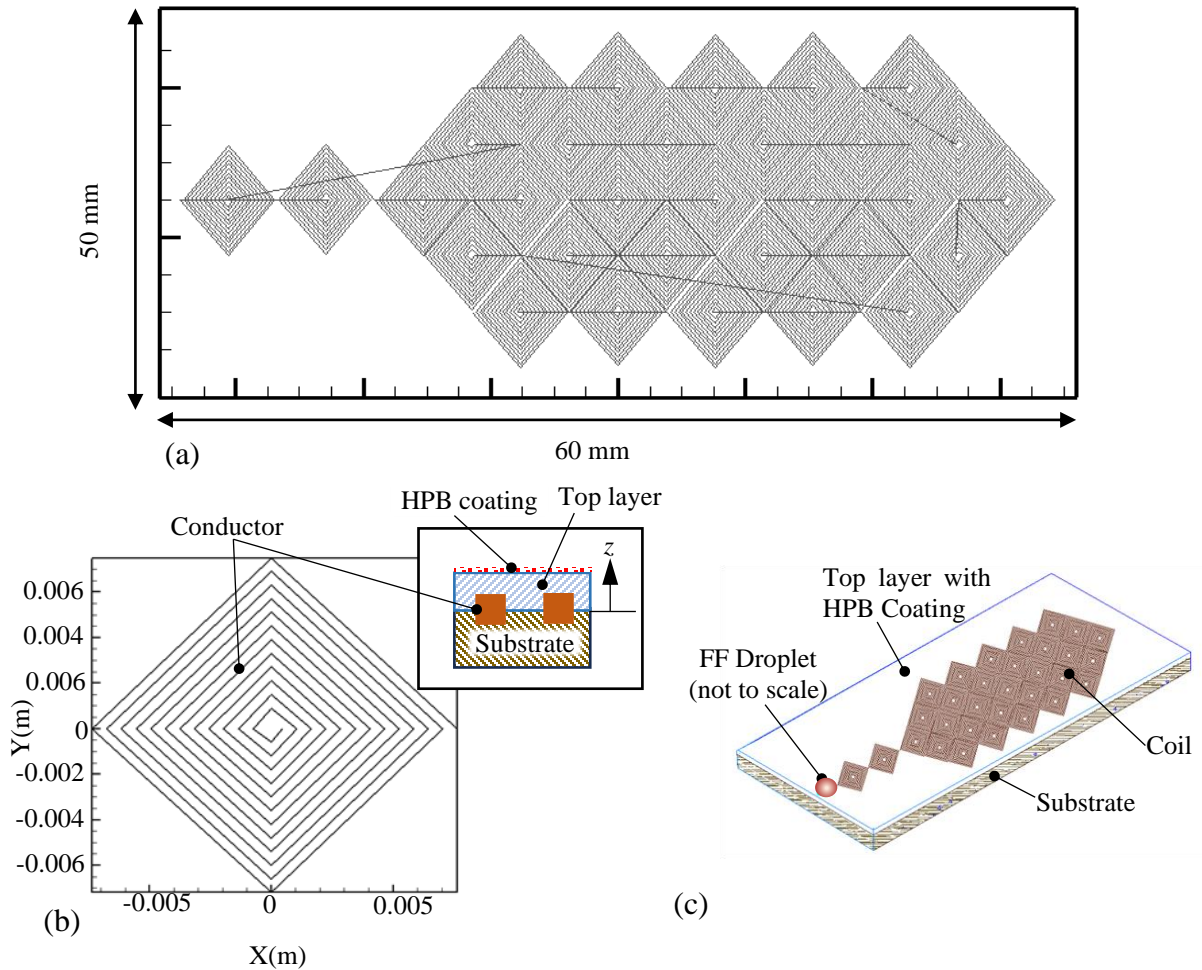


Figure 2.3: Arrangements of planar square coil (Third transport model): (a) Arrangement of a 31 planar square coil of 15 mm×15 mm size in a five stranded array with their coil number (b) Structure of the stranded array fabricated on a flat solid substrate (c) Single square coil structure with detailed specification; inset shows a cross-section view of the bottom substrate, embedded conductors, the overlaying substrate and the hydrophobic (HPB) coating on top

## 2.2. Magnetic field due to planar micro-coil

The Biot-Savart law [218] can be used to calculate the magnetic field produced by a current-carrying wire at a given point in space. In this study the planar microcoils are flat, square loop of wire, and the magnetic field can be calculated following the approach of Santra et al. [219] for each slender conductor segment in a coil and then by superposing the resulting fields.

### 2.2.1. Computation of magnetic field due to current through a loop

Figure 2.2 shows a single conductor segment of the coil placed in x-y plane. The magnetic field at a point P in the 3-D space for a single conductor can be calculated using the Biot Savart Law as

$$\vec{B} = \frac{\mu_0 I}{4\pi s} (\sin \varphi_2 - \sin \varphi_1) \hat{e} \quad (2)$$

The coordinates of endpoints of the conductors are known from the geometry and the orientation of the coil. The coordinate of the point  $P$  is an input parameter, where the field is to be measured. To determine the sine component of the initial and final angle  $\Phi_1$  and  $\Phi_2$  the lengths:  $D_{st}$ ,  $D_{nd}$  and  $P_{ln}$  are calculated from the geometry (see Figure 2.2).  $P_{ln}$  is the distance between the point  $P$  and the conductor (extended) which is mentioned as 's' in the Equation (2). Thus, after determining all the required distances, Equation (2) is applied to find the magnetic field of a single conductor segment. In a similar manner the magnetic field at point P for all the conductors in the x-y plane can be calculated. And then the superposition of the magnetic fields of all these segments results in the total magnetic field of the coil. Thus, for every point in the 3-D space the total magnetic field can be calculated for the planar spiral coil using a simple coordinate geometry and application of Biot-Savart's Law.

### 2.3. Magnetic force due to current carrying planar microcoil

The information of the local magnetic force field is important for predicting the magnetic manipulation of the microliter volume ferrofluid droplet. Considering each ferrofluid droplet to have homogeneous magnetization  $M$  induced due to an imposed field  $H$ , the magnetic force on such a droplet within the magnetic field is calculated from the general expression [219]

$$\vec{F}_{mag} = \mu_0 \int (M \cdot \nabla) H d^3r \quad (3)$$

The integral is taken over the volume of the magnetic object (the ferrofluid droplet is spherical for simplicity, irrespective of the magnetic field), and  $H$  is the magnetic field at the droplet center. In Eq. (3),  $H$  denotes the field in the absence of the magnetic object, i.e.,

it does not consider the demagnetization effect caused by the magnetic material due to magnetic polarization. To account for the demagnetization effect for a spherical droplet in a homogeneous magnetizing field, the magnetization  $M$  inside the bead is given by [220]

$$\chi_m = \frac{\chi_i}{\chi_i/3+1} = 3 \frac{\mu_r-1}{\mu_r+2} H \quad (4)$$

Where  $\chi_i$  the intrinsic susceptibility of the magnetic bead material is  $\chi_m$  the measured susceptibility of a single magnetic bead including demagnetization effects, and  $\mu_r = 1 + \chi_i$  is the relative permeability of the magnetic bead material. Substituting Eq. (4) in Eq. (3) and getting the force equation [219].

$$F_{mag} = \mu_0 \int (M \cdot \nabla) H d^3r = \mu_0 3 \frac{\mu_r-1}{\mu_r+2} \int (H \cdot \nabla) H d^3r \approx \frac{1}{2} \mu_0 V_{FF} \chi_m \nabla (|H|^2) \quad (5)$$

It is assumed that the integrand is constant over the volume  $V_{FF}$  of ferrofluid droplet with radius  $R_{FF}$  (valid for a very small drop size, such that the local field is almost constant over the entire volume of the droplet), and that  $H$  is curl free (since there are no free currents outside the copper coils).

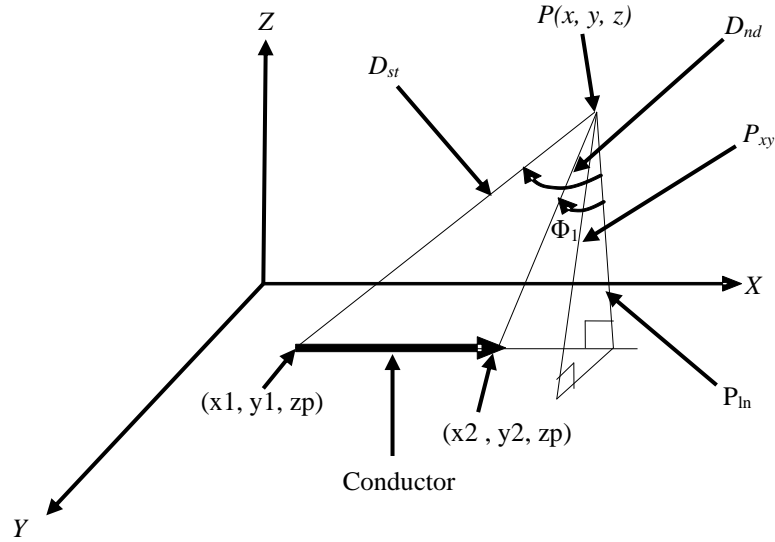


Figure 2.4: Geometrical configuration for calculation of the magnetic field due to a current carrying segment of conductor

## **2.4. Droplet transport model on open surface microfluidic platform**

This section illustrates the droplet transport model on an open surface magnetic digital microfluidic platform using electromagnetic micro coils. These micro coils generate localized magnetic fields that interact with magnetic particles within the droplets, enabling their manipulation and transport both within a liquid film and on a solid surface. This transport model is used to analyze the behavior of droplets under various external factors such as magnetic field strength, surface frictional drag, droplet size and contact angle hysteresis and help to design of optimal experimental conditions for droplet manipulation. It can be used to predict the movement and positioning of the droplets and to optimize the magnetic field parameters to achieve desired droplet operations such as sorting, merging, and pooling. In the case of a liquid film-based open surface magnetic digital microfluidic platform an array of electromagnetic micro coils is positioned beneath the liquid film. The liquid film acts as a medium for droplet transport, while the magnetic fields generated by micro coils control the movement of the droplets. This manipulation enables precise control over the position and movement of the droplets on the liquid film. In the case of a solid surface-based open surface magnetic digital microfluidic platform, electromagnetic micro coils are integrated into the surface. These micro coils generate localized magnetic fields that interact with the magnetic particles within the droplets, facilitating their manipulation and transport.

### **2.4.1. Droplet transport model within liquid film**

In this study the ferrofluid droplets stably floating on the aqueous film have been considered spherical droplets. The droplet creates a curvature on the water surface due to the mutual interaction of the ferrofluid and water surfaces (see the inset of Figure 2.3) which produces a net vertical contact force component  $F_s$  balancing the apparent weight  $W_a$  of the droplet and the vertical component of magnetic force  $F_{mz}$ . It has also been observed during experiment that the droplets remained afloat irrespective of the vertical component of the magnetic force (i.e., there is no appreciable droplet motion in the  $z$ -direction) for the entire course of manipulation.  $F_{mx}$  and  $F_{my}$  are the  $x$  and  $y$  components of magnetic force which produces a net acceleration of the ferrofluid droplet. As the droplet starts to move on the  $x$ -

y plane on the aqueous surface, a resistive fluidic drag  $D$  acts against the direction of motion.

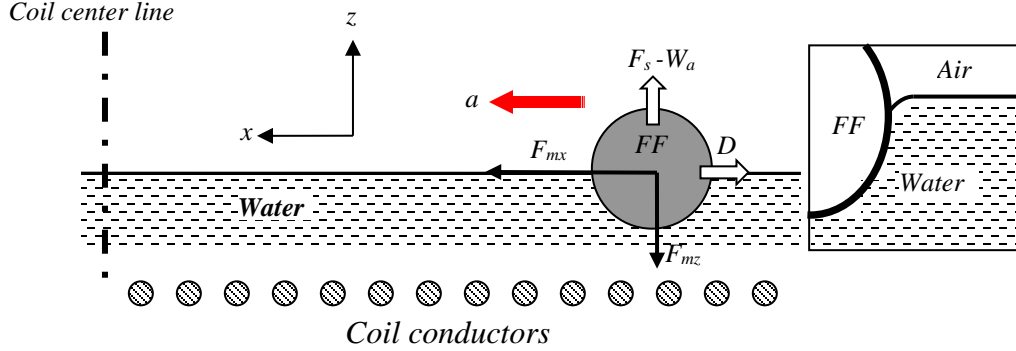


Figure 2.5: Forces on a ferrofluid droplet (FF), half-immersed at the surface of water.  $D$  denotes the fluid drag and  $F_s$  denotes vertical contact forces due the surface tension at the water-air-ferrofluid contact line (inset),  $W_a$  denotes the apparent weight (i.e., weight minus the buoyancy force) of a droplet

The equations of motion for the droplet of mass  $m_{FF}$  in terms of the  $x$  and  $y$  components are obtained by balancing the net unbalanced forces with the inertial one (the product of mass and acceleration), i.e.,

$$m_{FF} \frac{d^2x}{dt^2} = F_m(x, y, z) \hat{e}_x + D \quad (6)$$

$$m_{FF} \frac{d^2y}{dt^2} = F_m(x, y, z) \hat{e}_y + D \quad (7)$$

Along the  $z$  axis, it is assumed that the surface tension-induced reaction force can nullify the  $z$  component of magnetic force and the buoyancy force, i.e.

$$0 = F_s - F_m(x, y, z) \cdot \hat{e}_z - W_a \quad (8)$$

where  $W_a$  denotes the apparent weight (i.e., weight minus the buoyancy force) of the ferrofluid droplet. Clearly, the pertinent equations of motion for this case are only the Eqs. (6) and not (7), as the droplet does not exhibit any  $z$ -directional movement. The drag force on a fully immersed ferrofluid sphere of viscosity  $\eta_{FF}$  moving with a velocity  $U$  through another stationary fluid of viscosity  $\eta$  is obtained considering Stokes flow regime for the

droplets [221,222] (an assumption that is valid considering the extremely small size and velocity scales involved, so that  $Re = 2\rho UR_{FF}/\eta < 1$ ), so that

$$D_{sphere} = -2\pi R_{FF}\eta U \left( \frac{2+3\zeta}{1+\zeta} \right) \quad (9)$$

where,  $\zeta = \eta_{FF}/\eta$  Considering the ferrofluid droplet to be half-immersed, the drag force  $D$  is equal to half of  $D_{sphere}$  as predicted by Eq. (9).

Here  $U$  is the droplet velocity which consider  $dx/dt$  and  $dy/dt$  along  $x$  axis and  $y$  axis respectively and the Eq. (6) and (7) they can be written as:

$$m_{FF} \frac{d^2x}{dt^2} + \pi R_{FF}\eta U \left( \frac{2+3\zeta}{1+\zeta} \right) \frac{dx}{dt} - F_m(x, y, z) \hat{e}_x = 0 \quad (10)$$

$$m_{FF} \frac{d^2y}{dt^2} + \pi R_{FF}\eta U \left( \frac{2+3\zeta}{1+\zeta} \right) \frac{dy}{dt} - F_m(x, y, z) \hat{e}_y = 0 \quad (11)$$

Now the  $x$  and  $y$  components of magnetic force on a ferrofluid droplet from Eq. (5) are:

$$F_{mx} = \mu_0 \frac{4}{3} \pi R_{FF}^3 \chi_m \frac{\partial}{\partial x} \left( \frac{1}{2} H^2 \right) \quad \text{and} \quad F_{my} = \mu_0 \frac{4}{3} \pi R_{FF}^3 \chi_m \frac{\partial}{\partial y} \left( \frac{1}{2} H^2 \right)$$

So, Eq. (10) and (11) can be written as in following forms:

$$\frac{4}{3} \pi R_{FF}^3 \rho_{FF} \frac{d^2x}{dt^2} + \pi R_{FF}\eta \left( \frac{2+3\zeta}{1+\zeta} \right) \frac{dx}{dt} - \mu_0 \frac{4}{3} \pi R_{FF}^3 \chi_m \frac{\partial}{\partial x} \left( \frac{1}{2} H^2 \right) = 0 \quad (12)$$

$$\frac{4}{3} \pi R_{FF}^3 \rho_{FF} \frac{d^2y}{dt^2} + \pi R_{FF}\eta \left( \frac{2+3\zeta}{1+\zeta} \right) \frac{dy}{dt} - \mu_0 \frac{4}{3} \pi R_{FF}^3 \chi_m \frac{\partial}{\partial y} \left( \frac{1}{2} H^2 \right) = 0 \quad (13)$$

Thus, the equations of motion of the ferrofluid droplets (Eq. (12) and (13)) assume the following forms:

$$\frac{d^2x}{dt^2} + \frac{3}{4} \left( \frac{2+3\zeta}{1+\zeta} \right) \frac{\eta}{R_{FF}^2 \rho_{FF}} \frac{dx}{dt} - \frac{\mu_0 \chi_m}{\rho_{FF}} f(x) \mu_0 \frac{4}{3} \pi R_{FF}^3 \chi_m \frac{\partial}{\partial x} \left( \frac{1}{2} H^2 \right) = 0 \quad (14)$$

$$\frac{d^2y}{dt^2} + \frac{3}{4} \left( \frac{2+3\zeta}{1+\zeta} \right) \frac{\eta}{R_{FF}^2 \rho_{FF}} \frac{dy}{dt} - \frac{\mu_0 \chi_m}{\rho_{FF}} f(y) \mu_0 \frac{4}{3} \pi R_{FF}^3 \chi_m \frac{\partial}{\partial y} \left( \frac{1}{2} H^2 \right) = 0 \quad (15)$$

Here  $f(x) = \frac{\partial}{\partial x} \left( \frac{1}{2} H^2 \right)$  and  $f(y) = \frac{\partial}{\partial y} \left( \frac{1}{2} H^2 \right)$  are derived from the computed magnetic field profile (see Section 2.2) using central differencing finite difference approximation



[219]. Equations (14) & (15) are second order ordinary differential equations, which are solved with initial conditions of stationary droplet at the point of their release, i.e., at  $t = 0$ ,  $x = x_0$  and  $dx/dt=0$  for Eq. (14),  $y = y_0$  and  $dy/dt=0$  for Eq. (15). The locus of a ferrofluid droplet is obtained from numerical integration of Eqs. (14) and (15) using an explicit Euler integration method [223]. The time step of the integration is chosen so that the droplet does not travel more than  $1/100^{\text{th}}$  of its diameter in a single time step to accurately simulate the motion of a droplet and ensure stability in simulations.

#### 2.4.2. Droplet transport model on solid surface

The transport of the droplet on the solid surface can be modeled using a combination of resistive surface frictional drag, contact angle hysteresis, and the magnetic force acting on the droplet. The droplet will move along the surface in response to the magnetic force, with the direction and speed of motion depending on the strength and direction of the magnetic field. In this study spherical cap ferrofluid droplets are assumed to move on a solid hydrophobic surface under actuation of magnetic force generated by planar electromagnet coil (shown in set of Figure 2.4). Here a resistive surface frictional drag and contact angle hysteresis force act against the droplet motion.  $F_{Mag(x,y)}$  is the x and y components of magnetic force which produces a net acceleration of the ferrofluid droplet against opposing forces. As the droplet starts to move on the x-y plane on the solid hydrophobic surface, a resistive friction  $F_{n(x,y)}$  acts against the direction of motion along with another resistive force due to contact angle hysteresis  $F_{hyst(x,y)}$ . The equation of motion for the spherical cap ferrofluid droplet of mass  $m_{FF}$  in the x-y plane on a solid surface is obtained by balancing the net unbalanced forces due to frictional drag and contact angle hysteresis, i.e.,

$$m_{FF} \frac{d^2 S}{dt^2} = F_{mag(x,y)} - F_{hyst(x,y)} - F_{n(x,y)} \quad (16)$$

Where  $m_{FF}$  and  $S$  denote the mass and position vector of spherical cap ferrofluid droplet on the x-y plane respectively.

Mass of the droplet  $m_{FF} = V_{sd} \rho$ , where  $\rho$  is the density of droplet and  $V_{sd}$  is the volume of spherical cap ferrofluid droplet at rest or equilibrium condition is [154] (without effect of contact angle hysteresis).

$$V_{sd} = \frac{\pi D^3}{24} \left( \frac{2-3 \cos \theta + \cos^3 \theta}{\sin^3 \theta} \right) \quad (17)$$

Where  $D$  is the diameter of circular footprint of the spherical cap droplet and  $h$  is the height of droplet. Droplet equilibrium contact angle is  $\theta$ . The volume of asymmetrical spherical cap ferrofluid droplet sliding on a solid substrate due to an external force (with effect of contact angle hysteresis) is discussed in Appendix A1.

Resistive frictional drag on the spherical cap ferrofluid droplet acting against the sliding motion on solid hydrophobic surface can be obtained. This frictional drag determined by the following equation [ 224] is:

$$\text{Frictional drag } F_n = 3\eta_{FF}\pi r U \int_{x_{min}}^{x_{max}} \frac{dx}{\xi(x)} \quad (18)$$

Where  $\eta_{FF}$  and  $r$  are the viscosity and foot-print radius of the cap volume droplet respectively. Where  $U = dS/dt$  represents velocity of the droplet in  $x$ - $y$  plane.

$\xi(x) = 0.5(-2R \cos \theta + \sqrt{(2R \cos \theta)^2 - 4(x^2 - 2x \sin \theta)})$  (See details in Appendix A2)

$$\xi(x) = 0.5(-2R \cos \theta + \sqrt{(2R \cos \theta)^2 - 4(x^2 - 2xR \sin \theta)})$$

The upper limit  $x_{max}$  of integration on the right-hand side of Equation 18 arises from the physical length-scale of the droplet, so that  $x_{max} = D$  (the foot-print diameter of the spherical cap droplet). The lower limit  $x_{min} = 10^{-9}$  mm [224] is of the order of molecular length scale [225]. Physically consistent quantitative values of this lower length-scale obtained from molecular dynamic simulations [226] also conforms closely with this value.

The effect of Contact Angle Hysteresis is an important issue in digital microfluidics for successful droplet manipulation. This can be achieved through careful selection of surface materials and surface modification techniques. By minimizing contact angle hysteresis, digital microfluidic systems can achieve more precise and reliable droplet manipulation, which is critical for a wide range of applications. For a liquid drop resting on a flat, horizontal solid surface, the static contact angle is defined as the angle formed by the intersection of the liquid-solid interface and the liquid-vapor interface ( $\theta_m$ ). The interface where solid, liquid, and vapor co inside is referred to as the “three phase contact line”. If

the three-phase contact line is in actual motion, the contact angle produced is called a “dynamic” contact angle [151]. In particular, the contact angles formed by expanding and contracting the liquid are referred to as the advancing contact angle  $\theta_A$  and the receding contact angle  $\theta_R$ , respectively. Contact angle hysteresis is defined as difference in advancing contact angle  $\theta_A$  and the receding contact angle  $\theta_R$  although the term also used to describe the expression  $(\cos \theta_R - \cos \theta_A)$  [152]. Several numerical studies proposed to predict droplet profile and motion on an inclined plane under the action of a gravitational force, the advancing and receding contact angles for different droplet sizes and surface inclinations. Eisherbini et al. experimentally described the geometric shapes of liquid drops on vertical and inclined plane surfaces [153]. The retentive force due to the contact angle hysteresis is given by

$$F_{hyst} = \gamma_{lv} R k (\cos \theta_R - \cos \theta_A) \quad (19)$$

Where  $k$  is a constant,  $\gamma_{lv}$  is the liquid–vapor surface tension, and  $R$  is a length scale taken as the equivalent radius of the droplet contour, as recommended in prior work of Eisherbini [154]. Initially when droplet velocity  $U = 0$  then both advancing and receding contact angle are equal to static contact angle ( $\theta_A = \theta_R = \theta_m$ ). Initially despite certain force applied to the droplet, it will not move although the advancing contact angle  $\theta_A$  and the receding contact angle  $\theta_R$  start varying ( $\theta_A$  increases and  $\theta_R$  decreases). The maximum force for the droplet about to start is called static contact angle hysteresis. As soon as the applied force conquered static contact angle hysteresis, droplets start moving and the difference  $(\theta_A - \theta_R)$  increases with increasing capillary number ( $Ca = \eta U / \gamma$ ), which denotes the ratio of viscous to surface tension force [227]. This hysteresis is called dynamic contact angle hysteresis. A combined molecular-hydrodynamic model [228] derived from a combination of hydrodynamic model [229, 230] and molecular kinetic model [231, 232] is used to calculate modified advancing contact angle  $\theta_A$  and the receding contact angle  $\theta_R$  for every new velocity,

$$\theta_A^3 = \left[ \cos^{-1} \left\{ \cos \theta_m - \frac{2k_B T}{\gamma_{lv} \lambda^2} \sinh^{-1} \left( \frac{U}{2k^0 \lambda} \right) \right\} \right]^3 + 9Ca \ln \left( \frac{L}{L_s} \right) \theta_A^3 =$$

$$\left[ \cos^{-1} \left\{ \cos \theta_m - \frac{2k_B T}{\gamma_{lv} \lambda^2} \sinh^{-1} \left( \frac{U}{2k^0 \lambda} \right) \right\} \right]^3 + 9Ca \ln \left( \frac{L}{L_s} \right) \quad (20)$$

$$\theta_R^3 = \left[ \cos^{-1} \left\{ \cos \theta_m + \frac{2k_B T}{\gamma_{lv} \lambda^2} \sinh^{-1} \left( \frac{U}{2k^0 \lambda} \right) \right\} \right]^3 - 9Ca \ln \left( \frac{L}{L_s} \right) \theta_R^3 = \left[ \cos^{-1} \left\{ \cos \theta_m + \frac{2k_B T}{\gamma_{lv} \lambda^2} \sinh^{-1} \left( \frac{U}{2k^0 \lambda} \right) \right\} \right]^3 - 9Ca \ln \left( \frac{L}{L_s} \right) \quad (21)$$

Where  $k_B$  is Boltzmann Constant,  $L$  is characteristic capillary length and  $L_s$  is the slip length,  $T$  is the absolute temperature. Here,  $k^0$  and  $\lambda$  are the fitting parameters. Now substituting all the forces in equation (4) can be reduces to

$$V_{sd} \rho \frac{d^2 S}{dt^2} = \frac{1}{2} \mu_0 V_{sd} \chi_m \nabla (|H^2|) - \gamma_{lv} R k (\cos \theta_R - \cos \theta_A) - 3\eta_{FF} \pi r U \int_{x_{min}}^{x_{max}} \frac{dx}{\xi(x)} \quad (22)$$

Rearranging, the equations of motion of the spherical cap ferrofluid droplets in following forms

$$\frac{d^2 S}{dt^2} = \frac{1}{2} \frac{\mu_0 \chi_m \nabla (|H^2|)}{\rho} - \frac{\gamma_{lv} R k}{V_{sd} \rho} (\cos \theta_R - \cos \theta_A) - \frac{3\eta_{FF} \pi r}{V_{sd} \rho} U \int_{x_{min}}^{x_{max}} \frac{dx}{\xi(x)} \quad (23)$$

Equation (23) is a second order ordinary differential equation for droplet position vector  $S$ , which is solved with initial condition of droplet released velocity at the point of their release, i.e., at  $t = 0$ ,  $U = U_0$ ,  $S = S_0$  and  $z = z_0$ . Here an explicit Euler integration method [223] is used to obtain the locus of this ferrofluid droplet from numerical integration of Eq. (22).

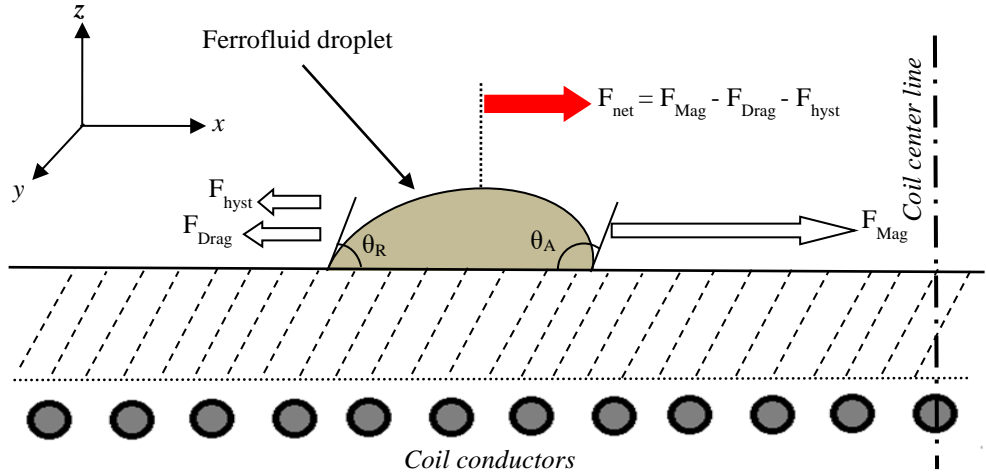


Figure 2.6: Forces model of a spherical cap ferrofluid droplets on a solid hydrophobic surface over planar electromagnet coil.  $F_{mag}$  denotes the magnetic force,  $F_n$  and  $F_{hyst}$  acts against the droplet motion representing resistive surface frictional drag and contact angle hysteresis force respectively

All over this chapter the theoretical formulation of different transport models used in this study along with the design of planar coil and coil array and its magnetic field computation are described. Objective equations of droplet transport models are also derived. Now it is important to focus on the field plot of different coil in the coil array, the motion of ferrofluid droplets and its trajectories and validation of mentioned transport models. Next chapter describes all the mentioned issues along with effect of different driving parameters on time of flight of droplets of the droplets.

## Chapter 3: Results and Discussion

In this chapter the motion two distinct types of droplet manipulation strategy in magnetic digital microfluidic platform have been discussed. In one configuration, the ferrofluid droplet floats on an immiscible liquid film on the surface, while in the second configuration, the ferrofluid droplet slides over a hydrophobic solid surface. In both cases, the planar electromagnetic micro coil provides the actuating magnetic field, and their sequence and duration of switching lends the controllability. The response of the ferrofluid droplet to the actuating field and the precise manipulation is characterized in terms of the droplet trajectory, velocity and transport time. Influence of specific parameters, such as the field current in the coil, coil design, fluid viscosity and droplet size are portrayed for various manipulation processes in a realistic magnetic digital microfluidic configuration.

### 3.1. Description of magnetic field plot for different coil structures

A field plot of different coil structures typically refers to a visual representation of the magnetic field distribution around different coil configurations. Coil structures in the present study is varied in terms of their shape, size, number of turns, and orientation, resulting in different magnetic field patterns. Different arrays of square electromagnetic microcoils are used to actuate the ferrofluid droplets to enable precise manipulation and control over droplet movement. Square coil allows more compact and space-efficient design resulting in a higher and uniform magnetic field distribution within their plane. These features are desirable for generating consistent and controllable magnetic forces on ferrofluid droplets to ensure predictable and precise manipulation. Computation method of magnetic field distribution at any point P for all the conductors of a planar square coil in a x-y plane already discussed in previous section. Magnetic field plot of three distinct square coils with different specifications and orientation shown in Figure 3.1. Figure 3.1 (d),(e) and (f) show Magnetic field (Tesla) computed at a height of 2 mm from the coil shown in Figure 3.1 (a), (b) and (c) respectively. As can be seen from magnetic field plot that the magnetic field peaks at the center of the spiral and it drops sharply towards the periphery.

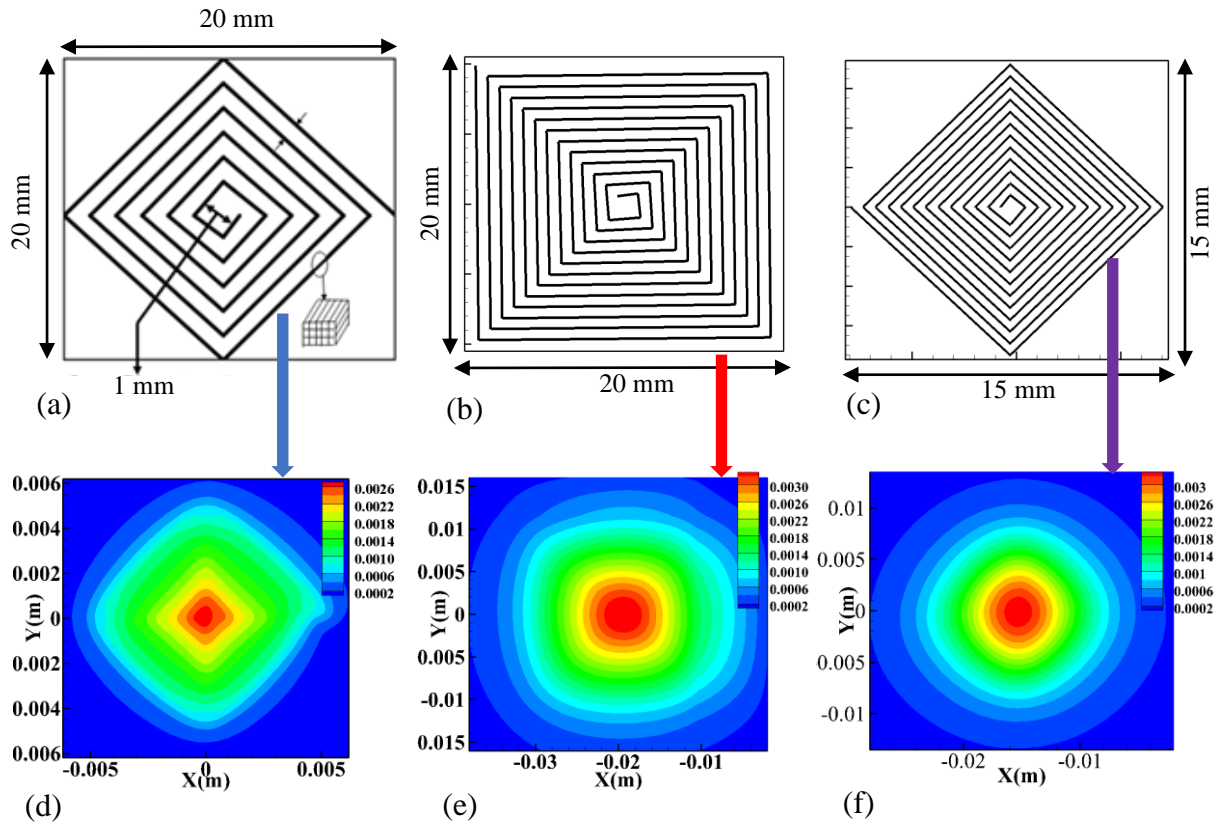


Figure 3.1: Magnetic field plot of square coils: (a) to (c): Three distinct square coils different size and orientation. (d) to (f): Magnetic field (Tesla) computed on the hydrophobic surface (i.e., at  $z = 2000 \mu\text{m}$ ) for square coils shown in (a) to (c) respectively

### 3.2 Motion of ferrofluid droplets stably floating on the aqueous film

Here the motion of a half immersed stably floating ferrofluid droplet on the aqueous film atop a solid substrate has been discussed. An array of planar electromagnetic micro coil is placed beneath an aqueous film, an electromagnetic field is generated. The ferrofluid droplet contains magnetic nanoparticles that respond to the magnetic field. By controlling the current passing through the planar coil, the magnetic field strength and direction can be manipulated. The magnetic field interacts with the magnetic nanoparticles in the droplet, exerting a force on the droplet. By varying the magnetic field strength and direction, the droplet can be manipulated on the aqueous film. The precise manipulation of the magnetic field allows for the precise control of the droplet's position and movement on the aqueous

film. Predictions of the magnetic force field and the resulting transient transport of ferrofluid droplet are validated experimentally in a single-coil configuration with the numerical model by comparing the predicted and observed motions of ferrofluid droplet.

### 3.2.1. Validation of the droplet transport model

The proposed transport model was validated with prior experimental result [233]. Figure 3.2 (a) illustrate schematic of experimental configuration for which the validation was carried out. In [233], the experiment was repeated for different initial droplet positions and for two levels of current, i.e.,  $I = 1.85$  and  $2.25$  A. Figure 3.b (b) shows the processed composite image showing the droplet trajectory. Simulation of droplet motion was carried out under the same geometrical configuration. The properties of EFH-1 (Ferrotec, USA) ferrofluid were chosen from the literature [234, 235]:  $\rho_{FF} = 1169 \text{ kg/m}^3$ ,  $\chi_i = 1.0$ , saturation magnetization =  $398 \text{ G}$ ,  $\eta_{FF} = 0.006 \text{ Pa.s}$  (at  $27^\circ\text{C}$ ). In the experiment, ferrofluid droplets of  $\sim 0.5 \text{ }\mu\text{L}$  volume has been used, which correspond to  $R_{FF} = 500 \text{ }\mu\text{m}$ . Also, for water, at room temperature,  $\eta = 0.001 \text{ Pa.s}$  has been chosen. Figure 3.2 (c) shows the radial variation of the x component of  $\text{grad}(H^2)$  at different heights  $z$  above the coil for different current strengths. Spatial variation of  $\text{grad}(H^2)$  is used to calculate the  $F_m(x, y, z)\hat{e}_x$  and  $F_m(x, y, z)\hat{e}_y$  in Eq. (10) and (11), which enable computing the droplet trajectory (refer to the plots in Figure 3.2 (d)). Figure 3.2 (d) shows the times-of-flight of the ferrofluid droplets as observed experimentally, superposed on the same data obtained from simulation. Results show a reasonably good match between the simulation and the experiment. The time-of-flight increases sharply as the initial dispensing distance  $x_0$  is increases. Also, the time is smaller for the larger current through the coil. The simulated and observed results match well particularly at the lower field values ( $I = 1.85 \text{ A}$ ) and dispensing distance. The difference between the theoretically predicted and experimentally observed transport-times in Figure 3.2(d) can be attributed to the variability in the dispensed droplet size and departure in droplet. Nevertheless, the results match in their order of magnitude, justifying the validity of the assumptions made for the analysis of droplet motion.



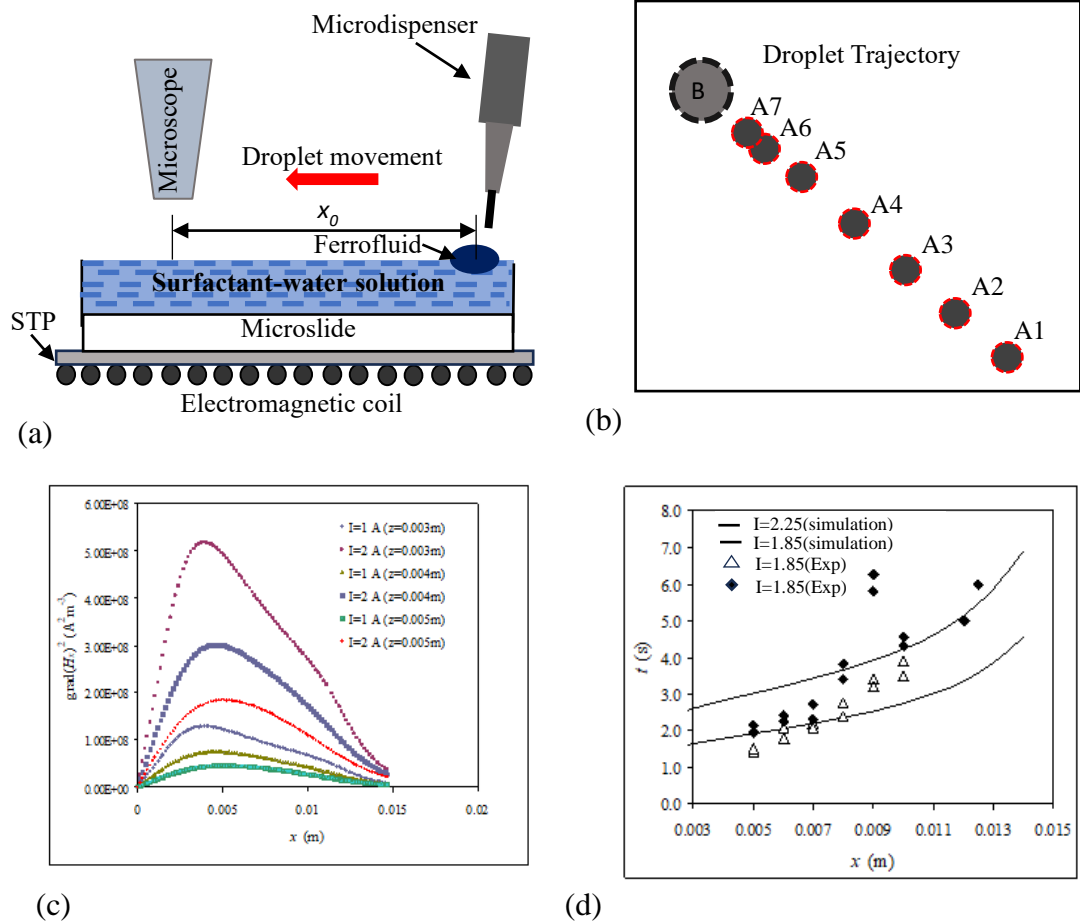


Figure 3.2: Validation of the droplet transport model: (a) Schematics diagram of experimental setup (b) processed composite image showing droplet trajectory. Legend: A1–A7: moving ferrofluid droplet at different time-stamps (B) ferrofluid accumulated from previously transported droplets Validation of droplet transport model (c) Theoretically calculated  $x$  component of  $grad(H^2)$  (d) Variation of the predicted time-of-flight of ferrofluid droplets validation between simulation and experimental results

### 3.2.2. Ferrofluid droplet trajectory using sequentially switchable array of microcoils

This section illustrated the half immersed stably floating ferrofluid droplet trajectory using a sequentially switchable array of electromagnetic micro-coils described in Figure 2.1(a). As a base case, a 1.7 mm diameter (the chosen droplet size is typical of an open-surface digital microfluidic platform [236]) ferrofluid droplet having viscosity  $\eta_{FF}=0.005 \text{ Pa.s}$  [179] is manipulated by a current of 2.5 A. The droplet is assumed to be suspended on the surface of an immiscible liquid ( $\eta = 0.003 \text{ Pa.s}$ , which is nearly three times larger than that

of water, is chosen to include the possibility of using biological samples of higher viscosity) film of 2 mm thickness (i.e., which is enough to suspend the ferrofluid droplet) deposited over the micro-coil array substrate.

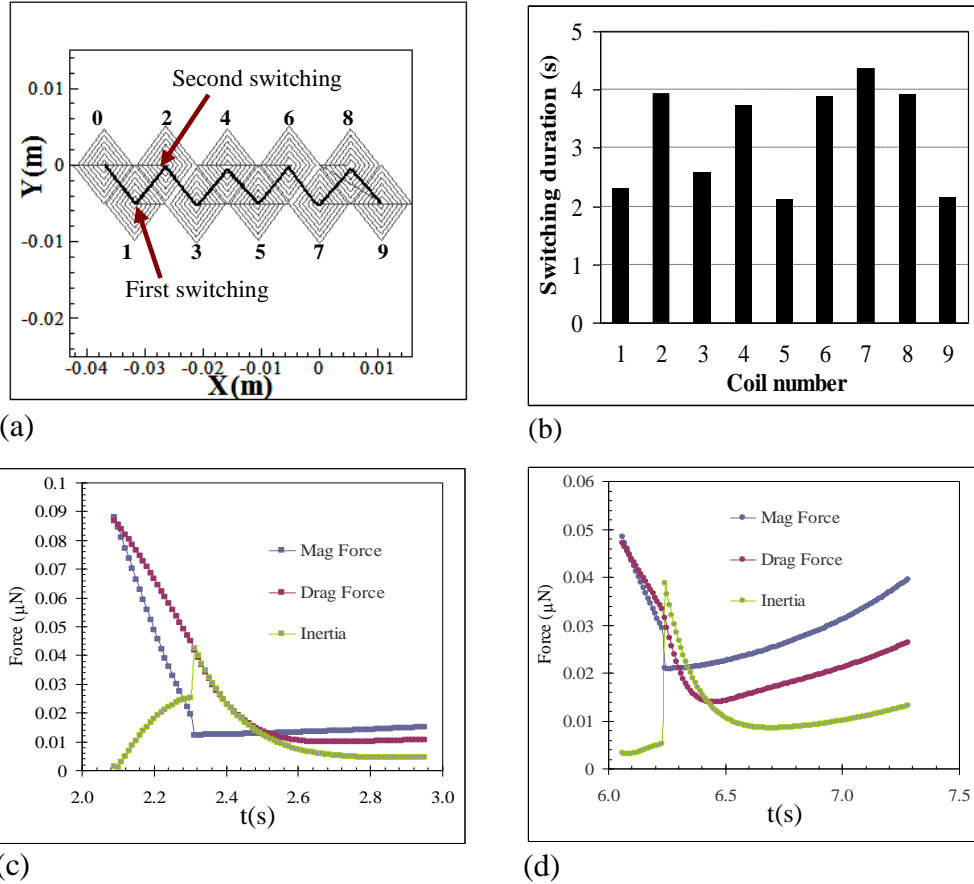


Figure 3.3: Ferrofluid droplet trajectory and corresponding coil switching (a) Trajectory of a 1.1 mm diameter ferrofluid droplet at  $z=2$  mm (b) The corresponding switching durations (for which the relevant coil was at “switched on” states) of coil-1 through coil-9 which are turned ‘on’ and ‘off’ in sequence. Time evolution of the magnetic, drag and inertial forces on the droplet at the instants of (c) the first switching (coil-1 turns off, coil-2 turns on) and (d) the second switching (coil-2 turns off, coil-3 turns on)

Figure 3.3 (a) shows the trajectory of the ferrofluid droplet at  $z=2$  mm with the coils of the double stranded array energized in a sequence from coil-1 to coil-9. The trajectory of the droplet shown in Figure 17 (a) corresponds to the base case. Figure 3.3 (b) shows the corresponding switching interval of coil-1 to coil-9, i.e., the duration for which a given coil

remained switched on as the ferrofluid droplet was transported over the coil array. In the beginning, the ferrofluid droplet is released at the center of coil-0 when coil-1 is switched on. The coil-1 remains switched on, passing a current of 2.5 A, until the  $x$  position of the droplet exceeds the  $x$ -location of the center of coil-1, after which coil-2 is turned on (passing the same current of 2.5 A). The instantaneous velocity of the droplet at this location is 0.0028 m/s, corresponding to a drag force of 0.045  $\mu\text{N}$  on the droplet. As the coil-1 is turned off and coil-2 is turned on, the magnetic force changes instantly from 0.0195  $\mu\text{N}$  to 0.0122  $\mu\text{N}$  in magnitude, and in direction (by almost 90 degrees), a sudden spike in droplet inertia is observed (see Figure 3.3 (c)). Therefore, the magnetic force is strong enough to change the droplet trajectory towards the center of coil-2. Coil-2 remains energized with the same current as long the  $x$  position of the ferrofluid droplet remains in between the  $x$ -positions of the coil centers of coil-2 and coil-3. The coil-3 turns on as soon as coil-2 is switched off. The corresponding jump in magnetic force and the resulting inertial effect described in Figure 3.3 (d) clearly indicates another change in direction of the droplet. This way, each of the coils from coil-1 through coil-9 are sequentially energized as long as the  $x$  position of the ferrofluid droplet lies between the  $x$  locations of the centers of the pertinent coil and its predecessor. Under the action of the sequentially altered magnetic force field, the droplet is steered ultimately to coil-9 in a zigzag manner. Apparently, the odd-numbered coils (except coil-7) require less time of energizing (2 – 2.6 s) while the even-numbered coils required 3.5 – 4 seconds of excitation. The overall time of transport for the coil is 29 s. Having identified the global trajectory of the ferrofluid droplets under the influence of sequentially switched array of electromagnet coils, a parametric investigation has undertaken to check the effect of coil-current on the droplet trajectory for the same set of its starting and finishing points on the substrate. Variation of field current of micro-coils allowed precise control of the droplet movement and enables adjustments to ensure that the droplets were manipulated accurately and precisely. The current in the micro-coils can be adjusted to change the strength or direction of the magnetic field, which will affect the behavior of the droplet.

### 3.2.3. Effect of variation of field current

Figure 3.4 (a) shows variation of ferrofluid droplet trajectories (at  $z = 2$  mm) for different values of current in the coil. The rationale of sequential switching of the electromagnet is retained as described in Section 3.2.2 (the  $i^{\text{th}}$  coil remains energized as long as  $x_{i-1} \leq x < x_i$ , where  $x_i$  denotes the  $x$  position of the center of the  $i$ th coil). For current varying from 1.7A to 3.75 A, droplet trajectories are found not to deviate much from that of the base case although the total time taken by the droplet to move over the coil array decreases. As the ferrofluid droplet moves along the liquid-film surface over the array of planar micro coils, it primarily experiences two forces: the magnetic field towards center of the planar coil, and the opposing viscous force. However, at larger magnetic field, the driving force becomes large and the effect of droplet inertia on its trajectory becomes increasingly prominent. For  $I = 6$  A the droplet trajectory shows a small, but discernable deviation from the base case, albeit it still follows a zigzag trajectory passing over all the coil centers. The trajectory differs further as current in the planar coil increases. For  $I = 8$  A, the magnetic force exceeds the viscous force appreciably (the difference being the inertia force) so that the droplet can no longer execute a sharp turn on every coil. For example, the magnetic force on the droplet by the coil-1 becomes so large that the droplet acquires a high velocity ( $\sim 0.055$  m/s) as it travels over the center of coil-1. The drag force on the droplet right at the instant when coil-1 is switched off is  $0.863 \mu\text{N}$ , which in the instantaneous decline of magnetic field (from  $0.45 \mu\text{N}$  to  $0.38 \mu\text{N}$ ; the closest coil-1 being switched off, and the coil-2 offering very weak force due to its distance from the droplet) should be comparable to the inertia force. The momentum of the droplet allows it to keep moving in straight line even after crossing the center of coil-1. This over-travel reduces the influence of coil-2 on the droplet. The droplet only partially passes over coil-2. On the other hand, relative initial proximity of the droplet to the coil-3 at the time of its switching on leads to an enhanced magnetic pull. Therefore, the droplet passes over the coil center with such a high inertia that it escapes the attraction of coil-4. Downstream, the droplet similarly passes over the centers of coil-5, coil-7, and coil-9 with high velocity, bypassing coil-6 and partially covering coil-8. For  $I = 10$  A, the trajectory differs even further, as the effect of inertia becomes more prominent. The droplet distinctly bypasses coil-2, coil-5 and coil-8, finally reaching coil-9. Although the trajectories differed considerably for different values of

currents, particularly above  $I = 3.75\text{A}$ , the overall time-of-flight of the droplet over the entire coil array decreased monotonically. This is obvious, as the increased magnetic force propels the droplets faster. Figure 3.4 (b) shows that at or below  $I = 3.75\text{A}$ , when the droplet trajectory did not differ much from the base case, the time-of-flight follows the relationship  $t \propto I^{-1.95}$  (thus giving in a straight line in a logarithmic plot). The plot in figure 3.4(b) deviates from a straight line (on the logarithmic I scale) at larger currents, indicating the influence of droplet inertia. Figure 3.4 (b) also shows that the operating condition for base case falls well within the straight-line regime (the viscous regime) of the plot. To evaluate the relative influence of inertial effect, temporal variations of the force magnitudes (on the droplet) are plotted. Figure 3.4 (c) shows the time evolution of the magnitudes of the magnetic, drag and inertial forces on the droplet during its passage for  $I = 2.5\text{ A}$ . The kinks in the plot approximately denote the instants of coil-switching. Although the inertial effect becomes comparable at the instants of switching, its overall magnitude for the base case remains considerably smaller than the magnetic and viscous drag forces. The time averaged magnetic, drag and inertial forces for base case ( $I = 2.5\text{ A}$ ) are  $0.047$ ,  $0.035$  and  $0.015\ \mu\text{N}$ , respectively, implying that the inertial force is only  $\sim 32\%$  of the magnetic force. However, for the case of  $I = 8\text{ A}$ , these are found to be  $0.503$ ,  $0.279$ , and  $0.383\ \mu\text{N}$ , respectively. Thus, the inertial force accounts for nearly  $76\%$  of the magnetic force, which also corroborates to the relatively larger peaks of inertial forces in Figure 3.4 (d).

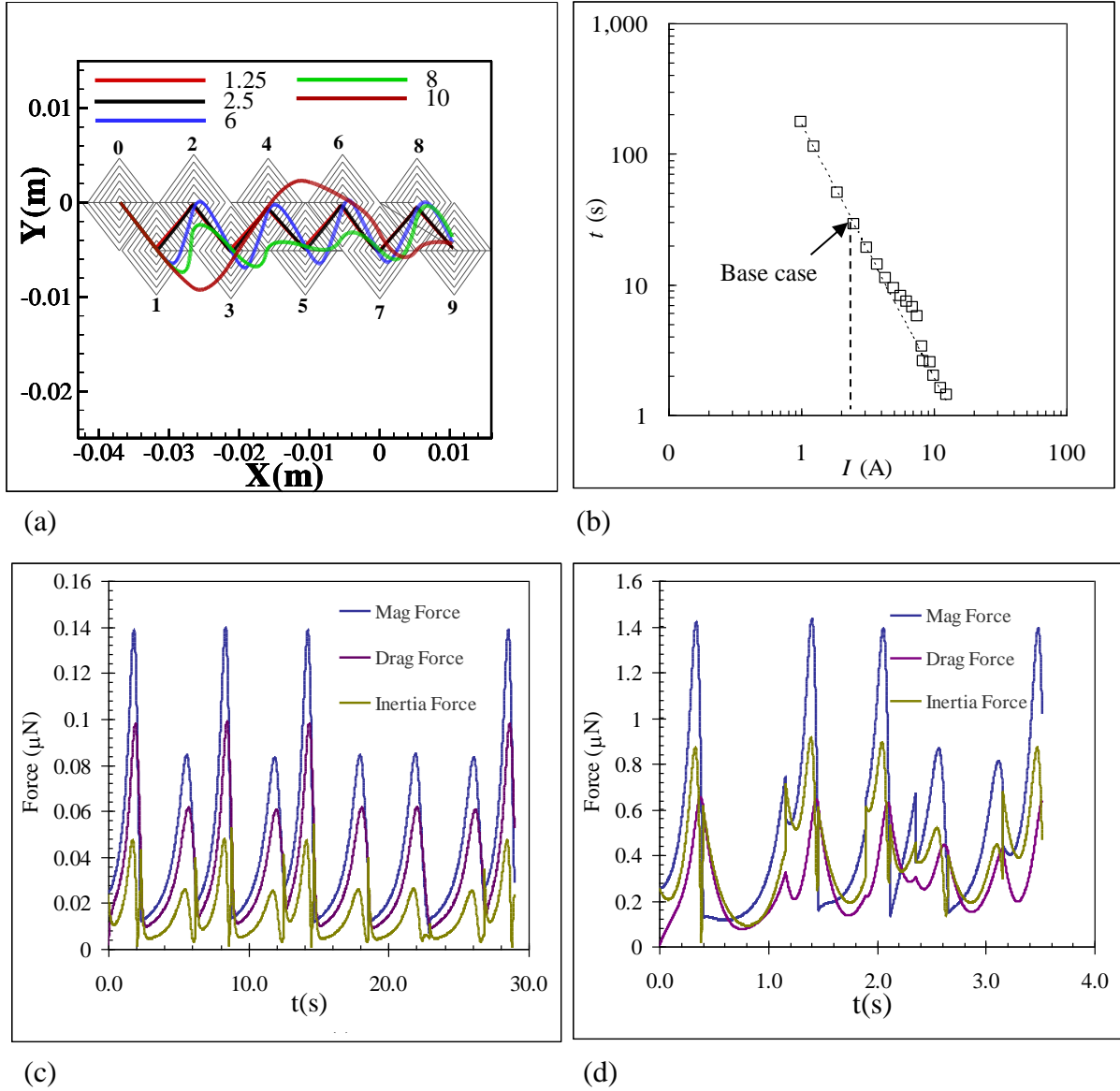


Figure 3.4: Droplet trajectories for different values of current in the coil and force plot (a) Variation of 1.7 mm diameter ferrofluid droplet trajectories (at  $z = 2$  mm) for different values of current in the coil (in terms of percentage of the base current of 2.5 A) (b) The total time-of-flight required decreases with increasing current in the coils ( $\square$  simulation results,---- trendline  $t \propto I^{-1.95}$ ). Time evolutions of the magnitudes of magnetic, viscous drag and inertial forces on the droplets for (c)  $I= 2.5$  A, and (d)  $I= 8$  A. The peaks in inertial force denote sharp turns of the droplets (difficult to differentiate the forces)

The variation of host fluid viscosity during transport of immiscible ferrofluid droplets on a fluid film atop a solid substrate is also important as viscosity influences the speed of droplet movement. By manipulating the host fluid viscosity, droplet transport can be precisely controlled and the accuracy and predictability of droplet manipulation enhanced.

### 3.2.4. Effect of variation of host fluid viscosity

Figure 3.5 (a) shows the variation of ferrofluid droplet trajectories for different values of host fluid viscosity (keeping the ferrofluid viscosity constant at 0.005 Pa.s). Droplet trajectories are portrayed for five values of fluid viscosity starting from 0.0005 Pa.s to 0.01 Pa.s, which correspond to a realistic range of fluids being transported in a surface microfluidic device. For fluid viscosity values between 0.003 – 0.01 Pa.s, the droplet trajectories do not differ much, although the total transport time taken by the droplet increases (see Figure 3.5(b)). The identity of droplet trajectories arises because with increased viscosity both the x and y components of viscous drags are equally strengthened. On the other hand, with increasing viscosity a proportionately lower slip velocity (between the ferrofluid droplet and the host fluid, see Eq. (14) and (15)) can produce a drag force comparable to the magnetic force, thus resulting in increased time-of-flight. For  $\eta = 0.0015$  Pa.s, minor variation of trajectory is observed. A larger droplet velocity is warranted at this viscosity for the drag force to compete with the magnetic force, implying that the droplet inertia is larger. This is manifested in the departure of the droplet trajectory from the base case. This deviation increases further as the viscosity is lowered to 0.001 Pa.s, even though the droplet still executes the zigzag path. With further reduction of viscosity, e.g., at  $\eta = 0.0005$  Pa.s, the inertia dominates so much over the viscous force that the droplet bypasses coil-2, coil-5 and coil-8 finally reaching coil-9. The reduced drag force leads to a monotonic reduction in the droplet time-of-flight. It is important to note that the effect of varying fluid viscosity manifests in the equation of motion of the droplet (Eqs. 14 and 15) through the product of  $[(2 + 3\zeta)/(1 + \zeta)]$  and  $\eta$  instead of the latter alone. Therefore, the droplet time of flight in Figure 9(b) is plotted against the parameter  $[\eta(2 + 3\zeta)/(1 + \zeta)]$  instead of against  $\eta$  alone. Above a host fluid viscosity of 0.0025 Pa.s, the plot is almost linear ( $t \propto [\eta(2 + 3\zeta)/(1 + \zeta)]^{0.98}$ ) denoting a viscosity dominated regime. For smaller viscosity values the plot departs from linearity, indicating the effect of inertia.

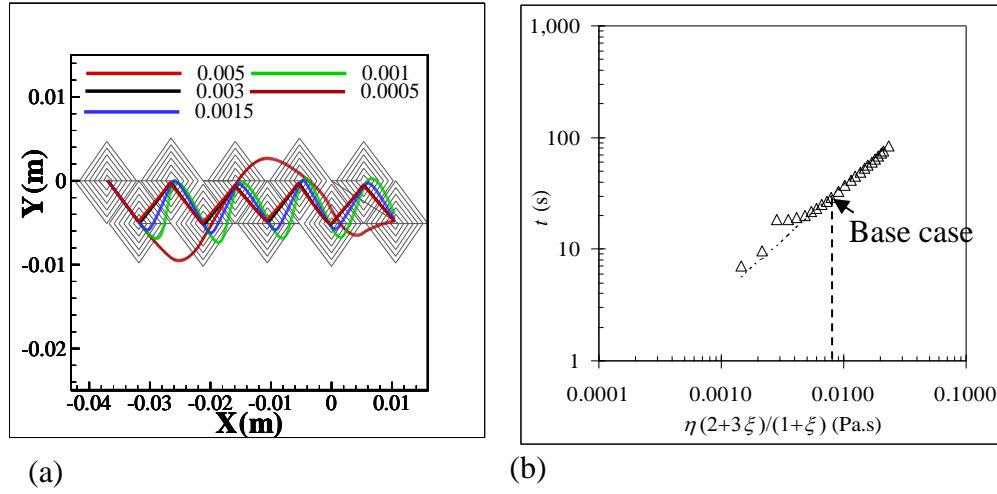


Figure 3.5: Droplet trajectories for different values of host fluid viscosity and corresponding time of flight plot (a) Variation of 1.1 mm diameter ferrofluid droplet trajectories at  $z = 2$  mm for different values of host fluid viscosity (expressed in Pa.s) (b) The total time required as a function of the parameter  $\eta(2+3\xi)/(1+\xi)$  ( $\Delta$  simulation results, ----- trendline  $t \propto [\eta(2+3\xi)/(1+\xi)]^{0.98}$ )

Variation of droplet size is important for droplet actuation in magnetic digital microfluidics because it affects the behaviour of the droplet when subjected to a magnetic field. This understanding can help optimize the parameters used to manipulate the droplets, including the current flow through the micro-coils and the switching sequence used to generate the magnetic field.

### 3.2.5. Effect of ferrofluid droplet size

It is apparent from the foregoing discussions that the droplet trajectories remain nearly unchanged as long as the effect of inertia remains negligible, although the time-of-flight decreases as the magnetic force becomes dominant over the viscous one due to a change in current or the host fluid viscosity. A third possibility of having nontrivial inertial effect would arise if the droplet mass (i.e., size) increases. Figure 3.6 (a) shows variation of ferrofluid droplet trajectories for different realistic values of droplet radius relevant for surface microfluidic devices [236], starting from 300  $\mu\text{m}$  to 1900  $\mu\text{m}$ . It can be seen from



Figure 3.8 (a), the droplet trajectory does not alter appreciably for the given set of operating conditions for droplet radii of 425  $\mu\text{m}$  and 850 $\mu\text{m}$ . However, the total time taken to transfer the droplet decreases. The effect of droplet inertia (and resulting departure from the base trajectory) is first observed for ferrofluid droplet radius of 1062.5  $\mu\text{m}$ . Figure 3.6(a) also shows that up to  $R_{FF} = 1275 \mu\text{m}$ , the droplet trajectory remains confined in zigzag path though. For a droplet radius of 1870  $\mu\text{m}$ , the inertial effect becomes dominant enough so that the droplet bypass coil coil-2, coil-5 and coil-8 before reaching coil coil-9. If the droplet radius is increased to 300 % of base value the droplet bypasses coil-2, coil-5 and coil-8, before reaching coil-9. The time-of-flight of the droplet is found to vary as  $t \propto R_{FF}^{-1.98}$  (Figure 3.6(b)), i.e., almost inversely with the square of the droplet radius, for droplet radius below 977.5  $\mu\text{m}$ . This corresponds to a regime where the droplet trajectory is influenced by the competing magnetic and viscous forces and the effect of inertia is negligible. For droplets having  $R_{FF}$  greater than 1 mm, the effect of droplet inertia becomes apparent as the time-of-flight data departs from the relationship  $t \propto R_{FF}^{-1.98}$ .

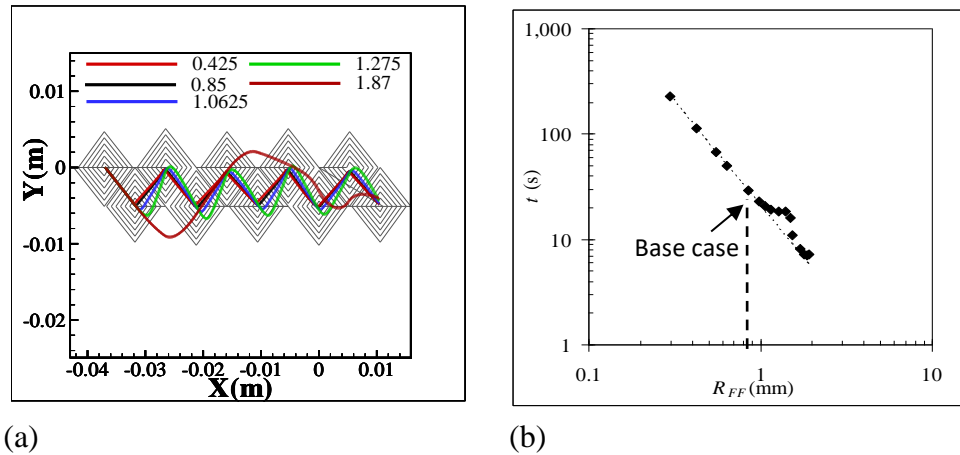


Figure 3.6: Droplet trajectories for different values of radius  $R_{FF}$  of the droplet and corresponding time of flight plot (a) Variation of ferrofluid droplet trajectories (at  $z = 2$  mm) for different values of radius  $R_{FF}$  of the droplet. (b) The total time required decreases with increasing radius of the droplet ( $\diamond$  denotes simulation results, ----- denotes the trendline  $t \propto R_{FF}^{-1.98}$ )

### 3.2.6. Scaling argument

Influence of the individual variations of the operating parameters (current and droplet radius) and fluid properties (host fluid viscosity) can lead to a wide variety of droplet trajectories and the times of flight, which is discussed in Sections 3.2.3 – 3.2.5. While the results clearly indicate the existence of two distinct regimes in which the droplet transport takes place (i.e., inertia-dominated and viscosity dominated), they also underscore the need for a more general criterion that alone can be used for identifying the operating regime. A scaling analysis of Eq. (14) shows for cases when the inertial effects are negligible,  $\frac{d^2x}{dt^2} \sim 0$ . Therefore, the second and the third terms would balance each other. Since the magnetic field function  $f(x) \sim I^2$ , a balance between the viscous and magnetic force term would warrant the droplet velocity to scale as  $\frac{dx}{dt} \sim R_{FF}^2 I^2 / \eta \left( \frac{2+3\zeta}{1+\zeta} \right)$ . Thus, the overall time-of-flight across the coil array is expected to scale as

$$t \sim \left( \frac{2+3\zeta}{1+\zeta} \right) \frac{\eta}{R_{FF}^2 I^2} x \quad (24)$$

Equation (24) clearly indicate that for traversing over a given length  $[(x_9 - x_0) \sim 49 \text{ mm}]$ , the time of flight would scale as the dimensional group-variable  $C = [\eta(2 + 3\zeta)/(1 + \zeta)]/[I^2 R_{FF}^2]$ . When the time-of-flight data from the parametric studies conducted in Sections 3.2.4 – 3.2.6 are plotted against this group variable  $C$  (see Figure 3.7), all the data points are found to merge on a single line for the viscosity-dominated regime. This validates the scaling hypothesis proposed in Eq. (24). For the inertia dominated regime, the overall time of flight is found to be higher than that proposed by Eq. (24) for nearly all the cases investigated in this paper. The increased time of flight can be attributed to the over-travels (beyond the coil centres in the positive and negative y- direction) exhibited by the droplets under inertia-dominated regimes.

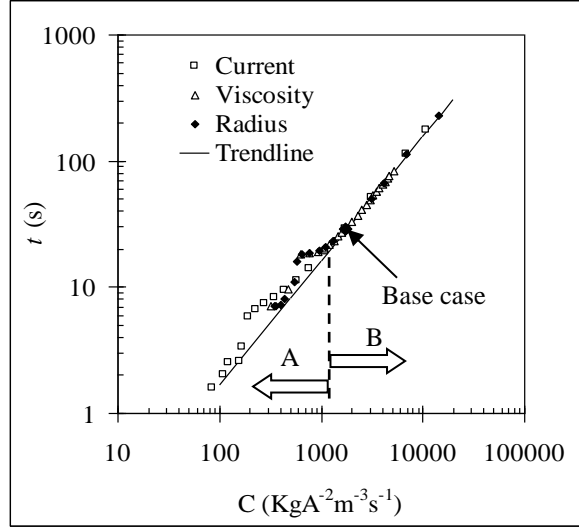


Figure 3.7: Combined plots of droplet transport time as function of the group-variable  $C = [\eta(2 + 3\zeta)/(1 + \zeta)]/[I^2 R_{FF}^2]$ . The plot on the left-hand side of the vertical dotted line (regime A) denotes inertia-dominated droplet transport, while the right-hand side (regime B) follows viscosity-controlled transport. Solid line denotes the curve-fit  $t \propto C$ .

Within the parametric regime investigated in the foregoing sections, the largest magnetic field encountered was 3.18 mT, which is an order of magnitude below the saturation magnetic field strength of EFH1 ( $\sim 400$  G). Therefore, the above scaling analysis leads to Eq. (24) did not have to account for magnetic saturation. For a more general scaling analysis, which would apply even to the cases where the imposed magnetic field exceeds the saturation magnetic field, the magnetic susceptibility of ferrofluid may be approximated as [218]:

$$\chi_m = \chi_{m0} \text{ for } H \leq H_{sat}, \text{ and } \chi_m = M_{sat}/H \text{ for } H > H_{sat}. \quad (25)$$

Below saturation magnetization, the expression of magnetic force is represented well by the right-most term of Eq. (5). For  $H > H_{sat}$ , the expression of magnetic force reduces to

$$F_m = \mu_0 \int (M \cdot \nabla) H d^3r = 3\mu_0 \frac{\mu_r - 1}{\mu_r + 2} (M_{sat} \cdot \nabla H) \quad (26)$$

Therefore, when the ferrofluid is magnetically saturated (thus resulting in a uniform magnetization  $|M_{sat}|$  irrespective of the imposed field) by the micro-coil current,  $F_m \sim I$ . A

balance between the viscous and magnetic force under this condition would warrant that the overall time-of-flight scales as:

$$t \sim \left( \frac{2+3\zeta}{1+\zeta} \right) \frac{\eta}{R_{FFI}^2} x \quad (27)$$

### 3.3 Motion of a spherical cap ferrofluid droplet on solid surface.

In the previous section a complex, two-dimensional manipulation of liquid droplets over a thin aqueous film on an open surface is explained where droplet is actuated using a periodically switched array of electromagnetic micro-coils. Despite precise and flexible droplet manipulation in liquid film, droplet speed could be restrained to some extent by surface tension and viscosity of the aqueous phase. Selection of host fluid medium is also a very important constraint so that some reagent carried by the droplet should not be influenced. Considering these limitations of droplet actuation in host fluid medium recent trends of digital microfluidics application demands droplet manipulation on solid surface for more precise control over droplet movement and positioning. It also reduces the risk of cross-contamination between different droplets, as the droplets are physically separated from each other on the solid surface. A host fluid medium may be incompatible with certain fluids which limits the range of applications whereas solid surface is typically non-reactive and making it compatible with a wide range of fluids. This section illustrated the motion of spherical cap ferrofluid droplets on a solid surface through the application of magnetic fields using a planar electromagnetic coil. Electromagnetic coil is positioned beneath the solid surface. The field generated by electromagnetic coil is applied to the droplet and aligned with the desired direction of motion. The magnetic nanoparticles within the droplet align with the field, causing the droplet to move accordingly. The field strength and gradient can be adjusted to control the droplet's movement. In this section two distinct transport models of spherical cap ferrofluid droplets on a solid surface have been studied based on the array of electromagnetic coils used to actuate the droplets and their unique manipulation strategies. In the first transport model a double layer array of electromagnetic micro-coil (see Figure 2.1(c)) is used to generate a spatio-temporal distribution of magnetic field that steers the ferrofluid droplet in a rectilinear path on a solid substrate. This two-dimensional manipulation of a microliter-volume droplet indicates the prospect of multifaceted on-chip

handling of numerous reaction processes that will enable simple and compact designs of surface microfluidic manipulator. In the other transport model, a concept of spherical cap ferrofluid droplet sorting on a solid hydrophobic surface is proposed where the droplets are actuated by array of electromagnetic micro-coils arranged in a five stranded row (see Figure 2.3(q)). This model also includes the operation of multiple droplets sequential merging as well as pooling on solid hydrophobic substrate which offers a versatile platform for performing a wide range of chemical and biological assays with high precision and accuracy. Sequential merging of multiple droplets increases the volume of liquid that can be manipulated on the substrate where small volumes of liquid need to be combined or diluted. It enables the mixing of their contents to initiate a chemical reaction. By pooling droplets, it is possible to create a higher concentration of a particular sample, or to combine different samples for analysis or reaction. All the equations of motion and different forces corresponding to the transport model of spherical cap ferrofluid droplets on a solid surface have been discussed in the previous section. Now validation of this droplet transport model is essential to establish its accuracy. It enhances the reliability and credibility of the model. In the following section validation of this transport model will be discussed.

### **3.3.1 Validation of the droplet transport model**

The numerical model to describe the manipulation of spherical cap volume droplets on solid substrate using periodically switching array of electromagnetic micro-coil was thoroughly validated against relevant experimental studies [210,237,238]. First, the computed magnetic field from substrate-embedded microcoils and the ensuing force fields were validated, and then the predicted motion of ferrofluid droplet under the magnetic field created by micro-coil is validated against prior experiments [233]. The technique of computing the magnetic field distribution by the electromagnet array which is described in section 2.2 was also being validated as shown in section 3.2.1 . For further validation, the magnetic force computed by the present model was compared with the results of Fulcrand et al. [210], who used, akin to the present work, multiple electromagnetic micro-coils to manipulate magnetic particles suspended in laminar flow inside a microfluidic channel with flow velocity below 1 $\mu$ m/min. Magnetic force on magnetic microbeads having diameter of 2.8  $\mu$ m, particle density of 1.6 g cm<sup>-3</sup> and an effective magnetic susceptibility of 0.17, was

calculated using Biot-Savart law for different z-distance of from the coils. Figure 3.8 (a) shows the coil-configurations (5 turn square coil) considered from the work of Fulcrand et al. [210] adopted for validating the transport model. Figure 3.8 (b) shows the comparison of magnetic force on the magnetic particles calculated as a function of height from the coil plane. Figure 3.8 (c) shows the microbead velocity as a function of its distance from the coil center obtained from both experiments as well as simulation. Having established the validity of the computed magnetic field and the resulting particle-transport model for a suspended magnetic bead, the magnetic fluid droplet transport model on a surface is validated thereafter. The closest configuration of transport of a spherical cap droplet, involving mutual interactions of the driving force, viscous drag and contact angle hysteresis force, has been found in the experimental observation of Podgorski et al. [237], who realized the droplet actuation in sliding mode on an inclined surface under the influence of gravity (transport model shown in Figure 3.8 (d)). In this model, the magnetic actuation force is replaced with the in-plane component of the weight of the droplet. Depending upon the droplet size, fluid viscosity and the inclination of the plate, the droplet velocity would vary. Figure 3.8 (e) and 3.8 (f) show the droplet sliding behavior in terms of the capillary number ( $Ca$ ) and Bond number ( $Bo = \rho g L^2 / \gamma$ ) for two different microdroplets sizes, i.e., 5.5  $\mu\text{m}^3$  and 3  $\mu\text{m}^3$ , respectively. The  $Ca$  vs  $Bo$  plots, describing the in-plane sliding behavior, as obtained from Podgorski's experiment and simulation match well with mean deviation of 4.8 and 5.6% only, for the 5.5  $\mu\text{L}$  and 3  $\mu\text{L}$  droplets, respectively. For a sliding spherical cap droplet, contact angle hysteresis leads to unequal contact angles at the advancing and receding ends of the droplet (see Figure 3.8 (g)); the advancing and receding contact angles depend on the substrate wettability and on droplet velocity [228]. This velocity dependency of advancing and receding contact angles of spherical cap droplet (as described in Eq. (21) and (28)) is also validated with experimental observations of Schneemilch et al. [238]. Figure 3.8 (h) and Figure 3.8 (i) shows the variations of advancing and the receding contact angles, respectively, against the droplet velocity for hexadecane; the plots indicate excellent match with experiments, with mean percentage deviations of 0.4 and 0.88, respectively, for the advancing contact angle and receding contact angle.

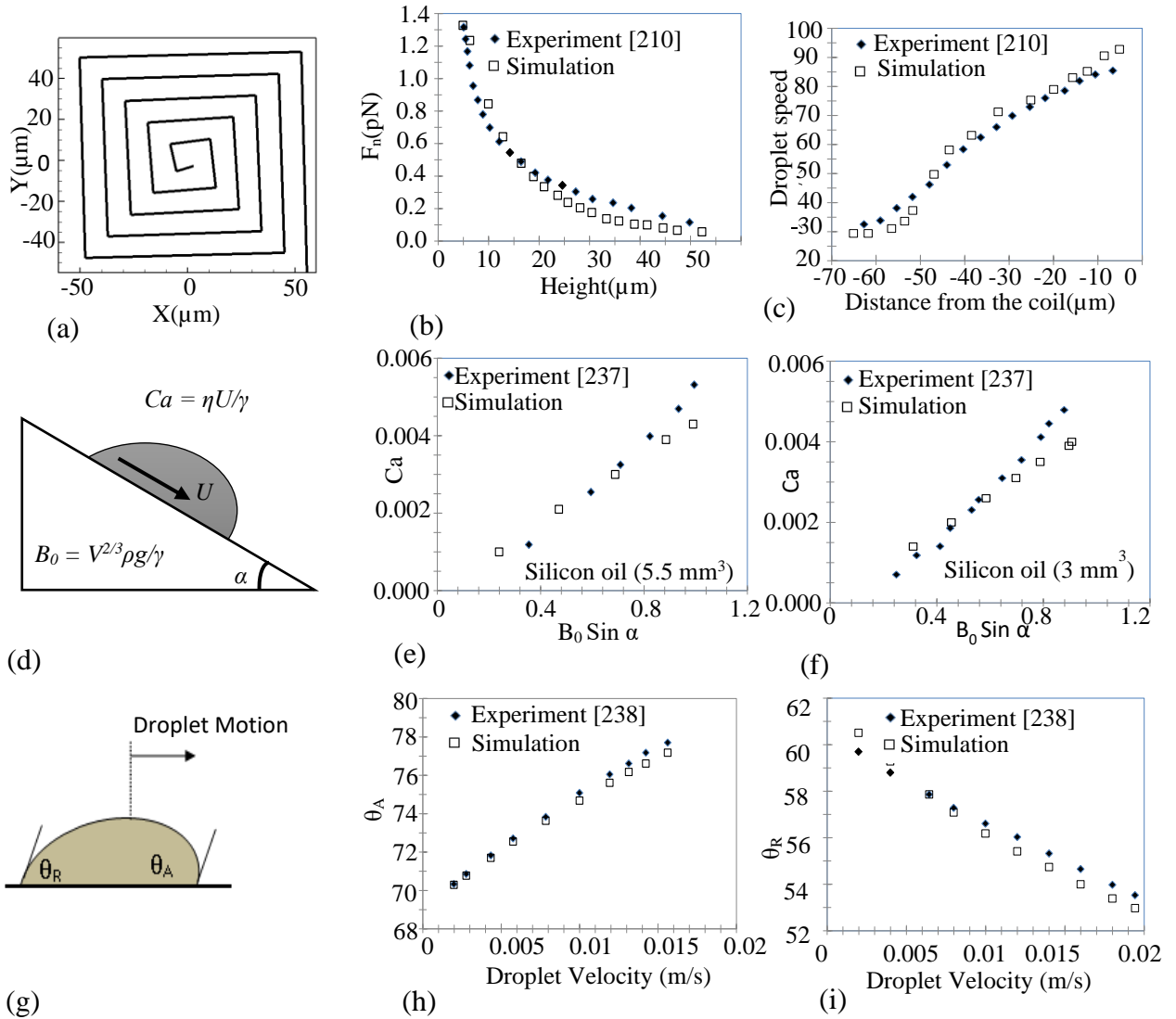


Figure 3.8: Validation of the droplet transport model on solid surface (a) 5 turn square coil (Fulcrand's Experiment[210]), (b) Comparison of magnetic force Vs height from the coil plane[210] (c) Comparison of microbead velocity vs distance from the coil (d) Spherical cap droplet in motion on inclined plane with angle  $\alpha$ .(e) and (f)[237]; Variation of capillary ( $ca$ ) Vs Bond number for silicon oil droplet of volume of 5.5  $\text{mm}^3$  and 3  $\text{mm}^3$  respectively (g) Deformation of spherical cap ferrofluid droplet in motion with advancing and receding contact angle. (h) and (i); Comparison of variation of advancing and receding contact angle with droplet speed respectively [238]

### 3.3.2 Spherical cap ferrofluid droplet trajectory using two-tier array of electromagnet coils

Having validated the droplet transport model, trajectory of a spherical cap ferrofluid droplet on the solid hydrophobic surface, under the actuation of magnetic force generated by the two-tier array of planar electromagnet coils implanted underneath the solid hydrophobic surface (shown in set of Figure 2.1(c)) is estimated. Figure 3.9 (a) shows the droplet trajectory where a 3mm [239] base diameter spherical cap volume ferrofluid droplet (viscosity of 0.005 Pa.s [234] and surface tension of 26.9 mN/m [75]) is released on the solid surface at the edge of coil number 1 (See Figure 3.9 (a)). Initially, the droplet starts from rest with very low acceleration as the net force acting on the droplet is very small due to its large distance from the coil center ahead of it. As it slowly moves towards center of the coil, the force, and hence the acceleration increases, and so does the droplet velocity. Here coil-1 is switched on for 0.77 s when a droplet is transported from the edge of this coil to the coil center. As soon as the droplet reaches the center of the first coil (Coil-1), it is switched off with simultaneous switching on of the next coil (the Coil-2). Right after this coil-switching, the droplet velocity falls sharply as the magnetic force on the droplet reduces suddenly because its large initial distance from Coil-2 immediately after the coil-switching event, but it again picks up as the droplet continues its journey towards the center of Coil-2. This sequential operation of Coil-1 and Coil-2 allows the droplet to move ahead in a straight line with a nearly saw-tooth type velocity profile. Figure 3.9 (a) shows the droplet actuation starting from edge of Coil-1 up to center of the Coil-5. Figure 3.9 (b) to 3.9 (f) shows the magnetic field (Tesla) plot computed on the hydrophobic surface (i.e., at  $z = 2$  mm) for coil-1 to coil-5 while droplet actuates by sequentially switching through the mentioned electromagnetic micro-coils. Figure 3.9 (g) shows variation of driving force (magnetic force,  $F_{mag}$ ) due to electromagnetic micro coil with frictional drag ( $F_{drag}$ ) and contact angle hysteresis force ( $F_{hyst}$ ) acting against the droplet motion. In the same way, to achieve two-dimensional transport, the droplet is further pulled by the next coils in sequence until the droplet finally reached coil-12. The complete droplet trajectory and detailed switching pulses of different coil used in this operation is shown in Figure 3.10



(a). There are three right-angle turns on the way of droplet transport (indicated by A, B and C in Figure 3.10 (a)) at the end of which, the droplet speed reduced to zero; this was achieved by switching off the particular coil (underneath the droplet) at an instant little sooner than when the droplet reached the coil-center (this is unlike the other coils which remain on until the droplet reaches its center) and a time delay of one second is applied prior to switching on next coil (pointed by A, B and C in Figure 3.10 (b)). In this way, the droplet can be turned at a right angle smoothly without over-travelling in the previous path. Figure 3.10 (b) shows the coil pulses (coil-1 to coil-12) used to actuate droplet by sequentially switching through the mentioned electromagnetic micro-coils for the entire droplet trajectory. The time delay between the consecutive coil switching events during every right turn is pointed by A, B and C. It has been observed that the pulse width for the coils after each right turn (coil-6, coil-8 and coil-12, as shown in figure) are higher compared to other coil pulses. Here droplet takes longer time to reach next coil (smaller coil at upper tier) primarily due to its higher distance from the predecessor coil (larger coil at lower tier) and moreover droplet starts from rest.

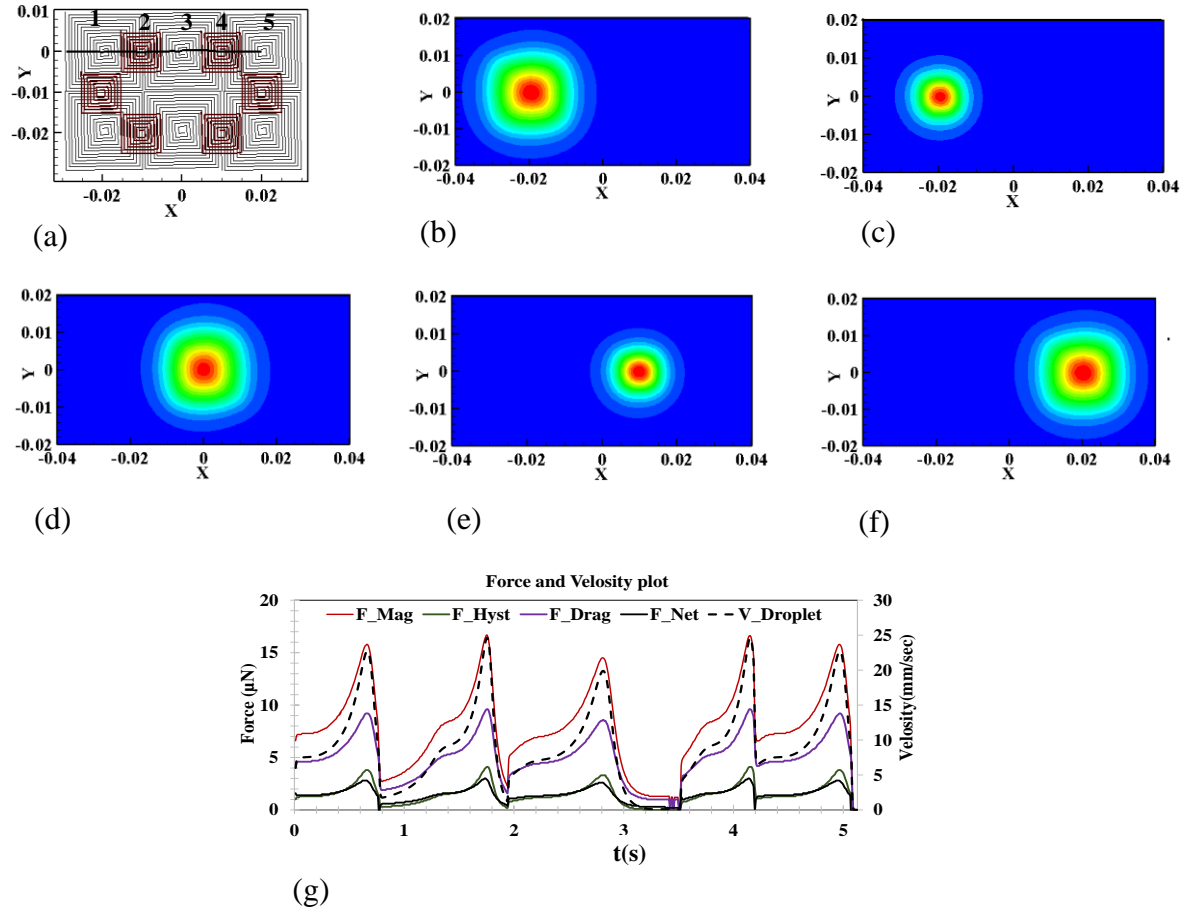


Figure 3.9: Magnetic field (Tesla) plot computed on the hydrophobic surface (i.e., at  $z = 2$  mm) with respect to coil switching and force plot (a) Droplet actuation starting from edge of coil 1 up to center of the coil 5. (b) - (f): Magnetic field (Tesla) plot computed on the hydrophobic surface (i.e., at  $z = 2$  mm) for coil 1 to coil 5 during sequential coil switching to actuate droplet. (g) Variation of driving force (Magnetic force) due to electromagnetic micro coil ( $F_{mag}$ ), frictional drag ( $F_{drag}$ ), contact angle hysteresis force ( $F_{hyst}$ ), Net force ( $F_{net}$ ) and Droplet speed

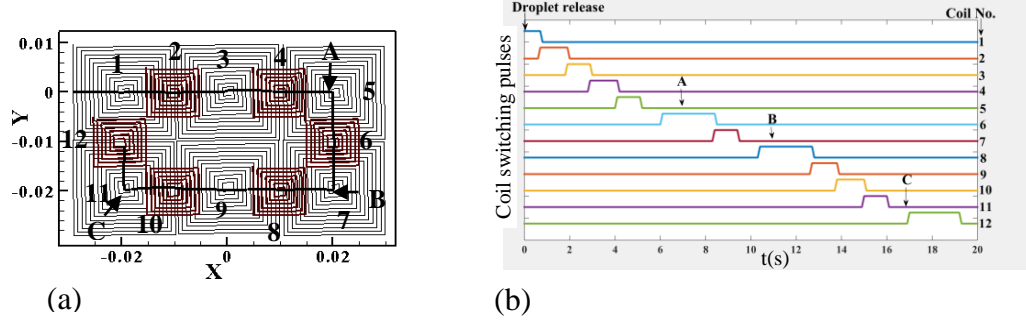


Figure 3.10: Complete droplet trajectory and respective coil switching pulse (a) Complete droplet trajectory starting from edge of coil 1 to its destination, center of the coil 12 (b) Sequential coil switching pulse corresponding to droplet actuation starting from Coil 1 to coil 12.

The force diagram in Fig. 3.9 can also be used to verify the assumption that the droplets retain spherical cap shape throughout the parametric range of simulation. Conformity of a droplet is governed by the Bond number  $Bo = \rho a D^2 / \gamma$ , where  $\rho$  denotes the liquid density,  $a$  the acceleration field,  $D$  the droplet diameter and  $\gamma$  the surface tension. Droplet retains its spherical shape for  $Bo < 1$ . Throughout the present study, the droplet size is small enough to remain in a low Bond number regime, and hence the possibility distortion and droplet-fragmentation is neglected. For example, for the case described Figure 3.9, a 3 mm base diameter ( $D$ ) spherical cap droplet is subjected to a peak magnetic force of  $F_{mag} \approx 16 \mu\text{N}$ . Neglecting other forces, the maximum droplet acceleration is  $a = F_{mag} / (\rho V_{droplet}) \approx 2.2 \text{ m/s}^2$ . In reality, the CAH and viscous resistance impede the droplet motion, and the actual acceleration is even less. Assuming a ferrofluid surface tension of  $\gamma \approx 27 \text{ mN/m}$  [75], this translates into a Bond number of  $Bo = \rho a D^2 / \gamma \approx 0.75$ . This is too small for even a tangible departure of droplet shape from spherical cap, let alone the possibility of droplet fragmentation. The viscous force on the same droplet, as evident from Fig 3.9, is less than  $10 \mu\text{N}$ , thus precluding the possibility of any shear-induced splitting of droplet either.

The analysis also assumes that the temperature of the planar surface is not altered despite the current flowing through the conductors. This is expected, since coils are energized for a very short duration, and the heat dissipation from each coil was considered to be negligible. To verify the veracity of this assumption, a transient heat conduction analysis is

carried out to estimate the temperature rise – due to sudden Joule heat flux from the coil – at the open surface of the substrate (e.g., the PDMS layer) that is interspaced between the coil and the droplet. Considering the coil structure of Figure 2.3 as an example, which has a total conductor length of 27.53 cm, and conductor cross-section of 500 $\mu\text{m}$   $\times$  500 $\mu\text{m}$  and taking the electrical resistivity of copper as 1.7 $\times 10^{-8}$   $\Omega\text{m}$ , the electrical resistance of each coil is found out to be 0.0187  $\Omega$ . A maximum current of 10 A (which is on the highest end of the parametric study) through the coil would entail a dissipation of 1.9 W of heat (corresponding to a heat flux  $q'' \sim 0.83$  W/cm<sup>2</sup>). Considering that this heat is conducted upward to the surface of the substrate of thickness  $\delta$  (2mm in the present situation), the temperature rise  $\Delta T_s$  of the surface of the substrate over a time  $t$  of coil-excitation is expressed as [240]:

$$\Delta T_s = \frac{2q''}{kA} \sqrt{\frac{\alpha t}{\pi}} e^{-(\delta^2/4\alpha t)} - \frac{q''\delta}{kA} \left[ 1 - \text{erf} \left( \frac{\delta}{2\sqrt{\alpha t}} \right) \right] \quad (28)$$

Taking the standard thermophysical properties of PDMS, viz., thermal conductivity  $k = 0.16$  W/mK, thermal diffusivity  $\alpha = 0.095$  mm<sup>2</sup>/s [241], the value of  $\Delta T_s$  turns out to be less than 1 mK. Therefore, the Joule heating produced within the wire is not expected to induce evaporation of the ferrofluid droplet or influence the liquid surface tension.

### **3.3.3 Spherical cap ferrofluid manipulation using array of single layer electromagnetic micro-coils arranged in a five stranded row**

Magnetic manipulation of the spherical cap volume droplet on the solid surface under the influence of the sequentially switched array of electromagnetic micro-coils shown in figure 3.11(a). Real-time monitoring and control of droplet movement are essential to ensure accurate and precise manipulation of droplets on surface microfluidic platforms. To achieve real-time connectivity, sensors can be used to monitor the position of the droplets as they move on the substrate under the influence of the magnetic field. This information can then be fed back to a control system, which would adjust the switching sequence of the micro-coils to ensure accurate and precise manipulation of the droplets. Ferrofluid droplet having 3 mm base diameter and a spherical cap shape is chosen for the simulation, the droplet size

is typical for open surface microfluidic manipulation and sorting [239]. Ferrofluid viscosity is chosen to be 0.005 Pa.s [234] while an actuating current of 4.5 A is applied through the coils. Figure 3.13(a) shows the droplet trajectory after being released near the edge of coil-12 and transported to coil-1 by sequentially actuating the intermediate coils coil-12, coil-13, coil-14, coil-11 and finally coil-1. Figure 3.11(b) shows the magnified view of the droplet trajectory over coil-12, coil-13, coil-14, coil-11 and coil-1. Initially ferrofluid droplet is released at a position before the coil-12 (shown by the vertical, blue arrow in Figure 3.11(b)) with this coil is turned on with a current of 4.5 A and is kept energized until the droplet passes over the center of the coil. As soon as coil-12 is turned off, Coil-13 is energized with the same current. The velocity of the droplet at the instant of switching (coil-13 on and coil-12 off) is 0.28 m/s in the  $x$ -direction, corresponding to a net force of 4.4  $\mu\text{N}$  on the droplet. During this switching, the magnetic force changes instantly from 8.55  $\mu\text{N}$  (due to coil-12) to 0.01  $\mu\text{N}$  (due to coil-13) in magnitude as now the droplet is far away from the active coil-13 center. At the same time, the opposing forces (drag plus contact angle hysteresis) still acting and net force is -4.13  $\mu\text{N}$ ; this results in the deceleration of the droplet. As the droplet velocity start to decrease, the velocity-dependent viscous drag and contact angle hysteresis force also decrease; at the same time droplet keeps moving towards the coil-13, when the magnetic force increases. This drives the net force to return to positive value within a short while (27 ms). Coil-13 remains energized as long as the ferrofluid droplet reaches the coil-13 center, after which it is switched off, and coil-14 energized. All corresponding forces on the droplet and the droplet velocity vary like that observed during the previous switching event. Figure 3.11(b) clearly shows after third switching, the droplet transport direction changes (almost  $45^\circ$ ) as coil-11 is turned on with simultaneous turning off coil-14. Figure 3.11(b) clearly shows that droplet slightly overshoots the center of the coil-14 due to inertia (droplet speed was the highest at the center of the coil-14) before it changes direction. After final switching (between coils-11 and coil-1) the droplet volume moves towards center of active coil-1 (destination). Finally, coil-1 is turned off when the droplet is marginally ahead of the coil center (unlike previous switching events that take place when the droplet gets transported past the coil centers). This is done deliberately so that the droplet stops at the coil enter of coil-1. Once coil-1 is switched off, the magnetic force and net force change instantly from 8.52  $\mu\text{N}$  and 4.87  $\mu\text{N}$  to zero and -4.07  $\mu\text{N}$ ,

respectively. Thereafter, the droplet speed start decreasing as the opposing forces still exist and the net force eventually turns zero when the droplet stops at the coil-1 center.

### **3.3.3.1 Time evolution of different forces on the spherical cap volume ferrofluid droplet**

Physical variation of different forces acting on droplets in motion on a solid surface is important because it can affect their behavior and trajectory. This understanding is essential for accurately predicting and controlling droplet movement warranted in different surface microfluidic tasks. To evaluate physical variation of different forces acting on droplet in motion on solid surface are plotted in Figure 3.11(c). This Figure shows the variation of the driving force (Magnetic force) due to electromagnetic micro coil ( $F_{mag}$ ) with frictional drag ( $F_{drag}$ ) and contact angle hysteresis force ( $F_{hyst}$ ) acting against the droplet motion. Both contending forces are velocity dependent. Initially released droplet at edge of the coil-12 starts with very low speed as lower magnetic force (due to its distance from coil center) acting on the droplet is counterbalanced by the force due to contact angle hysteresis and frictional drag. The droplet steadily moves with this low starting speed towards coil center still the magnetic force gets comparably higher than  $F_{drag}$  and  $F_{hyst}$  near the coil center which induces higher droplet speed. As soon as the droplet is reached at center of first coil (coil-12), it is turned off with simultaneous turning on the next coil. Magnetic force along with droplet speed are momentarily reduced to very low value due to a far distance from the next active coil center. The droplet accelerates from its low speed when magnetic force overshoots against the opposing forces near the next coil center. In the same way the droplet travels over the rest of the coils and finally reaches its assigned destination. To prevent overshoot due to inertia, the last coil is switched off ~0.11 s prior to the droplet reaching its center. It is clear from the force and velocity timelines that the droplet transport is strongly impeded by the drag and hysteresis forces. Also, the magnetic force is highly localized in nature, and the relative spacing of the coils and the switching sequence has an important role in ensuring seamless droplet transport.

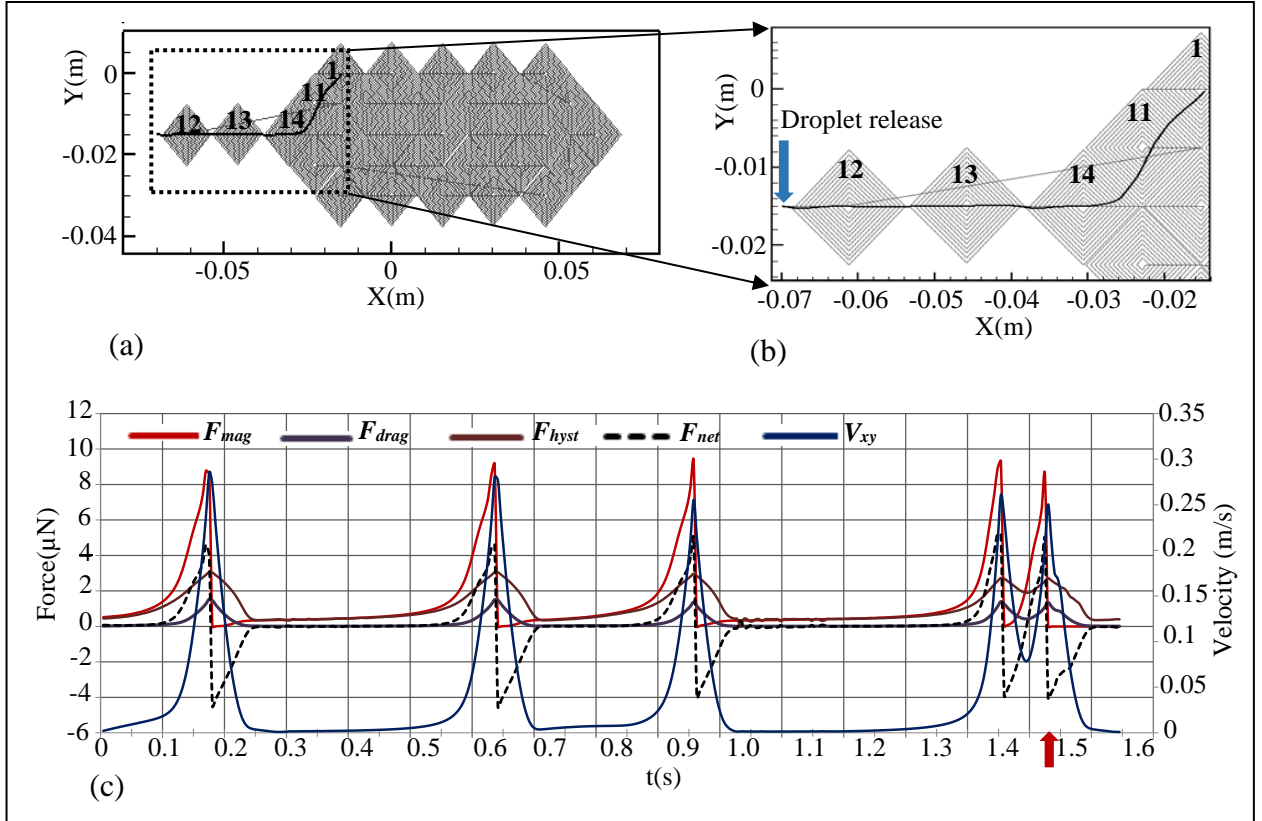


Figure 3.11: Spherical cap ferrofluid droplet trajectory and corresponding force plot (a) Trajectory of a spherical cap ferrofluid droplet having 3 mm base (footprint) diameter on solid substrate with coil current of 4.5 Amp, (b) inset view. (c) Temporal variation of the driving (magnetic) force ( $F_{mag}$ ), frictional drag ( $F_{drag}$ ) and contact angle hysteresis force ( $F_{hyst}$ ) on the droplet, and the resulting droplet speed (secondary axis) during the droplet motion. Coil activation starts at  $t = 0$ , and the final coil is switched off at  $t = 1.53$  s (shown by the brown arrow)

### 3.3.3.2 Effect of variation of field current

Having identified the global trajectory of the ferrofluid droplets under the influence of sequentially switched array of electromagnet coils, now a parametric investigation is undertaken to check the effect of coil-current on the droplet trajectory for the same set of its starting and finishing points on the substrate. Variation of field current of micro-coils allows precise control of the droplet movement and enables adjustments to ensure that the droplets are manipulated accurately and precisely. The current in the micro-coils can be adjusted to change the strength or direction of the magnetic field, which will affect the behavior of the

droplet. For this study, the current magnitude in all the pertinent coils (viz. coil-12, coil-13, coil-14, coil-11 and finally coil-1) are changed from the base value to the same extent, and their energization durations are adjusted such that the droplet trajectory remains nearly the same, but the overall travel time changes. The resulting droplet trajectories for different values of current through the specific coils (i.e., coil-12, coil-13, coil-14, coil-11 and coil-1) are overlaid in figure 3.12 (a). Sequencing of the coil-energization remains the same as in section 4.1 (implying that a particular coil remains energized as long as droplet outstrip its center). For current varying from 3 Amps to 6 Amps, droplet trajectories are found to vary only a little, although the total time taken by the droplet to move from the starting to the designated finishing point decreases (see figure 3.12(b)). Here magnetic force drives the droplet towards the center of the planar coil. At higher value coil magnetic field (Higher field current in the coil), the driving force becomes large and the effect of droplet inertia on its trajectory becomes slightly prominent where droplet swivels from its straight path shortly after coil-14 center. The time-of-flight of the droplet is found to vary as  $t \propto I^{3.9}$  (see figure 3.12(b)).



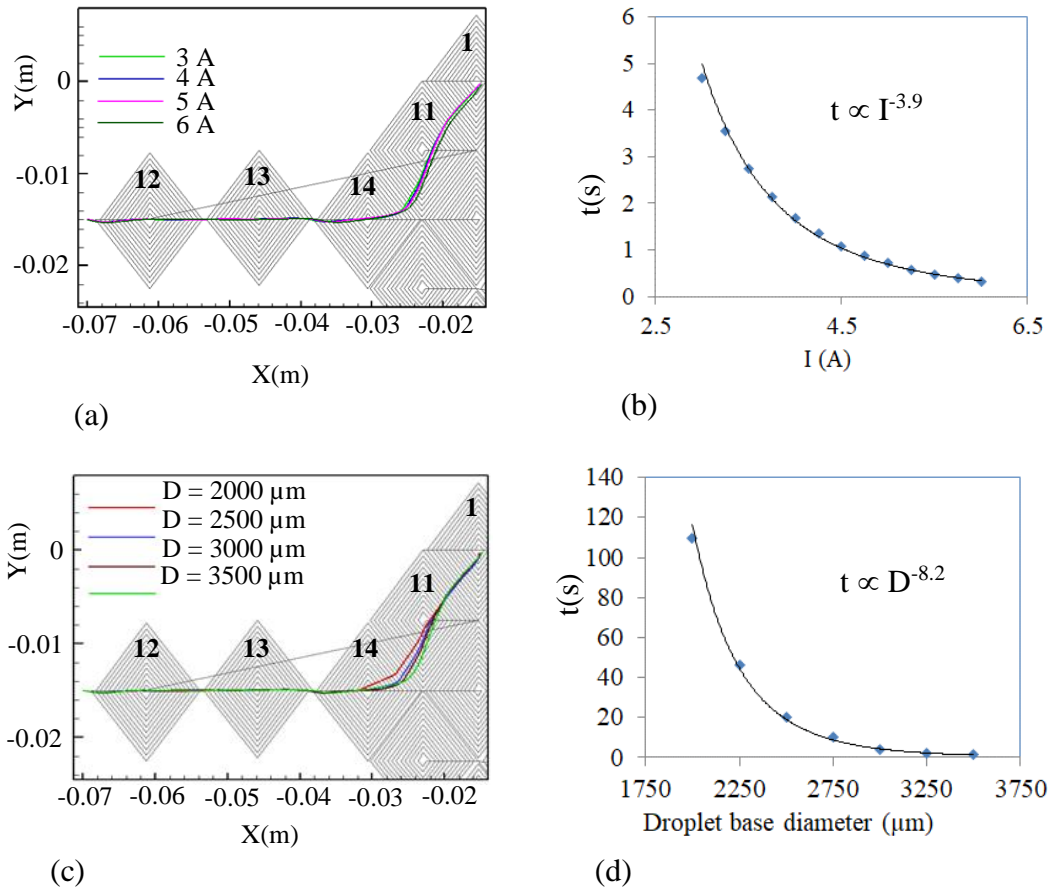


Figure 3.12: Variation of droplet trajectories and time of flight with respect to field current and droplet base diameter (a) Variation of 3 mm base diameter (footprint) spherical cap ferrofluid droplet trajectories on solid substrate for different values of current  $I$  (in A) passing through the coil (b) Time of flight to reach center of 1<sup>st</sup> electromagnetic coil from starting point with different actuation current in the coil (c) Variation of ferrofluid droplet trajectories on solid surface for different values of cap volume ferrofluid droplet base diameter (2000  $\mu\text{m}$  to 3500  $\mu\text{m}$ ). (d) Time of flight ( $t$ ) to reach center of 1<sup>st</sup> electromagnetic coil from starting point with different droplet base diameter

### 3.3.3.3 Effect of variation of droplet base diameter

Variation of droplet base diameter is important for droplet actuation on a solid surface in magnetic digital microfluidics because it affects the behavior of the droplet when subjected to a magnetic field. This understanding can help optimize the parameters used to manipulate

the droplets, including the current flow through the micro-coils and the switching sequence used to generate the magnetic field. figure 3.12 (c) shows variation of ferrofluid droplet trajectories on solid surface for different values of cap volume (corresponding to ferrofluid droplet ranging between 2000 – 3500  $\mu\text{m}$ ) over specific coils (coil-12, coil-13, coil-14, coil-11 and finally coil-1). It can be seen from figure 3.12 (c) that for different sized droplets, the trajectories do not differ noticeably in its straight part (i.e., during droplet transport over coil-12 and coil-13), but they deviate slightly from one another near the zone of its first turn (i.e., over coil-14). At higher base diameter of the spherical cap droplet, the trajectory swerves from its straight path later since the inertial effect becomes dominant. However, the total time taken by the droplet to move over the coil array decreases (see figure 3.12 (d)). The time-of-flight of the droplet is found to vary as  $t \propto D^{-8.2}$  (Figure 3.12(d)).

### **3.3.4. Droplet multiplexing and complex transport**

Controlled magnetophoretic transport of spherical cap ferrofluid droplets on solid substrate using sequentially switched planar micro-coils embedded underneath the substrate is demonstrated in the previous section. This section illustrates the feasibility of multiple droplets manipulation on the same array of micro-coils (Figure 3.13 (a)) by periodic sequential switching of the coils, to achieve droplet-specific predefined direction with respect to coil switching. This multiplexing and complex transport of multiple droplets has several advantages over traditional methods of bioassay and medical diagnostics, including reduced sample volumes, faster reaction times, and the ability to perform multiple assays simultaneously on a single platform. The droplets containing biological samples such as blood, saliva, or urine are manipulated to specific locations on the surface, where they can be combined with reagents or other samples for analysis. Here three different types of droplet manipulations strategy were reported. First, multiple monodisperse (11 droplets) droplets are manipulated where these droplets are released sequentially on PDMS substrate and consequently transported in different predefined destinations using appropriately timed switching of the microcoils as shown in Figure 3.13(a). In the second approach, five multiple polydisperse droplets are pooled and trapped in five different preordained destinations on the substrate using appropriately timed switching of planar micro coils as shown in Figure 3.14(a). Finally, sequential merging of multiple droplets and their pooling

on the substrate has been reported in Figure 3.15(a). All these mentioned droplet manipulations of droplets on a solid hydrophobic substrate in digital microfluidics offer a versatile platform for performing a wide range of chemical and biological assays with high precision and accuracy. Sequentially released multiple droplet manipulation can perform sequential chemical reactions, mixing, and sample analysis. Beforehand please Each droplet can contain different sensing elements for multi-parameter analysis in a single platform. The droplets can be transported to specific detection zones, where their contents are analyzed for rapid and precise testing in a compact format. Sequential merging of multiple droplets increases the volume of liquid that can be manipulated on the substrate where small volumes of liquid need to be combined or diluted. It enables the mixing of their contents to initiate a chemical reaction. By pooling droplets, it is possible to create a higher concentration of a particular sample, or to combine different samples for analysis or reaction.

#### **3.3.4.1. Targeted delivery of multiple monodisperse droplets**

Targeted delivery of multiple monodisperse droplets ensure consistency in size and properties which enables accurate delivery of specific volumes of reagents. Monodisperse droplets facilitate accurate and consistent screening across multiple experiments during high-throughput screening. For quantitative analysis monodisperse droplets are essential as consistent droplet sizes lead to accurate measurements of concentrations, reactions rates, and other quantitative parameters. This section demonstrates the driving concept of multiple monodisperse droplets on solid substrate. Eleven identical spherical cap ferrofluid droplets (having 3mm base diameter) are released sequentially on the PDMS substrate at 7 mm from the center of the Coil-12 and finally pooled along their pre-assigned independent paths, eventually trapping them at the centers of some pre-designated coils. Table 1 lists the coils to be energized in sequence for achieving this this for droplet 1 through 11. The last coil in each set (in bold) designates the target coil where the droplet is finally immobilized. Figure 3.13(a) shows droplet trajectories towards different destinations (shown by dark red arrow from D1 through D11) with droplet number with reference to their sequential release. Importance of such a trapping stem from the concept of holding multiplexed reactions on the same microfluidic platform. For example, all the destination locations (of trapping the ferrofluid droplet in Figure 3.13 (a)) may be construed as different

miniature reaction sites where the droplet needs to reside for the necessary reaction to occur. Multiple monodisperse droplets simultaneously react with numerous compositions at different reaction chambers at the same time. Thus, multiple studies can be performed on a single chip with reduced analysis time by manipulating each droplet independently on a single planar microcoil array. Here, the time gap between the releases of consecutive droplets is maintained at 2 seconds. This optimized intervening distance and frequency of release of ferrofluid droplet have been chosen carefully so that once a droplet passes over a certain coil (and it switches off, as shown in Figure 3.13 (b)) it traverses far enough (under the pull of the next downstream coil) and subsequent turning on of the upstream coil does not pull the droplet back.

Table 3.1: Set of coils to be energized to transport a specific droplet to a pre-designated location on the substrate. Each droplet is finally immobilized at the center of the last coils (in bold) of the sets (the sequence energizing the electromagnetic coils are assigned based on predefine path to target destination coil )

Droplet	Sequence of energizing the electromagnetic coils	Droplet	Sequence of energizing the electromagnetic coils
1 <sup>st</sup> Droplet	12,13,14,11, <b>1</b>	7 <sup>th</sup> Droplet	12,13,14,15,16,17,8, <b>4</b>
2 <sup>nd</sup> Droplet	12,13,14,26, <b>31</b>	8 <sup>th</sup> Droplet	12,13,14,15,16,17,23, <b>28</b>
3 <sup>rd</sup> Droplet	12,13,14,15,10, <b>2</b>	9 <sup>th</sup> Droplet	12,13,14,15,16,17,18,7, <b>5</b>
4 <sup>th</sup> Droplet	12,13,14,15,25, <b>30</b>	10 <sup>th</sup> Droplet	12,13,14,15,16,17,18,22, <b>27</b>
5 <sup>th</sup> Droplet	12,13,14,15,16,9, <b>3</b>	11 <sup>th</sup> Droplet	12,13,14,15,16,17,18,19, <b>20</b>
6 <sup>th</sup> Droplet	12,13,14,15,16,24, <b>29</b>		

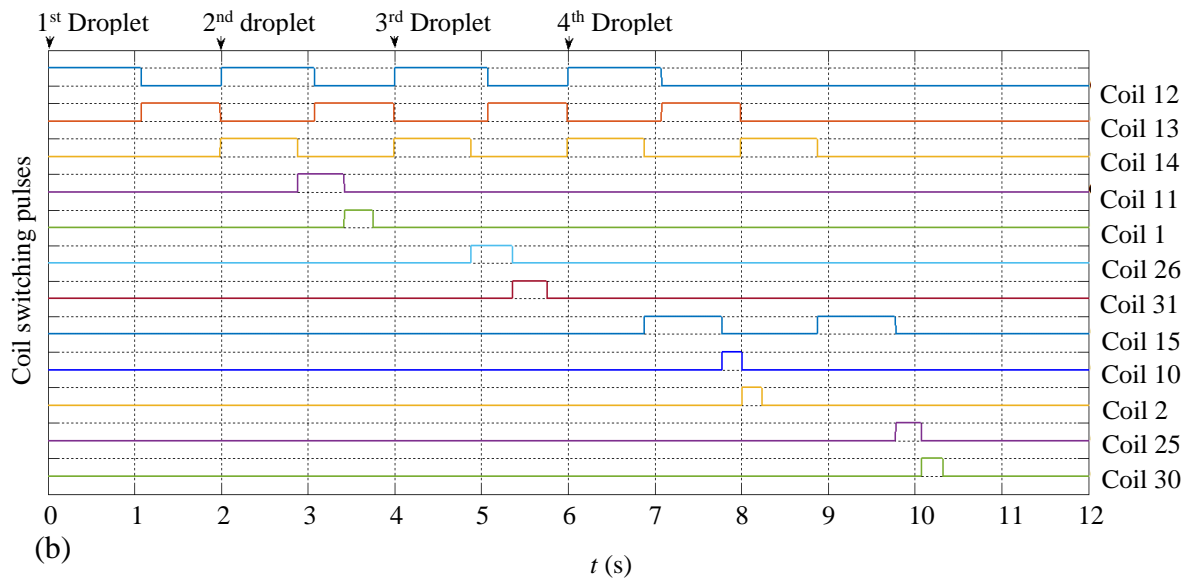
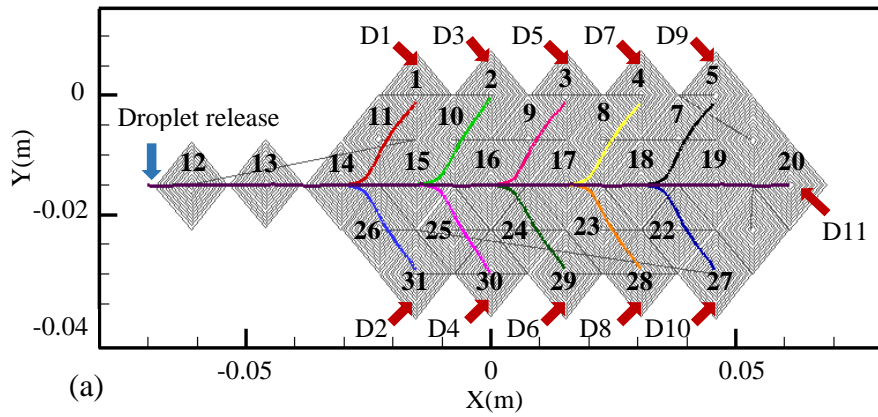


Figure 3.13: Monodisperse droplet trajectories and corresponding coil switching pulses (a) Transport of eleven monodispersed spherical cap ferrofluid droplets, released ahead of coil 12 (shown by the blue arrow), showing their trajectories towards different destinations (shown by dark red arrow from D1 through D11) on the same substrate; droplets are numbered with reference to their sequence of release. (b) Coil switching pulse for the first 4 droplets for the multiplexed droplet-manipulations.

The numbers under the pulses denote the droplet serials. Coil-switching pulses for the first four droplets are shown in Figure 3.13 (b). Initially, the first ferrofluid droplet is released at a position before the coil 12 (shown by the vertical, blue arrow in Figure 3.13 (a)) and finally transport through subsequent switching of specific coils (coil-12, coil-13, coil-14, coil-11 and finally coil-1), reaching a pre-ordained target (coil-1) at 3.75 second. While the

second droplet is released at the same location (denoted by the blue arrow in Figure 3.13 (a)) after 2 seconds and the coil-12 is switched on, the first droplet passes over the center of coil-13 at a velocity of 9.67 cm/s. From the coil-switching timeline (Figure 3.13 (b)) it is interesting to note that at this moment, both coils-12 and coil-14 are switched on, and coil 13 is turned off. Therefore, the first droplet would experience the magnetic influence of both coil-12 and coil-14. However, the forward velocity of the first droplet biases it more toward coil-14 and sweeps it out of the influence of coil-12. Timing of the subsequent switching of coils-14, coil-11 and coil-1 are synchronized to ensure the passage of the first droplet to coil-1 center. A similar sequence of coil switching (coil-12, coil-13, coil-14, coil-26 and finally coil coil-31; see Table 1) ensures the forward traction of the second droplet in the same manner down the line, leading to its entrapment over coil-31. For the third and fourth droplets, the coil switching sequences are coil coil-12, coil-13, coil-14, coil-15, coil-10, coil-2 and coil-12, coil-13, coil-14, coil-15, coil-25, coil-30 respectively (see Table 1) leading to the trapping of the droplets over coil-2 (third droplet) and coil-30 (fourth droplet). Droplet numbers are mentioned in respective coil pulses shown in Figure 3.13(b). The sorting scheme (e.g., the first droplet over coil-1, second over coil-31, third over coil-2 and the fourth over coil-30) is cited as an example only, and different temporal and spatial combinations are possible with the same configuration of coil assembly and different switching sequences. Such spatiotemporal separations offer viable tools for sample isolations on-chip according to different bioanalytical protocols. This underscores the operational flexibility of the droplet manipulating platform.

#### **3.3.4.2. Spatiotemporal separation of multiple polydisperse droplets**

Akin to the previous example, which proposed a sequential transport and spatial sorting of monodispersed droplets. The spatiotemporal separation of multiple polydisperse droplets in magnetic digital microfluidics enables the selective manipulation and sorting of droplets based on their physical properties such as size, shape, and composition. This can be useful in various applications, such as cell sorting, particle separation, and bioassays. By using different magnetic field strengths and gradients, droplets with different physical properties can be selectively moved and sorted in specific locations on the surface. Here spatiotemporal separation of five polydisperse droplets in specific target locations are

explained as shown in Figure 3.14 (a). Multiple applications can be performed sequentially on such a single DMF device by manipulating each droplet. Conforming to the typical DMF volumes, five different volumes of spherical cap ferrofluid droplets have been chosen, corresponding to base diameters of 3 mm to 3.4 mm respectively (with increment of 0.1 mm), released from the same location on the substrate (shown by the blue arrow in Figure 3.14 (a)), in a decreasing sequence of volume (i.e., the base diameter). Droplets are released with a time gap of 3 seconds (typical hiatus in common digital droplet dispensers) to avoid interfering “pull-back” force from adjacent coils during switching transitions and any resulting untoward reverse-motion or coalescence of the droplets, as they are and manipulated independently through distinct path to its respective destination. Initially, the first ferrofluid droplet of 3.4 mm base diameter is released on the substrate at the same starting position as mentioned earlier, and then pooled along and trapped at their pre-designated independent path (in straight line through subsequent switching of coil-12 through coil-20), and finally bringing the droplet at pre-set destination (at the center of coil-20) as shown in Figure 3.14(a) (pink line). Energizing current pulses of different coils used to drive these specific polydisperse droplets are shown in Figure 3.14(b). For the initial three droplets (which are comparatively heavier), no two alternate coils remain simultaneously active; thus, there is no chance of droplet coalescence till 11.5 second. When the fourth droplet passes over the center of coil-13 at 11.72 second, coil-14 is switched on with simultaneous switching-off of coil-13. In a short while (at  $t = 12$  s), the fifth droplet is released with coil-12 switched on. Interestingly, at this moment, two alternative coils (coil-12 and coil-14) remain active on either side of the fourth droplet. However, that does not impact the unidirectional motion of the fourth droplet, as it moves toward coil-14 due to its antecedent high velocity; and continues its transport through subsequent switching of coil-15, coil-16, coil-24 and finally coil-29. Afterward, in the same way, the fifth droplet is transported forward through alternate consecutive coil-3 and coil-15 are switched on during  $t = 13.27$  to  $14.68$  s and both coil-14 and coil-16 are switched on during  $t = 14.9$  to  $16.25$ s. Eventually, all the five droplets are manipulated individually through specific path to its corresponding target within 20.3s (see Figure 3.14(b)). Such operation underscores the feasibility of manipulating droplets of different functional tasks

through different parts (and hence possibly different biochemical conditions) of the same chip.

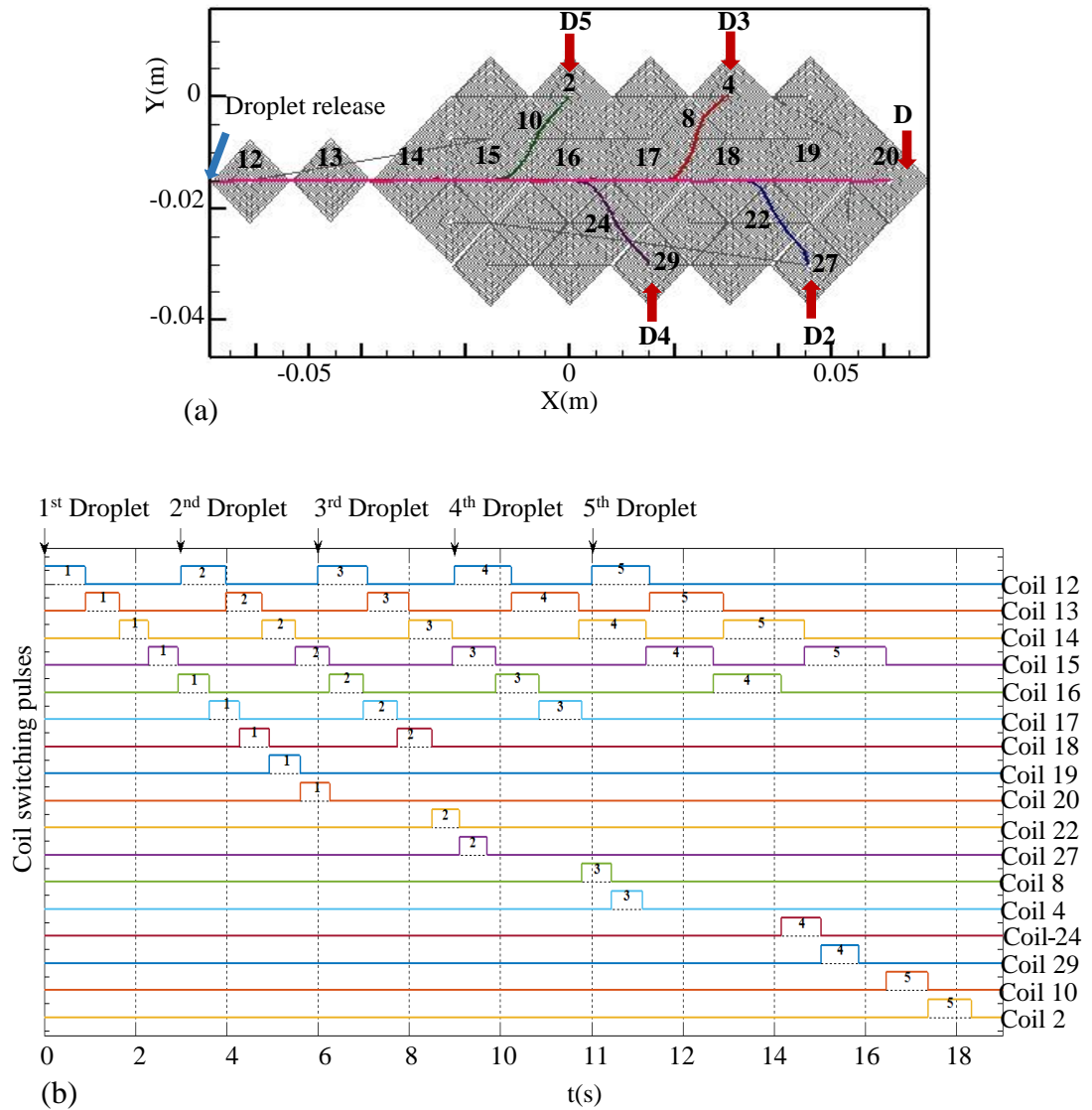


Figure 3.14: Polydisperse droplet trajectories and corresponding coil switching pulses (a) Sequential transport of five droplets of progressively diminishing size (base diameters of 3.4, 3.3, 3.2, 3.1, and 3 mm, respectively) towards specific targets on the chip. Blue arrow denotes the initial droplet dispensing location on the chip (b) Coil-switching pulse for the five poly-dispersed droplets. The numbers under the pulses denote the droplet serials



### 3.3.4.3. Multiple droplets merging and pooling

Merging and pooling of multiple droplets in magnetic digital microfluidics has a wide range of useful applications like in microreactors, medical diagnostics, and drug delivery. By coalescing discrete droplets containing measured quantities of different reagents and analyte samples, one may initiate an intended biochemical reaction, and then transport the resulting droplet containing the products to targeted areas on chip. Sequential merging and transport of droplets, in the same philosophy, may be used to carry out a sequence of biochemical reactions. This section demonstrates sequential merging of multiple droplets and subsequent pooling using the same array of microcoils, but a different switching strategy to suit the specific functional objective. Here, initially a seeding ferrofluid-droplet (D1) having a base diameter of 3.4 mm is released on the substrate at the starting position (shown by the blue arrow in Figure 3.15(a)). Thereafter, it is magnetically steered and sequentially merged with four identical ferrofluid daughter-droplets (D2, D3, D4 and D5, respectively, each spherical cap droplets having footprint diameter of 2 mm) that are dispensed at strategic times at different coil centers (viz., at position A, B, C and D, respectively, as shown in Figure 3.15 (a)) enroute the desired droplet actuation path (shown by the red line). In actual applications, the droplet merging locations (shown by the brown arrows in Figure 3.15. (a)) represent localized on-chip sites of specific reactions that need to take place in a pre-designated sequence [242,243]. This sequenced actuation and merging of droplets [102] create additional functionalities in digital microfluidics, such as immunoassay [244], cell manipulation, tissue culture, drug efficacy [245,121]. The time instants of these droplet-dispensing sequence are marked in Figure 3.15(b). Strategically, the respective coils are switched off immediately before the seeding droplet reaches the coil center (as it travels from the previous coil location). This allows the main droplet to decelerate to a near-zero velocity and merge impact-free with the daughter droplet. For this, a time delay of 1 second is allowed, before the subsequent coil is switched on and the merged droplet begins its onward journey and repeats similar merging operations. Detailed switching pulses of different coil is used in this operation as shown in Figure 3.15(b). At first, the droplet D1 is transported by successive switching on coil-12, coil-13 and coil-14. Coil-14 is switched off as the droplet reaches a point 3 mm ahead of the coil-center; the droplet inertia takes it slowly towards the center of coil-14. By this time the second

ferrofluid droplet D2 (footprint diameter 2mm) is released at position ‘A’ (see Figure8(b)), which merges with the first droplet. After merging, the merged spherical cap ferrofluid droplet (which now has a footprint diameter of 3.62 mm) is transported forward by successive switching of coils-11, coil-1, coil-2, coil-9, etc. Enroute, the droplet is pooled and merged with the third (D3), fourth (D4) and fifth (D5) daughter droplets at point B, C and D, respectively. Finally, the last formed droplet (footprint diameter 3.985 mm) is transported to the center of coil-10 through consecutive switching of coil-16 and coil-15 as shown in Figure8 (b).

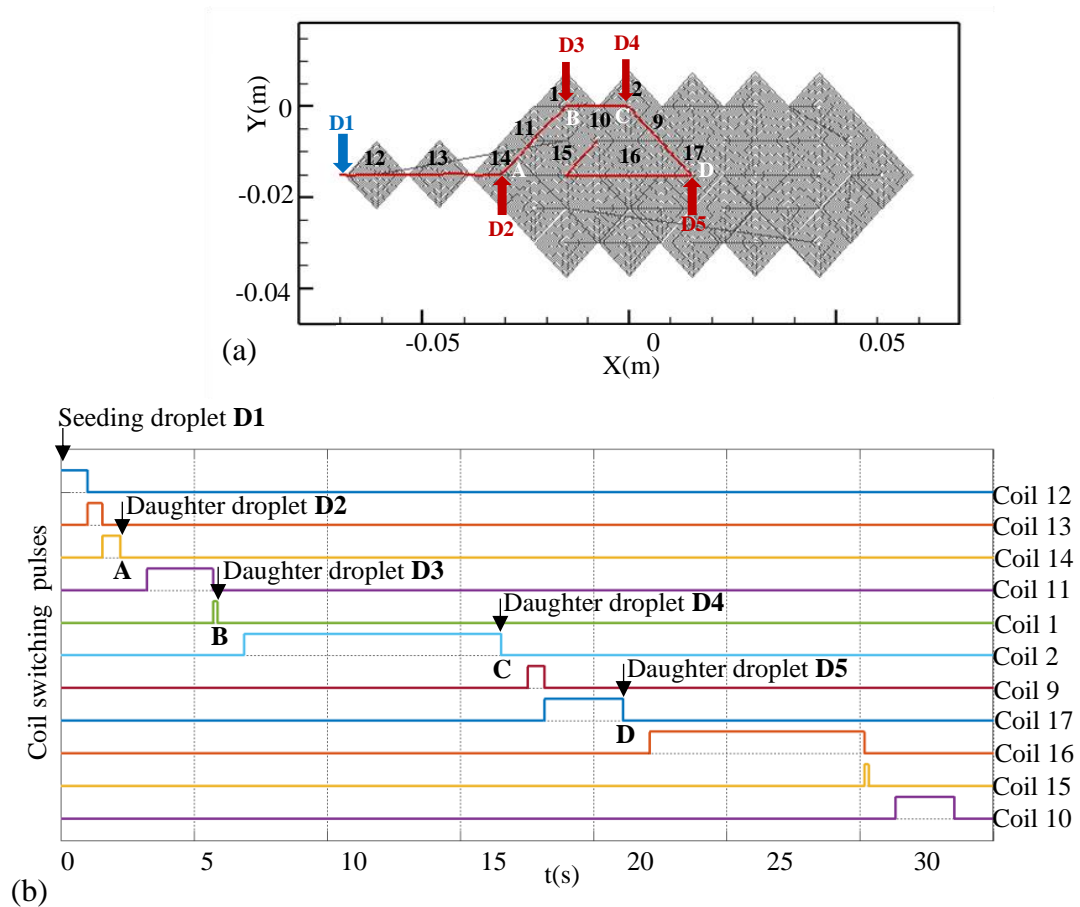


Figure 3.15: Multiple droplets merging and pooling trajectories and corresponding coil switching pulses (a) A spherical cap, seeding ferrofluid-droplet D1 of footprint diameter 3.4 mm droplet sequentially merged with ferrofluid daughter-droplets (D2 through D5, all having footprint diameter of 2 mm) and pooled *enroute* the droplet actuation path (the red line) and reached the preordained destination. (b) Coil-switching pulse for the intended droplet merging and pooling

### 3.4 Closing remark

It is worth noticing that the foregoing numerical simulations do not consider the effect of thermocapillary actuation. In case of a high circuit current (and a coil material of low or moderate electrical conductivity), Joule heating may create temperature gradient along the free surface, entailing thermocapillary migration of the droplet. This would alter the overall droplet transport and would impair the maneuverability, since the thermal signature of the coils would change sluggishly and will not be synchronized with the rapidly changing magnetic field. For systems handling higher currents (e.g., the system studied in some of the simulation cases), one must therefore ensure very good thermal insulation on the top side and excellent heat dissipation at the bottom side of the coils to curb the effect of thermocapillary migration. It must also be noted that for successful on-chip droplet manipulation, the droplet liquid (the host liquid of the ferrofluid in the present case) should be immiscible in the carrier liquid of the film. Thus, oil or lipid droplets in aqueous medium [18], water-based droplets in oil medium [7], droplet interface bilayers [246], or even droplets of aqueous two-phase system [5] would work, if the magnetic nanoparticles can be homogeneously pre-dispersed in the droplet liquid to enable the requisite magnetic actuation. Similar mode of droplet transport may also be realized in nano-liter scale droplets, impregnated with magnetic microspheres [163]. For all these cases, the droplet size (and therefore, the Capillary [247] and magnetic Bond [248] numbers) should be small enough to maintain the integrity of the liquid droplet even when the maximum magnetic and shear forces are at play.

## Chapter 4: Conclusions and Scope of future work

### 4.1. Conclusion:

Two versatile magnetic force-based droplet manipulation strategies have been proposed using an array of planar electromagnetic microcoils embedded in a substrate. The first approach demonstrates controlled manipulation of half-immersed ferrofluid droplets over a thin aqueous film on a flat solid substrate by a periodically switched array of square electromagnetic micro-coils. Magnetic actuation of the droplets is achieved using substrate-embedded array of current carrying micro-coils. First, the field produced by an individual micro-coil is simulated. Predictions of the magnetic force field from a single-coil configuration, and the resulting transient transport of ferrofluid droplet are validated experimentally. Subsequently, the numerical model is used to characterize two-dimensional manipulation of the ferrofluid droplets on the liquid film using periodically switchable array of square-electromagnetic micro-spirals embedded in the flat surface. Ferrofluid droplet motion induced by the micro-coil array is subsequently analyzed for different values of field current, fluid viscosity and droplet size. At relatively low current, ferrofluid droplets exhibit zigzag motion, passing through the centers of the excited coils. However, at larger field currents, the droplet picks up relatively larger momentum and requires high inertial force to steer their trajectories. For cases when the magnetic force falls short of the inertial one, droplet trajectory remains less sensitive to the switching of the coil, deviating from the zigzag path and missing a few coil centers during its transport. Similar behavior is also observed if the host fluid viscosity is reduced or the droplet size is increased since both leads to an increase in magnetic force over the viscous drag. For the regime of viscosity-dominated transport (e.g., at small current  $I$ , large fluid viscosity  $\eta$  or small droplet radius  $R_{FF}$ ), the droplet time-of-flight  $t$  over the coil-array (length of  $\sim 49$  mm) follows the relationships  $t \propto I^{-1.95}$ ,  $t \propto [\eta(2 + 3\xi)/(1 + \xi)]^{0.98}$  and  $t \propto R_{FF}^{-1.98}$ . Overall, the droplet transport time over the length of the active substrate is found to scale linearly with a group-variable  $C = [\eta(2 + 3\xi)/(1 + \xi)]/\chi_m I^2 R_{FF}^2$  for the viscosity-dominated regime of transport. For inertia-dominated transports (e.g., at higher  $I$ , smaller  $\eta$  or larger  $R_{FF}$ ), droplet time-of-flight slightly exceeds this scaling relationship due to inertia-driven over-travels in the positive and negative y-directions. The two-dimensional

manipulation of ferrofluid droplets reported here shows the possibility of complex on-chip handling of biochemically functionalized droplets for different microfluidic tasks. The study can also serve as the basis of a general design criterion for similar ferrofluid droplet-based micro-manipulation devices.

In the second approach two distinct transport models have been discussed where cap volume ferrofluid droplet was manipulated on solid surface. In the first transport model an array of double layer electromagnetic micro-coils is used to actuate a cap volume ferrofluid droplet in a rectilinear path on a solid substrate. Droplet motion was actuated by a periodically switched array of a double layer electromagnetic micro-coils. The two-dimensional rectilinear path of the droplet indicates the prospect of multifaceted on-chip handling of numerous reaction processes. The second transport model demonstrates three exclusive two-dimensional droplet manipulations on a solid hydrophobic surface in the context of proposing a configurable, multitasking surface microfluidic platform by sequentially switched array of electromagnetic micro-coils. In the first two approaches, multiple monodispersed as well as polydispersed ferrofluid droplets were pooled and trapped in different preordained destinations on the chip. In the third embodiment, sequential merging of a seeding ferrofluid droplet with four daughter ferrofluid-droplets at four locations on the chip and pooling of the merged droplets to a target location on the substrate were designed. This magnetic fluid droplet transport model is validated against prior experimental results of gravity-driven sliding on an inclined plane. The velocity dependency of advancing and receding contact angles of the spherical-cap droplet was also validated with experimental observation. It was observed that the droplet transport is strongly impeded by the drag and hysteresis forces. The highly localized nature of the magnetic force implies that the relative spacing of the coils and the switching sequences have important roles in ensuring seamless droplet transport. For the demonstrated on-chip directional transport of the droplet, the transport time  $t$  was found to scale with the droplet diameter  $D$  and the coil current  $I$  as  $t \propto I^{-3.9}$  and  $t \propto D^{-8.2}$ . All these complex on-chip handling of microliter-volume droplets were achieved with the same design of substrate-embedded coils, only with different switching strategies. The study shows the prospect of developing programmable, multitasking on-chip droplet manipulation for versatile surface microfluidic applications.

## 4.2. Scope of future work

Droplet-based Magnetic Digital Microfluidics is an emerging area and holds significant potential for upcoming development and several uses with promising future prospects. It combines the principles of microfluidics, droplet manipulation, and magnetic actuation to enable precise control and manipulation of droplets on a digital platform. Some potential future scopes of work in this field are as follows:

- 1. CFD simulation of droplet transport including the simulations of the transient switching of the electromagnetic coils:** The model will consider solutions of the Navier Stokes equation and will implement volume of fluid (VoF) method to capture the free surface of the droplet. The effect of the transient magnetic field, due to coil-switching, will be considered by appropriately solving Maxwell equations. The effect coil-heating due to the current will be considered by incorporating conjugate heat transfer through the substrate into the liquid. The ensuing temperature gradient may be strong enough to induce thermocapillary actuation, which will also be considered. At a later stage, simulation of multi-component mixing and droplet-mediated biochemical reactions may also be conducted.
- 2. Experimental demonstration of droplet transport and complex manipulation strategies:** As suggested in the present work, surface fabrication may be done on a simple PDMS platform with electrodeposited coils. Surface functionalization may be realized on the top layer of the substrate using Teflon-coating or grafting a self-assembled monolayer of a fluoroalkylsilane.
- 3. Device level integration:** At the third stage, device level integration of an OMDMF-based microfluidic sensor may be taken up. Configurability of the actuating field may be enhanced by real-time feedback of the droplet position signal to actuate the substrate-embedded coils.

Present level serves as the starting point for accomplishing the aforementioned future work. Findings of the present work serves as the design bases for developing the experimental OMDMF platforms. A first-hand idea on the choice of electromagnet size, current level, coil position, switching sequence, substrate size and the target manipulations of the droplet may be derived from the present work. Even at the design and implementation phases in

these future works, the present model and the numerical model may be used for getting quick prediction of the target mode of droplet transport.

## Appendix

### A1: Volume of asymmetrical spherical cap ferrofluid droplet sliding on a solid substrate due to an external force

A liquid drop on a horizontal plane takes the shape of a spherical cap, where the base contour is circular, and the contact angle is constant around the base.

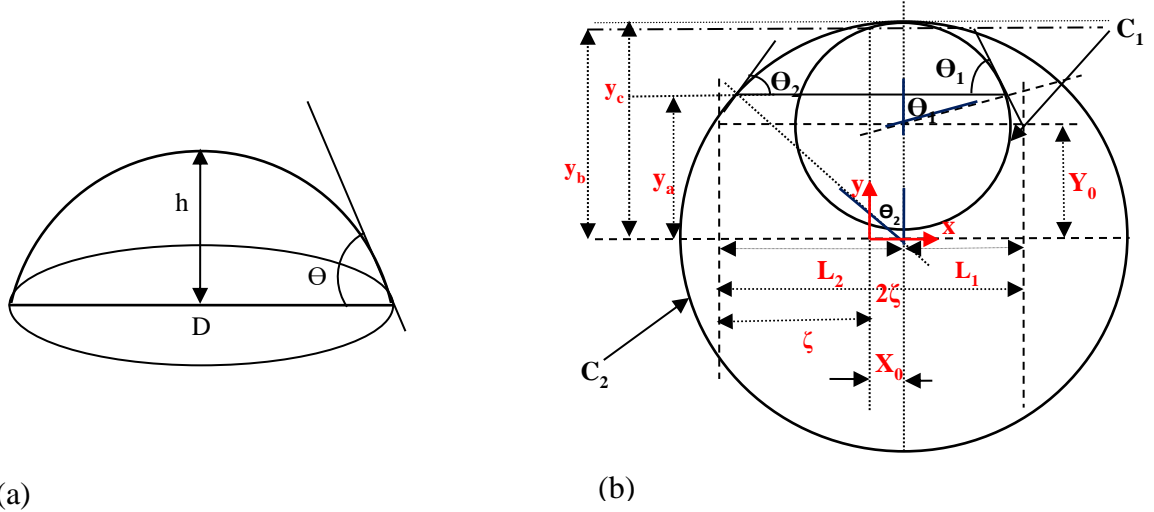


Figure A1: Schematic of a spherical cap droplet and its sliding profile with nomenclature with two-circle method: (a) Schematic diagram of a spherical cap ferrofluid droplet (b) Midsection of spherical cap droplet profile sliding on a solid substrate due to an external force  $F$  with the nomenclature for the two-circle method [154]. Inset figures A1(b) reproduced with permission from Elsevier

A schematic diagram of a spherical cap droplet is shown in Figure 1(a) where  $D$  is the diameter of circular footprint of the spherical cap droplet and  $h$  is the height of droplet. Droplet equilibrium contact angle is  $\theta$ . The volume of spherical cap ferrofluid droplet at rest or equilibrium condition is (without effect of contact angle hysteresis)

$$V = \frac{\pi D^3}{24} \left( \frac{2 - 3\cos\theta + \cos^3\theta}{\sin^3\theta} \right) \quad [A1]$$

Now when droplet tends to move or slide on a solid substrate due to any external force  $F$ , then droplet will not retain in equilibrium shape due to contact angle hysteresis. The volume



of asymmetrical spherical cap droplet was determined by Eisherbini et al can be obtained from Figure A1(b) [154].

The length at the base of the droplet is given as  $2\zeta$ , and the contact angles  $\theta_1$  and  $\theta_2$  are advancing contact angle and receding contact angle respectively. These two circles meet at the highest point of the profile, where  $x = X_0$  and  $y = Y_0$ . The circle with a contact angle  $\theta_1$  and  $\theta_2$  is named C1 (origin  $X_0, 0$ ) and C2 ( $X_0, Y_0$ ) respectively. Equating the height of the droplet from C1 and C2,

$$\frac{L_1}{\sin\theta_1} - \frac{L_1}{\sin\theta_1} \cos\theta_1 = \frac{L_2}{\sin\theta_2} - \frac{L_2}{\sin\theta_2} \cos\theta_2 \quad [\text{A2}]$$

$$\text{Or } \frac{L_1}{L_2} = \frac{\sin\theta_1(1 - \cos\theta_2)}{\sin\theta_2(1 - \cos\theta_1)} \quad [\text{A3}]$$

For simplification  $L_1$  can be expressed as  $L_1 = L_2 L_f$  where  $L_f = \frac{\sin\theta_1(1 - \cos\theta_2)}{\sin\theta_2(1 - \cos\theta_1)}$

In figure 2(b),  $\theta_1$  means  $\theta_A$  (Advance contact angle) and  $\theta_2$  means  $\theta_R$  (Receding contact angle)

Since  $L_1 + L_2 = 2\zeta$  (length of the base of the droplet under CAH),

The variable  $L_1$  and  $L_2$  can be expressed as

$$L_1 = \frac{2\zeta L_f}{1 + L_f}, \quad L_2 = \frac{2\zeta}{1 + L_f}$$

$$y_a = L_2 \tan\theta_2, \quad y_b = \frac{L_2}{\sin\theta_2}, \quad y_c = \sqrt{\frac{L_2^2}{\sin^2\theta_2} - X_0^2} \quad \text{Where } X_0 = \zeta - L_1$$

$$Y_0 = y_a - L_1 \cot\theta_1 = y_b - \frac{L_1}{\sin\theta_1}$$

$V_1$  and  $V_2$  represent the part of the volume of ferrofluid droplet generated by C1 and C2 respectively.

$$V_1 = \int_0^{\frac{\pi}{2}} \left[ \frac{(y_b - Y_0)^3}{3} (2 - 3 \cos \theta_1 + \cos^3 \theta_1) + X_0 (y_b - Y_0)^2 \theta_1 - X_0 (y_a - Y_0)(y_b - Y_0) \sin \theta_1 \right. \\ \left. + X_0^2 (y_b - y_a) - \frac{2}{3} y_b^3 + \frac{2}{3} y_b^2 y_c - X_0^2 y_b + \frac{X_0^2}{3} y_c + X_0 y_b^2 \left( \frac{\pi}{2} - \sin^{-1} \left( \frac{y_c}{y_b} \right) \right) \right] d\phi$$

[A4]

$$V_2 = \int_{\pi}^{\frac{3\pi}{2}} \left[ y_c \left( \frac{2}{3} y_b^2 + \frac{X_0^2}{3} \right) - y_b^2 y_a + \frac{y_a^3}{3} - X_0^2 y_a + X_0 y_a y_b \sin \theta_2 - X_0 y_b^2 \left( \sin^{-1} \left( \frac{y_c}{y_b} \right) - \frac{\pi}{2} + \theta_2 \right) \right] d\phi$$

[A5]

Total volume of the droplet  $V = V_1 + V_2$

## A2: Derivation of the equation to determine thickness or height of the droplet to find resistive frictional drag on the spherical cap ferrofluid droplet

A liquid droplet on a horizontal plane takes the shape of a spherical cap, where the base contour is circular, and the contact angle is constant around the base.

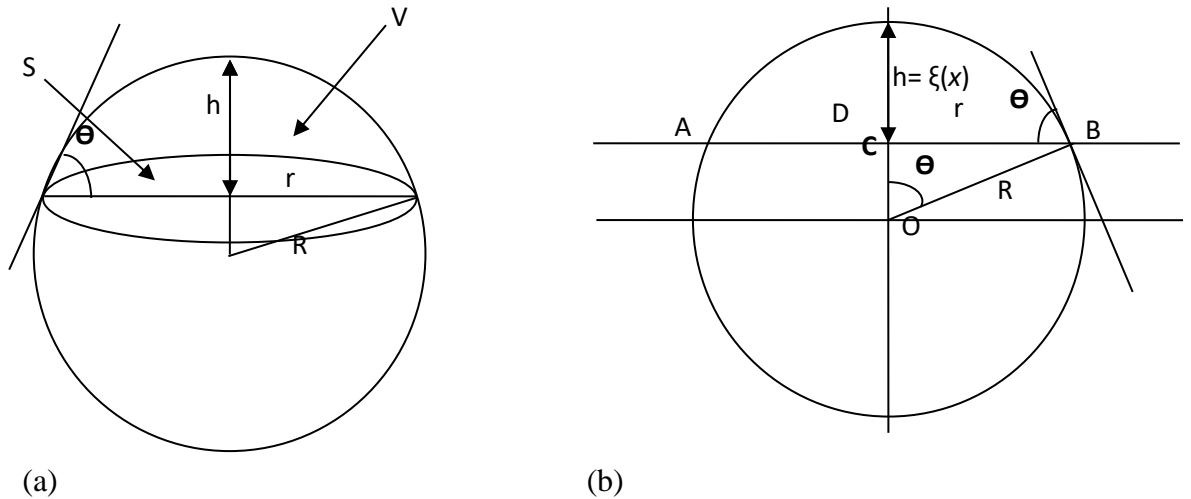


Figure A2: The schematic diagram of extended sphere profile of cap volume droplet at equilibrium position (a) Extended sphere profile of cap volume droplet at equilibrium

position. (b) Midsection profile of spherical cap droplet at rest on a horizontal surface fit by extended circle

Figure 2 (a) shows the schematic diagram of extended sphere profile of cap volume droplet at equilibrium position where  $S$  is the footprint of the spherical cap droplet and  $R$  is the radius of extended sphere. Figure 2(b) represents midsection profile of spherical cap droplet at rest on a horizontal surface fit by extended circle where  $r$  is the radius footprint,  $R$  radius of the extended circle. Here  $AB$  is the droplet diameter. Let co-ordinate of  $A$  is  $(0, 0)$  and Straight-line  $AB$  on the  $x$  axis. So, height of arc from different position of  $AB$  is nothing but the co-ordinate of  $y$  which therefore represents the height or thickness of the droplet from different position of its footprint diameter ( $\xi(x)$ ). Then

$$AC = R \sin\theta, OC = R \cos\theta$$

So, co-ordinate of center of circle is  $(R \sin\theta, -R \cos\theta)$

So, equation of arc is nothing but equation of circle itself.

Hence

$$(x - R \sin\theta)^2 + (y + R \cos\theta)^2 = R^2 \quad [A6a]$$

$$y^2 + 2yR\cos\theta + R^2\cos^2\theta = R^2 - x^2 + 2xR\sin\theta - R^2\sin^2\theta \quad [A6b]$$

$$y^2 + 2yR\cos\theta + (x^2 - 2xR\sin\theta) = 0 \quad [A6c]$$

$$y = \frac{-2R\cos\theta \pm \sqrt{(2R\cos\theta)^2 - 4(x^2 - 2xR\sin\theta)}}{2} \quad [A6d]$$

considering only +ve sign to satisfy above figure.

$$y = \frac{-2R\cos\theta + \sqrt{(2R\cos\theta)^2 - 4(x^2 - 2xR\sin\theta)}}{2} \quad [A6e]$$

Here  $y$  represents instantaneous value of height of the droplet with respect to its footprint diameter  $\xi(x)$  so,

$$\xi(x) = 0.5(-2R\cos\theta + \sqrt{(2R\cos\theta)^2 - 4(x^2 - 2xR\sin\theta)}) \quad [A7]$$

Resistive frictional drag on the spherical cap ferrofluid droplet represented by

$$F_n = 3\eta_{FF}\pi r U \int_{x_{min}}^{x_{max}} \frac{dx}{\xi(x)} \quad [A8]$$

Where  $\eta_{FF}$  and  $r$  are the viscosity and foot-print radius of the cap volume droplet respectively. Where  $U = dS/dt$   $U = dS/dt$  represents velocity of the droplet in x-y plane.

## References

- 1 Dittrich, Petra S., Kaoru Tachikawa, and Andreas Manz. "Micro total analysis systems. Latest advancements and trends." *Analytical Chemistry* 78, no. 12 (2006): 3887-3908.
- 2 Manz, Andréas, N. Graber, and H.M Widmer. "Miniaturized total chemical analysis systems: a novel concept for chemical sensing." *Sensors and Actuators B: Chemical* 1, no. 1-6 (1990): 244-248.
- 3 Neethirajan, Suresh, Isao Kobayashi, Mitsutoshi Nakajima, Dan Wu, Saravanan Nandagopal, and Francis Lin. "Microfluidics for food, agriculture and biosystems industries." *Lab on a Chip* 11, no. 9 (2011): 1574-1586.
- 4 Scanlon, Thomas C., Sarah M. Dostal, and Karl E. Griswold. "A high-throughput screen for antibiotic drug discovery." *Biotechnology and Bioengineering* 111, no. 2 (2014): 232-243.
- 5 Hardt, Steffen, and Thomas Hahn. "Microfluidics with aqueous two-phase systems." *Lab on a Chip* 12, no. 3 (2012): 434-442.
- 6 Washizu, Masao. "Electrostatic actuation of liquid droplets for micro-reactor applications." *IEEE Transactions on Industry Applications* 34, no. 4 (1998): 732-737.
- 7 Tice, Joshua D., Helen Song, Adam D. Lyon, and Rustem F. Ismagilov. "Formation of droplets and mixing in multiphase microfluidics at low values of the Reynolds and the capillary numbers." *Langmuir* 19, no. 22 (2003): 9127-9133.
- 8 Berry, Scott M., Elaine T. Alarid, and David J. Beebe. "One-step purification of nucleic acid for gene expression analysis via Immiscible Filtration Assisted by Surface Tension (IFAST)." *Lab on a Chip* 11, no. 10 (2011): 1747-1753.
- 9 Zhang, Yi, Seungkyung Park, Kelvin Liu, Jennifer Tsuan, Samuel Yang, and Tza-Huei Wang. "A surface topography assisted droplet manipulation platform for biomarker detection and pathogen identification." *Lab on a Chip* 11, no. 3 (2011): 398-406.
- 10 Shamsi, Mohtashim H., Kihwan Choi, Alphonsus HC Ng, and Aaron R. Wheeler. "A digital microfluidic electrochemical immunoassay." *Lab on a Chip* 14, no. 3 (2014): 547-554.
- 11 White, A. K., K. A. Heyries, C. Doolin, M. Vaninsberghe, and C. L. Hansen. "High-throughput microfluidic single-cell digital polymerase chain reaction." *Analytical Chemistry* 85, no. 15 (2013): 7182-7190.
- 12 Zhu, Zhi, Gareth Jenkins, Wenhua Zhang, Mingxia Zhang, Zhichao Guan, and Chaoyong James Yang. "Single-molecule emulsion PCR in microfluidic droplets." *Analytical and Bioanalytical Chemistry* 403 (2012): 2127-2143.
- 13 Bogojevic, Dario, M. Dean Chamberlain, Irena Barbulovic-Nad, and Aaron R. Wheeler. "A digital microfluidic method for multiplexed cell-based apoptosis assays." *Lab on a Chip* 12, no. 3 (2012): 627-634.
- 14 Mary, Pascaline, Vincent Studer, and Patrick Tabeling. "Microfluidic droplet-based liquid-liquid extraction." *Analytical Chemistry* 80, no. 8 (2008): 2680-2687.
- 15 Golberg, Alexander, Martin L. Yarmush, and Tania Konry. "Picoliter droplet microfluidic immunosorbent platform for point-of-care diagnostics of tetanus." *Microchimica Acta* 180 (2013): 855-860.
- 16 Atencia, Javier, and David J. Beebe. "Controlled microfluidic interfaces." *Nature* 437, no. 7059 (2005): 648-655.
- 17 Darhuber, Anton A., and Sandra M. Troian. "Principles of microfluidic actuation by modulation of surface stresses." *Annu. Rev. Fluid Mech.* 37 (2005): 425-455.

- 18 Teh, Shia-Yen, Robert Lin, Lung-Hsin Hung, and Abraham P. Lee. "Droplet microfluidics." *Lab on a Chip* 8, no. 2 (2008): 198-220.
- 19 Tabeling, P. "A brief introduction to slippage, droplets and mixing in microfluidic systems." *Lab on a Chip* 9, no. 17 (2009): 2428-2436.
- 20 Shembekar, Nachiket, Chawaree Chaipan, Ramesh Utharala, and Christoph A. Merten. "Droplet-based microfluidics in drug discovery, transcriptomics and high-throughput molecular genetics." *Lab on a Chip* 16, no. 8 (2016): 1314-1331.
- 21 Davanlou, Ashkan, and Ranganathan Kumar. "Passive mixing enhancement of microliter droplets in a thermocapillary environment." *Microfluidics and Nanofluidics* 19 (2015): 1507-1513.
- 22 Sattari, Amirmohammad, Pedram Hanafizadeh, and Mina Hoorfar. "Multiphase flow in microfluidics: From droplets and bubbles to the encapsulated structures." *Advances in Colloid and Interface Science* 282 (2020): 102208.
- 23 Amirifar, Leyla, Mohsen Besanjideh, Rohollah Nasiri, Amir Shamloo, Fatemeh Nasrollahi, Natan Roberto de Barros, Elham Davoodi et al. "Droplet-based microfluidics in biomedical applications." *Biofabrication* 14, no. 2 (2022): 022001.
- 24 Nooranidoost, Mohammad, Daulet Izbassarov, and Metin Muradoglu. "Droplet formation in a flow focusing configuration: Effects of viscoelasticity." *Physics of Fluids* 28, no. 12 (2016).
- 25 Fu, Taotao, Yining Wu, Youguang Ma, and Huai Z. Li. "Droplet formation and breakup dynamics in microfluidic flow-focusing devices: From dripping to jetting." *Chemical Engineering Science* 84 (2012): 207-217.
- 26 Li, Yuehao, Mranal Jain, Yongting Ma, and Krishnaswamy Nandakumar. "Control of the breakup process of viscous droplets by an external electric field inside a microfluidic device." *Soft Matter* 11, no. 19 (2015): 3884-3899.
- 27 Teo, Adrian JT, Say Hwa Tan, and Nam-Trung Nguyen. "On-demand droplet merging with an AC electric field for multiple-volume droplet generation." *Analytical chemistry* 92, no. 1 (2019): 1147-1153.
- 28 Kahkeshani, Soroush, and Dino Di Carlo. "Drop formation using ferrofluids driven magnetically in a step emulsification device." *Lab on a Chip* 16, no. 13 (2016): 2474-2480.
- 29 Chong, Zhuang Zhi, Say Hwa Tan, Alfonso M. Gañán-Calvo, Shu Beng Tor, Ngiap Hiang Loh, and Nam-Trung Nguyen. "Active droplet generation in microfluidics." *Lab on a Chip* 16, no. 1 (2016): 35-58.
- 30 Yan, Qifan, Shouhu Xuan, Xiaohui Ruan, Jie Wu, and Xinglong Gong. "Magnetically controllable generation of ferrofluid droplets." *Microfluidics and Nanofluidics* 19 (2015): 1377-1384.
- 31 Huang, Jin-Pei, Xue-Hui Ge, Jian-Hong Xu, and Guang-Sheng Luo. "Controlled formation and coalescence of paramagnetic ionic liquid droplets under magnetic field in coaxial microfluidic devices." *Chemical Engineering Science* 152 (2016): 293-300.
- 32 Ghaderi, Atena, Mohammad Hassan Kayhani, Mohsen Nazari, and Keivan Fallah. "Drop formation of ferrofluid at co-flowing microchannel under uniform magnetic field." *European Journal of Mechanics-B/Fluids* 67 (2018): 87-96.
- 33 Liang, Di, Pengcheng Ma, Chunying Zhu, Taotao Fu, Youguang Ma, Kai Wang, and Guangsheng Luo. "Manipulable formation of ferrofluid droplets in Y-shaped flow-focusing

- microchannels." *Industrial & Engineering Chemistry Research* 58, no. 41 (2019): 19226-19238.
- 34 Tan, Say Hwa, and Nam-Trung Nguyen. "Generation and manipulation of monodispersed ferrofluid emulsions: The effect of a uniform magnetic field in flow-focusing and T-junction configurations." *Physical Review E* 84, no. 3 (2011): 036317.
- 35 Tan, Say-Hwa, Nam-Trung Nguyen, Levent Yobas, and Tae Goo Kang. "Formation and manipulation of ferrofluid droplets at a microfluidic T-junction." *Journal of Micromechanics and Microengineering* 20, no. 4 (2010): 045004.
- 36 Zhang, Qindan, Huajun Li, Chunying Zhu, Taotao Fu, Youguang Ma, and Huai Z. Li. "Micro-magnetofluidics of ferrofluid droplet formation in a T-junction." *Colloids and Surfaces A: Physicochemical and Engineering Aspects* 537 (2018): 572-579.
- 37 Alegret, Salvador, ed. Integrated analytical systems. Vol. 39. *Gulf Professional Publishing*, 2003.
- 38 Liu, Jing, Yit Fatt Yap, and Nam-Trung Nguyen. "Numerical study of the formation process of ferrofluid droplets." *Physics of Fluids* 23, no. 7 (2011).
- 39 Ahn, Byungwook, Kangsun Lee, Rajagopal Panchapakesan, and Kwang W. Oh. "On-demand electrostatic droplet charging and sorting." *Biomicrofluidics* 5, no. 2 (2011).
- 40 Link, Darren R., Erwan Grasland-Mongrain, Agnes Duri, Flavie Sarrazin, Zhengdong Cheng, Galder Cristobal, Manuel Marquez, and David A. Weitz. "Electric control of droplets in microfluidic devices." *Angewandte Chemie International Edition* 45, no. 16 (2006): 2556-2560.
- 41 Ahn, Byungwook, Kangsun Lee, Romain Louge, and Kwang W. Oh. "Concurrent droplet charging and sorting by electrostatic actuation." *Biomicrofluidics* 3, no. 4 (2009).
- 42 Singh, Pushpendra, and Nadine Aubry. "Transport and deformation of droplets in a microdevice using dielectrophoresis." *Electrophoresis* 28, no. 4 (2007): 644-657.
- 43 Cho, Sung Kwon, Hyejin Moon, and Chang-Jin Kim. "Creating, transporting, cutting, and merging liquid droplets by electrowetting-based actuation for digital microfluidic circuits." *Journal of Microelectromechanical Systems* 12, no. 1 (2003): 70-80.
- 44 Sen, Uddalok, Souvick Chatterjee, Swarnendu Sen, Manish K. Tiwari, Achintya Mukhopadhyay, and Ranjan Ganguly. "Dynamics of magnetic modulation of ferrofluid droplets for digital microfluidic applications." *Journal of Magnetism and Magnetic Materials* 421 (2017): 165-176.
- 45 Zhang, Kai, Qionglin Liang, Sai Ma, Xuan Mu, Ping Hu, Yiming Wang, and Guoan Luo. "On-chip manipulation of continuous picoliter-volume superparamagnetic droplets using a magnetic force." *Lab on a Chip* 9, no. 20 (2009): 2992-2999.
- 46 Surenjav, Enkhtuul, Craig Priest, Stephan Herminghaus, and Ralf Seemann. "Manipulation of gel emulsions by variable microchannel geometry." *Lab on a Chip* 9, no. 2 (2009): 325-330.
- 47 Roodan, Venos Amiri, Jenifer Gómez-Pastora, Ioannis H. Karampelas, Cristina González-Fernández, Eugenio Bringas, Inmaculada Ortiz, Jeffrey J. Chalmers, Edward P. Furlani, and Mark T. Swihart. "Formation and manipulation of ferrofluid droplets with magnetic

- fields in a microdevice: A numerical parametric study." *Soft Matter* 16, no. 41 (2020): 9506-9518.
- 48 Hatch, Andrew C., Apurva Patel, N. Reginald Beer, and Abraham P. Lee. "Passive droplet sorting using viscoelastic flow focusing." *Lab on a Chip* 13, no. 7 (2013): 1308-1315.
- 49 Murshed, SM Sohel, Say-Hwa Tan, and Nam-Trung Nguyen. "Temperature dependence of interfacial properties and viscosity of nanofluids for droplet-based microfluidics." *Journal of Physics D: Applied Physics* 41, no. 8 (2008): 085502.
- 50 Yap, Yit-Fatt, Say-Hwa Tan, Nam-Trung Nguyen, SM Sohel Murshed, Teck-Neng Wong, and Levent Yobas. "Thermally mediated control of liquid microdroplets at a bifurcation." *Journal of Physics D: Applied Physics* 42, no. 6 (2009): 065503.
- 51 Franke, Thomas, Adam R. Abate, David A. Weitz, and Achim Wixforth. "Surface acoustic wave (SAW) directed droplet flow in microfluidics for PDMS devices." *Lab on a Chip* 9, no. 18 (2009): 2625-2627.
- 52 Schmid, Lothar, David A. Weitz, and Thomas Franke. "Sorting drops and cells with acoustics: acoustic microfluidic fluorescence-activated cell sorter." *Lab on a Chip* 14, no. 19 (2014): 3710-3718.
- 53 Nam, Jeonghun, Hyunjung Lim, Choong Kim, Ji Yoon Kang, and Sehyun Shin. "Density-dependent separation of encapsulated cells in a microfluidic channel by using a standing surface acoustic wave." *Biomicrofluidics* 6, no. 2 (2012).
- 54 Li, Sixing, Xiaoyun Ding, Feng Guo, Yuchao Chen, Michael Ian Lapsley, Sz-Chin Steven Lin, Lin Wang, J. Philip McCoy, Craig E. Cameron, and Tony Jun Huang. "An on-chip, multichannel droplet sorter using standing surface acoustic waves." *Analytical Chemistry* 85, no. 11 (2013): 5468-5474.
- 55 Maddala, Jeevan, Babji Srinivasan, Swastika S. Bithi, Siva A. Vanapalli, and Raghunathan Rengaswamy. "Design of a model-based feedback controller for active sorting and synchronization of droplets in a microfluidic loop." *AIChE Journal* 58, no. 7 (2012): 2120-2130.
- 56 Fradet, Etienne, Craig McDougall, Paul Abbyad, Rémi Dangla, David McGloin, and Charles N. Baroud. "Combining rails and anchors with laser forcing for selective manipulation within 2D droplet arrays." *Lab on a Chip* 11, no. 24 (2011): 4228-4234.
- 57 Harada, Yu, Dong Hyun Yoon, Tetsushi Sekiguchi, and Shuichi Shoji. "Size-oriented passive droplet sorting by using surface free energy with micro guide groove." In *2012 IEEE 25th International Conference on Micro Electro Mechanical Systems (MEMS)*, pp. 1105-1108. IEEE, 2012.
- 58 Numakunai, Satoshi, Afshan Jamsaid, Dong Hyun Yoon, Tetsushi Sekiguchi, and Shuichi Shoji. "Multiple size-oriented passive droplet sorting device and basic approach for digital chemical synthesis." In *2014 IEEE 27th International Conference on Micro Electro Mechanical Systems (MEMS)*, pp. 92-95. IEEE, 2014.
59. Pethig, Ronald. "Dielectrophoresis: Status of the theory, technology, and applications." *Biomicrofluidics* 4, no. 2 (2010).
- 60 Wu, Tianzhun, Yuji Suzuki, and Nobuhide Kasagi. "Electrostatic droplet manipulation using electret as a voltage source." In *2008 IEEE 21st International Conference on Micro Electro Mechanical Systems*, pp. 591-594. IEEE, 2008.



- 61 Wu, Tianzhun, Yuji Suzuki, and Nobuhide Kasagi. "Low-voltage droplet manipulation using liquid dielectrophoresis on electret." *Journal of Micromechanics and Microengineering* 20, no. 8 (2010): 085043.
- 62 Fan, Shih-Kang, Tsung-Han Hsieh, and Di-Yu Lin. "General digital microfluidic platform manipulating dielectric and conductive droplets by dielectrophoresis and electrowetting." *Lab on a Chip* 9, no. 9 (2009): 1236-1242.
- 63 Geng, Hongyao, Jian Feng, Lisa Marie Stabryla, and Sung Kwon Cho. "Droplet manipulations by dielectrowetting: Creating, transporting, splitting, and merging." In *2017 IEEE 30th International Conference on Micro Electro Mechanical Systems (MEMS)*, pp. 113-116. IEEE, 2017.
- 64 Pollack, Michael G., Alexander D. Shenderov, and Richard B. Fair. "Electrowetting-based actuation of droplets for integrated microfluidics." *Lab on a Chip* 2, no. 2 (2002): 96-101.
- 65 Geng, Hongyao, Jian Feng, Lisa Marie Stabryla, and Sung Kwon Cho. "Dielectrowetting manipulation for digital microfluidics: Creating, transporting, splitting, and merging of droplets." *Lab on a Chip* 17, no. 6 (2017): 1060-1068.
- 66 Chiu, Cheng-Pu, Shang-Chih Lin, and Shih-Kang Fan. "Droplet manipulation by electrowetting on polymer dispersed liquid crystal." In *Transducers 2007-2007 International Solid-State Sensors, Actuators and Microsystems Conference*, pp. 295-298. IEEE, 2007.
- 67 Fan, Shih-Kang, Craig Hashi, and Chang-Jin Kim. "Manipulation of multiple droplets on N/spl times/M grid by cross-reference EWOD driving scheme and pressure-contact packaging." In *The Sixteenth Annual International Conference on Micro Electromechanical Systems, 2003. MEMS-03 Kyoto. IEEE*, pp. 694-697. IEEE, 2003.
- 68 Howell, Nathan, and Weihua Li. "Modeling and simulation of droplet translocation and fission by electrowetting-on-dielectrics (EWOD)." *Frontiers of Mechanical Engineering in China* 5 (2010): 376-388.
- 69 Lu, Hsiang-Wei, Frederic Bottausci, Jesse D. Fowler, Andrea L. Bertozzi, and Carl Meinhart. "A study of EWOD-driven droplets by PIV investigation." *Lab on a Chip* 8, no. 3 (2008): 456-461.
- 70 Guttenberg, Zeno, Helena Müller, Heiko Habermüller, Andreas Geisbauer, Jürgen Pipper, Jana Felbel, Mark Kielpinski, Jürgen Scriba, and Achim Wixforth. "Planar chip device for PCR and hybridization with surface acoustic wave pump." *Lab on a Chip* 5, no. 3 (2005): 308-317.
- 71 Beyssen, D., L. Le Brizoual, O. Elmazria, and P. Alnot. "Microfluidic device based on surface acoustic wave." *Sensors and Actuators B: Chemical* 118, no. 1-2 (2006): 380-385.
- 72 Luo, J. K., Yong Qing Fu, Yifan Li, X. Y. Du, A. J. Flewitt, A. J. Walton, and W. I. Milne. "Moving-part-free microfluidic systems for lab-on-a-chip." *Journal of Micromechanics and Microengineering* 19, no. 5 (2009): 054001.
- 73 Cecchini, Marco, Salvatore Girardo, Dario Pisignano, Roberto Cingolani, and Fabio Beltram. "Acoustic-counterflow microfluidics by surface acoustic waves." *Applied Physics Letters* 92, no. 10 (2008).
- 74 Thalhammer, S. "Programmable lab-on-a-chip system for single cell analysis." In *Nanotechnology IV*, SPIE, 7364(2009), 63-77.

- 75 Yakhshi-Tafti, Ehsan, Hyoung J. Cho, and Ranganathan Kumar. "Droplet actuation on a liquid layer due to thermocapillary motion: Shape effect." *Applied Physics Letters* 96, no. 26 (2010).
- 76 Jiao, Z. J., X. Y. Huang, and Nam-Trung Nguyen. "Manipulation of a droplet in a planar channel by periodic thermocapillary actuation." *Journal of Micromechanics and Microengineering* 18, no. 4 (2008): 045027.
- 77 Teste, Bruno, Nicolas Jamond, Davide Ferraro, Jean-Louis Viovy, and Laurent Malaquin. "Selective handling of droplets in a microfluidic device using magnetic rails." *Microfluidics and Nanofluidics* 19 (2015): 141-153.
- 78 Chiou, Chi-Han, Dong Jin Shin, Yi Zhang, and Tza-Huei Wang. "Topography-assisted electromagnetic platform for blood-to-PCR in a droplet." *Biosensors and Bioelectronics* 50 (2013): 91-99.
- 79 Ghazimirsaeed, Erfan, Masoud Madadelahi, Mahdi Dizani, and Amir Shamloo. "Secondary flows, mixing, and chemical reaction analysis of droplet-based flow inside serpentine microchannels with different cross sections." *Langmuir* 37, no. 17 (2021): 5118-5130.
- 80 Sinha Mahapatra, Pallab, Ranjan Ganguly, Aritra Ghosh, Souvick Chatterjee, Sam Lowrey, Andrew D. Sommers, and Constantine M. Megaridis. "Patterning wettability for open-surface fluidic manipulation: fundamentals and applications." *Chemical Reviews* 122, no. 22 (2022): 16752-16801.
- 81 Yang, Chen, Qinghong Zeng, Jinxia Huang, and Zhiguang Guo. "Droplet manipulation on superhydrophobic surfaces based on external stimulation: A review." *Advances in Colloid and Interface Science* 306 (2022): 102724.
- 82 Subramanian, R. Shankar, Nadjoua Moumen, and John B. McLaughlin. "Motion of a drop on a solid surface due to a wettability gradient." *Langmuir* 21, no. 25 (2005): 11844-11849.
- 83 Ciria, Nate J., Adrien Benusiglio, and Manu Prakash. "Vapour-mediated sensing and motility in two-component droplets." *Nature* 519, no. 7544 (2015): 446-450.
- 84 Xing, Siyuan, Jia Jiang, and Tingrui Pan. "Interfacial microfluidic transport on micropatterned superhydrophobic textile." *Lab on a Chip* 13, no. 10 (2013): 1937-1947.
- 85 Yang, Xiaolong, Biao Qi, Yao Lu, Wang Zhang, and Xiaolei Wang. "Bionic surface diode for droplet steering." *Droplet* (2023): e46.
- 86 Shastry, Ashutosh, Marianne J. Case, and Karl F. Böhringer. "Directing droplets using microstructured surfaces." *Langmuir* 22, no. 14 (2006): 6161-6167.
- 87 Sommers, A. D., T. J. Brest, and K. F. Eid. "Topography-based surface tension gradients to facilitate water droplet movement on laser-etched copper substrates." *Langmuir* 29, no. 38 (2013): 12043-12050.
- 88 Khoo, H. S., and F-G. Tseng. "Self-directed movements of droplets on radially patterned surfaces based on self-assembled monolayers." In *2006 International Conference on Microtechnologies in Medicine and Biology*, pp. 273-276. IEEE, 2006.
- 89 Lai, Yu-Hsuan, Jing-Tang Yang, and Dar-Bin Shieh. "A microchip fabricated with a vapor-diffusion self-assembled-monolayer method to transport droplets across superhydrophobic to hydrophilic surfaces." *Lab on a Chip* 10, no. 4 (2010): 499-504.
- 90 Yang, Xiaolong, Jinlong Song, Ni Chen, and Xin Liu. "Open surface multifunctional droplet manipulation platform fabricated by micromilling." *Journal of Materials Science* 54, no. 15 (2019): 10715-10727.

- 91 Morrissette, Jared M., Aritra Ghosh, Raymond Campos, Joseph E. Mates, Joseph M. Mabry, and Constantine M. Megaridis. "Fluorinated Nanocomposite Coatings for Confinement and Pumpless Transport of Low-Surface-Tension Liquids." *Advanced Materials Interfaces* 6, no. 19 (2019): 1901105.
- 92 Park, Jae Woo, Sangcheol Na, Myeongwoo Kang, Sang Jun Sim, and Noo Li Jeon. "PDMS microchannel surface modification with Teflon for algal lipid research." *BioChip Journal* 11 (2017): 180-186.
- 93 Manoharan, Kapil, Mohd Tahir Anwar, and Shantanu Bhattacharya. "Development of hydrophobic paper substrates using silane and sol-gel based processes and deriving the best coating technique using machine learning strategies." *Scientific reports* 11, no. 1 (2021): 11352.
- 94 Quéré, David. "Wetting and roughness." *Annual Review. Mater. Of Res.* 38 (2008): 71-99.
- 95 Nakae, Hideo, Ryuichi Inui, Yosuke Hirata, and Hiroyuki Saito. "Effects of surface roughness on wettability." *Acta Materialia* 46, no. 7 (1998): 2313-2318.
- 96 Ghosh, Aritra, Ranjan Ganguly, Thomas M. Schutzius, and Constantine M. Megaridis. "Wettability patterning for high-rate, pumpless fluid transport on open, non-planar microfluidic platforms." *Lab on a Chip* 14, no. 9 (2014): 1538-1550.
- 97 Morrissette, Jared M., Pallab Sinha Mahapatra, Aritra Ghosh, Ranjan Ganguly, and Constantine M. Megaridis. "Rapid, self-driven liquid mixing on open-surface microfluidic platforms." *Scientific reports* 7, no. 1 (2017): 1800.
- 98 Li, Yan, Jinrong Li, Liwu Liu, Yufeng Yan, Qiuya Zhang, Na Zhang, Linlin He et al. "Switchable wettability and adhesion of micro/nanostructured elastomer surface via electric field for dynamic liquid droplet manipulation." *Advanced Science* 7, no. 18 (2020): 2000772.
- 99 Jin, Yuankai, Wanghui Xu, Huanhuan Zhang, Ruirui Li, Jing Sun, Siyan Yang, Minjie Liu, Haiyang Mao, and Zuankai Wang. "Electrostatic tweezer for droplet manipulation." *Proceedings of the National Academy of Sciences* 119, no. 2 (2022): e2105459119.
- 100 Frozanpoor, Iman, Michael D. Cooke, Vibin Ambukan, Andrew J. Gallant, and Claudio Balocco. "Continuous droplet-actuating platforms via an electric field gradient: electrowetting and liquid dielectrophoresis." *Langmuir* 37, no. 21 (2021): 6414-6422.
- 101 Mats, Lili, Rachel Young, Graham TT Gibson, and Richard D. Oleschuk. "Magnetic droplet actuation on natural (Colocasia leaf) and fluorinated silica nanoparticle superhydrophobic surfaces." *Sensors and Actuators B: Chemical* 220 (2015): 5-12.
- 102 Yang, Chao, Zongwei Zhang, and Gang Li. "Programmable droplet manipulation by combining a superhydrophobic magnetic film and an electromagnetic pillar array." *Sensors and Actuators B: Chemical* 262 (2018): 892-901.
- 103 Darhuber, Anton A., Joseph P. Valentino, Sandra M. Troian, and Sigurd Wagner. "Thermocapillary actuation of droplets on chemically patterned surfaces by programmable microheater arrays." *Journal of Microelectromechanical Systems* 12, no. 6 (2003): 873-879.
- 104 Dai, Qingwen, Yajuan Ji, Wei Huang, and Xiaolei Wang. "On the thermocapillary migration on radially microgrooved surfaces." *Langmuir* 35, no. 28 (2019): 9169-9176.

- 105 Du, X. Y., Yong Qing Fu, J. K. Luo, A. J. Flewitt, and W. I. Milne. "Microfluidic pumps employing surface acoustic waves generated in ZnO thin films." *Journal of Applied Physics* 105, no. 2 (2009).
- 106 Wang, Zhuochen, and Jiang Zhe. "Recent advances in particle and droplet manipulation for lab-on-a-chip devices based on surface acoustic waves." *Lab on a Chip* 11, no. 7 (2011): 1280-1285.
- 107 Huang, C. J., M. S. Ke, and J. T. Yang. "A pneumatic open-surface microfluidic platform for droplet manipulation." In *2013 Transducers & Eurosensors XXVII: The 17th International Conference on Solid-State Sensors, Actuators and Microsystems (TRANSDUCERS & EUROSENSORS XXVII)*, pp. 313-316. IEEE, 2013.
- 108 Huang, C. J., W. F. Fang, M. S. Ke, H. Y. E. Chou, and J. T. Yang. "A biocompatible open-surface droplet manipulation platform for detection of multi-nucleotide polymorphism." *Lab on a Chip* 14, no. 12 (2014): 2057-2062.
- 109 Xu, Wanghui, Yuankai Jin, Wanbo Li, Yuxin Song, Shouwei Gao, Baoping Zhang, Lili Wang, Miaomiao Cui, Xiantong Yan, and Zuankai Wang. "Triboelectric wetting for continuous droplet transport." *Science Advances* 8, no. 51 (2022): eade2085.
- 110 Zhang, Yi, Dong Jin Shin, and Tza-Huei Wang. "Serial dilution via surface energy trap-assisted magnetic droplet manipulation." *Lab on a Chip* 13, no. 24 (2013): 4827-4831.
- 111 Maenaka, Hirosuke, Masumi Yamada, Masahiro Yasuda, and Minoru Seki. "Continuous and size-dependent sorting of emulsion droplets using hydrodynamics in pinched microchannels." *Langmuir* 24, no. 8 (2008): 4405-4410.
- 112 Joensson, Haakan N., Mathias Uhlén, and Helene Andersson Svahn. "Droplet size based separation by deterministic lateral displacement—separating droplets by cell-induced shrinking." *Lab on a Chip* 11, no. 7 (2011): 1305-1310.
- 113 Niu, Xize, Mengying Zhang, Suili Peng, Weijia Wen, and Ping Sheng. "Real-time detection, control, and sorting of microfluidic droplets." *Biomicrofluidics* 1, no. 4 (2007).
- 114 Ahn, Keunho, Charles Kerbage, Tom P. Hunt, R. M. Westervelt, Darren R. Link, and David A. Weitz. "Dielectrophoretic manipulation of drops for high-speed microfluidic sorting devices." *Applied Physics Letters* 88, no. 2 (2006).
- 115 Milsom, Robert F., N. H. C. Reilly, and Martin Redwood. "Analysis of generation and detection of surface and bulk acoustic waves by interdigital transducers." *IEEE Transactions on Sonics Ultrasonics* 24 (1977): 147-166.
- 116 Murshed, SM Sohel, Say Hwa Tan, Nam Trung Nguyen, Teck Neng Wong, and Levent Yobas. "Microdroplet formation of water and nanofluids in heat-induced microfluidic T-junction." *Microfluidics and Nanofluidics* 6 (2009): 253-259.
- 117 Zhang, Qiang, Peiran Zhang, Yetian Su, Chunbo Mou, Teng Zhou, Menglong Yang, Jian Xu, and Bo Ma. "On-demand control of microfluidic flow via capillary-tuned solenoid microvalve suction." *Lab on a Chip* 14, no. 24 (2014): 4599-4603.
- 118 Zhang, Kai, Qionglin Liang, Xiaoni Ai, Ping Hu, Yiming Wang, and Guoan Luo. "On-demand microfluidic droplet manipulation using hydrophobic ferrofluid as a continuous-phase." *Lab on a Chip* 11, no. 7 (2011): 1271-1275.
- 119 Zhang, Jun, Sheng Yan, Dan Yuan, Qianbin Zhao, Say Hwa Tan, Nam-Trung Nguyen, and Weihua Li. "A novel viscoelastic-based ferrofluid for continuous sheathless microfluidic separation of nonmagnetic microparticles." *Lab on a Chip* 16, no. 20 (2016): 3947-3956.

- 120 Al-Hetlani, Entesar, Oliver J. Hatt, Martin Vojtišek, Mark D. Tarn, Alexander Iles, and Nicole Pamme. "Sorting and manipulation of magnetic droplets in continuous flow." In *AIP Conference Proceedings*, vol. 1311, no. 1, pp. 167-175. *American Institute of Physics*, 2010.
- 121 Ray, Ayan, Vijaykumar B. Varma, Zhaomeng Wang, Zhiping Wang, P. J. Jayaneel, Natteri M. Sudharsan, and Raju V. Ramanujan. "Magnetic droplet merging by hybrid magnetic fields." *IEEE Magnetics Letters* 7 (2016): 1-5.
- 122 Varma, Vijaykumar Babulalji, Ayan Ray, Zhao Meng Wang, Zhi Ping Wang, and Raju Vijayaraghavan Ramanujan. "Droplet merging on a lab-on-a-chip platform by uniform magnetic fields." *Scientific Reports* 6, no. 1 (2016): 37671.
- 123 Ray, Ayan, Vijaykumar Babulalji Varma, P. J. Jayaneel, N. M. Sudharsan, Z. P. Wang, and Raju V. Ramanujan. "On demand manipulation of ferrofluid droplets by magnetic fields." *Sensors and Actuators B: Chemical* 242 (2017): 760-768.
- 124 Chatterjee, Debalina, Boonta Hetayothin, Aaron R. Wheeler, Daniel J. King, and Robin L. Garrell. "Droplet-based microfluidics with nonaqueous solvents and solutions." *Lab on a Chip* 6, no. 2 (2006): 199-206.
- 125 Millman, Jeffrey R., Ketan H. Bhatt, Brian G. Prevo, and Orlin D. Velev. "Anisotropic particle synthesis in dielectrophoretically controlled microdroplet reactors." *Nature Materials* 4, no. 1 (2005): 98-102.
- 126 Dubois, Philippe, Gilles Marchand, Yves Fouillet, Jean Berthier, Thierry Douki, Fatima Hassine, Said Gmouh, and Michel Vaultier. "Ionic liquid droplet as e-microreactor." *Analytical Chemistry* 78, no. 14 (2006): 4909-4917.
- 127 Jebraïl, Mais J., Alphonsus HC Ng, Vishal Rai, Ryan Hili, Andrei K. Yudin, and Aaron R. Wheeler. "Synchronized synthesis of peptide-based macrocycles by digital microfluidics." *Angewandte Chemie* 122, no. 46 (2010): 8807-8811.
- 128 Keng, Pei Yuin, Supin Chen, Huijiang Ding, Saman Sadeghi, Gaurav J. Shah, Alex Dooraghi, Michael E. Phelps et al. "Micro-chemical synthesis of molecular probes on an electronic microfluidic device." *Proceedings of the National Academy of Sciences* 109, no. 3 (2012): 690-695.
- 129 Sista, Ramakrishna S., Allen E. Eckhardt, Tong Wang, Carrie Graham, Jeremy L. Rouse, Scott M. Norton, Vijay Srinivasan et al. "Digital microfluidic platform for multiplexing enzyme assays: implications for lysosomal storage disease screening in newborns." *Clinical Chemistry* 57, no. 10 (2011): 1444-1451.
- 130 Vergauwe, Nicolas, Daan Witters, Yegermal T. Atalay, Bert Verbruggen, Steven Vermeir, Frederik Ceyskens, Robert Puers, and Jeroen Lammertyn. "Controlling droplet size variability of a digital lab-on-a-chip for improved bio-assay performance." *Microfluidics and Nanofluidics* 11 (2011): 25-34.
- 131 Choi, Kihwan, Ezel Boyacı, Jihye Kim, Brendon Seale, Luis Barrera-Arbelaez, Janusz Pawliszyn, and Aaron R. Wheeler. "A digital microfluidic interface between solid-phase microextraction and liquid chromatography–mass spectrometry." *Journal of Chromatography A* 1444 (2016): 1-7.
- 132 Witters, Daan, Nicolas Vergauwe, Rob Ameloot, Steven Vermeir, Dirk De Vos, Robert Puers, Bert Sels, and Jeroen Lammertyn. "Digital microfluidic high-throughput printing of single metal-organic framework crystals." *Advanced Materials* 24, no. 10 (2012): 1316-1320.

- 133 Welch, Erin R. Ferguson, Yan-You Lin, Andrew Madison, and Richard B. Fair. "Picoliter DNA sequencing chemistry on an electrowetting-based digital microfluidic platform." *Biotechnology Journal* 6, no. 2 (2011): 165-176.
- 134 Srinivasan, Vijay, Vamsee K. Pamula, and Richard B. Fair. "Droplet-based microfluidic lab-on-a-chip for glucose detection." *Analytica Chimica Acta* 507, no. 1 (2004): 145-150.
- 135 Luk, Vivienne N., Gary CH Mo, and Aaron R. Wheeler. "Pluronic additives: a solution to sticky problems in digital microfluidics." *Langmuir* 24, no. 12 (2008): 6382-6389.
- 136 Au, Sam H., Paresh Kumar, and Aaron R. Wheeler. "A new angle on pluronic additives: advancing droplets and understanding in digital microfluidics." *Langmuir* 27, no. 13 (2011): 8586-8594.
- 137 Perry, Guillaume, Vincent Thomy, Manash R. Das, Yannick Coffinier, and Rabah Boukherroub. "Inhibiting protein biofouling using graphene oxide in droplet-based microfluidic microsystems." *Lab on a Chip* 12, no. 9 (2012): 1601-1604.
- 138 Yang, Hao, Vivienne N. Luk, Mohamed Abelgawad, Irena Barbulovic-Nad, and Aaron R. Wheeler. "A world-to-chip interface for digital microfluidics." *Analytical Chemistry* 81, no. 3 (2009): 1061-1067.
- 139 Barbulovic-Nad, Irena, Hao Yang, Philip S. Park, and Aaron R. Wheeler. "Digital microfluidics for cell-based assays." *Lab on a Chip* 8, no. 4 (2008): 519-526.
- 140 Fiddes, Lindsey K., Vivienne N. Luk, Sam H. Au, Alphonsus HC Ng, Victoria Luk, Eugenia Kumacheva, and Aaron R. Wheeler. "Hydrogel discs for digital microfluidics." *Biomicrofluidics* 6, no. 1 (2012).
- 141 George, Subin M., and Hyejin Moon. "Digital microfluidic three-dimensional cell culture and chemical screening platform using alginate hydrogels." *Biomicrofluidics* 9, no. 2 (2015).
- 142 Hung, Ping-Yi, Pei-Shing Jiang, Erh-Fang Lee, Shih-Kang Fan, and Yen-Wen Lu. "Genomic DNA extraction from whole blood using a digital microfluidic (DMF) platform with magnetic beads." *Microsystem Technologies* 23 (2017): 313-320.
- 143 Zeng, Zhi, Kaidi Zhang, Wei Wang, Weijiang Xu, and Jia Zhou. "Portable electrowetting digital microfluidics analysis platform for chemiluminescence sensing." *IEEE Sensors Journal* 16, no. 11 (2016): 4531-4536.
- 144 Sista, Ramakrishna, Zhishan Hua, Prasanna Thwar, Arjun Sudarsan, Vijay Srinivasan, Allen Eckhardt, Michael Pollack, and Vamsee Pamula. "Development of a digital microfluidic platform for point of care testing." *Lab on a Chip* 8, no. 12 (2008): 2091-2104.
- 145 Kim, Hanyoup, Michael S. Bartsch, Ronald F. Renzi, Jim He, James L. Van de Vreugde, Mark R. Claudnic, and Kamlesh D. Patel. "Automated digital microfluidic sample preparation for next-generation DNA sequencing." *JALA: Journal of the Association for Laboratory Automation* 16, no. 6 (2011): 405-414.
- 146 Yafia, Mohamed, Ali Ahmadi, Mina Hoorfar, and Homayoun Najjaran. "Ultra-portable smartphone controlled integrated digital microfluidic system in a 3D-printed modular assembly." *Micromachines* 6, no. 9 (2015): 1289-1305.
- 147 West, Jonathan, Marco Becker, Sven Tombrink, and Andreas Manz. "Micro total analysis systems: latest achievements." *Analytical Chemistry* 80, no. 12 (2008): 4403-4419.
- 148 Schneider, John, Ana Egatz-Gómez, Sonia Melle, S. Lindsay, P. Dominguez-Garcia, M. A. Rubio, M. Marquez, and Antonio A. García. "Motion of viscous drops on

- superhydrophobic surfaces due to magnetic gradients." *Colloids and Surfaces A: Physicochemical and Engineering Aspects* 323, no. 1-3 (2008): 19-27.
- 149 Marston, J. O., Sigurdur T. Thoroddsen, W. K. Ng, and R. B. H. Tan. "Experimental study of liquid drop impact onto a powder surface." *Towder Technology* 203, no. 2 (2010): 223-236.
- 150 Yonemoto, Yukihiro, Shosuke Suzuki, Sae Uenomachi, and Tomoaki Kunugi. "Sliding behaviour of water-ethanol mixture droplets on inclined low-surface-energy solid." *International Journal of Heat and Mass Transfer* 120 (2018): 1315-1324.
- 151 Dupont, Jean-Baptiste, and Dominique Legendre. "Numerical simulation of static and sliding drop with contact angle hysteresis." *Journal of Computational Physics* 229, no. 7 (2010): 2453-2478.
- 152 ElSherbini, A. I., and Anthony M. Jacobi. "Liquid drops on vertical and inclined surfaces: I. An experimental study of drop geometry." *Journal of Colloid and Interface Science* 273, no. 2 (2004): 556-565.
- 153 ElSherbini, Abdelrahman I. *Modeling condensate drops retained on the air-side of heat exchangers*. University of Illinois at Urbana-Champaign, 2003.
- 154 ElSherbini, A. I., and A. M. Jacobi. "Retention forces and contact angles for critical liquid drops on non-horizontal surfaces." *Journal of colloid and interface science* 299, no. 2 (2006): 841-849.
- 155 Annapragada, S. Ravi, Jayathi Y. Murthy, and Suresh V. Garimella. "Droplet retention on an incline." *International Journal of Heat and Mass Transfer* 55, no. 5-6 (2012): 1457-1465.
- 156 Annapragada, S. Ravi, Jayathi Y. Murthy, and Suresh V. Garimella. "Prediction of droplet dynamics on an incline." *International Journal of Heat and Mass Transfer* 55, no. 5-6 (2012): 1466-1474.
- 157 Ahmed, Gulraiz, Mathieu Sellier, Mark Jermy, and Michael Taylor. "Modeling the effects of contact angle hysteresis on the sliding of droplets down inclined surfaces." *European Journal of Mechanics-B/Fluids* 48 (2014): 218-230.
- 158 Chaudhury, Manoj K., and George M. Whitesides. "How to make water run uphill." *Science* 256, no. 5063 (1992): 1539-1541.
- 159 Kooij, Ernst S., H. P. Jansen, O. Bliznyuk, Bene Poelsema, and Henricus JW Zandvliet. "Directional wetting on chemically patterned substrates." *Colloids and surfaces A: Physicochemical and Engineering Aspects* 413 (2012): 328-333.
- 160 Lv, Cunjing, and Pengfei Hao. "Driving droplet by scale effect on microstructured hydrophobic surfaces." *Langmuir* 28, no. 49 (2012): 16958-16965.
- 161 Yang, Jing-Tang, Zong-Han Yang, Chien-Yang Chen, and Da-Jeng Yao. "Conversion of surface energy and manipulation of a single droplet across micropatterned surfaces." *Langmuir* 24, no. 17 (2008): 9889-9897.
- 162 Chandesris, Benoit, Ulrich Soupremanien, and Nicolas Dunoyer. "Uphill motion of droplets on tilted and vertical grooved substrates induced by a wettability gradient." *Colloids and Surfaces A: Physicochemical and Engineering Aspects* 434 (2013): 126-135.

- 163 Moumen, Nadjoua, R. Shankar Subramanian, and John B. McLaughlin. "Experiments on the motion of drops on a horizontal solid surface due to a wettability gradient." *Langmuir* 22, no. 6 (2006): 2682-2690.
- 164 Shikida, Mitsuhiro, Kentaro Takayanagi, Kohta Inouchi, Hiroyuki Honda, and Kazuo Sato. "Using wettability and interfacial tension to handle droplets of magnetic beads in a micro-chemical-analysis system." *Sensors and Actuators B: Chemical* 113, no. 1 (2006): 563-569.
- 165 Bliznyuk, O., H. Patrick Jansen, E. Stefan Kooij, Harold JW Zandvliet, and Bene Poelsema. "Smart design of stripe-patterned gradient surfaces to control droplet motion." *Langmuir* 27, no. 17 (2011): 11238-11245.
- 166 Zhang, Yi, and Nam-Trung Nguyen. "Magnetic digital microfluidics—a review." *Lab on a Chip* 17, no. 6 (2017): 994-1008.
167. Zhang, Yi, and Tza-Huei Wang. "Full-range magnetic manipulation of droplets via surface energy traps enables complex bioassays." *Advanced Materials* 25, no. 21 (2013): 2903-2908.
- 168 Lehmann, Ulrike, Smail Hadjidj, Virendra K. Parashar, Caroline Vandevyver, Amar Rida, and Martin AM Gijs. "Two-dimensional magnetic manipulation of microdroplets on a chip as a platform for bioanalytical applications." *Sensors and Actuators B: Chemical* 117, no. 2 (2006): 457-463.
- 169 Sharma, Himani, Kimberley John, Anvesh Gaddam, Ambuja Navalkar, Samir K. Maji, and Amit Agrawal. "A magnet-actuated biomimetic device for isolating biological entities in microwells." *Scientific Reports* 8, no. 1 (2018): 12717.
- 170 Zhang, Yi, and Tza-Huei Wang. "Micro magnetic gyromixer for *Analytical* speeding up reactions in droplets." *Microfluidics and Nanofluidics* 12 (2012): 787-794.
- 171 Goya, Gerardo F., S. L. Gómez, and Suhaila Maluf Shibli. "Magnetic dynamics of iron-oxide nanoparticles in frozen ferrofluids and ferronematics." *Journal of Metastable and Nanocrystalline Materials* 22 (2004): 33-38.
- 172 Rosensweig, Ronald E. Ferrohydrodynamics. *Courier Corporation*, (2013), ISBN 978-0-486-67834-4
- 173 Shin, Dong Jin, and Tza-Huei Wang. "Magnetic droplet manipulation platforms for nucleic acid detection at the point of care." *Annals of Biomedical Engineering* 42 (2014): 2289-2302.
- 174 Ng, Alphonsus HC, Kihwan Choi, Robert P. Luoma, John M. Robinson, and Aaron R. Wheeler. "Digital microfluidic magnetic separation for particle-based immunoassays." *Analytical Chemistry* 84, no. 20 (2012): 8805-8812.
- 175 Huang, Cheng-Yeh, Po-Yen Tsai, I. Lee, Hsin-Yun Hsu, Hong-Yuan Huang, Shih-Kang Fan, Da-Jeng Yao, Cheng-Hsien Liu, and Wensyang Hsu. "A highly efficient bead extraction technique with low bead number for digital microfluidic immunoassay." *Biomicrofluidics* 10, no. 1 (2016).
- 176 Coudron, Loïc, Martin B. McDonnell, Ian Munro, Daniel K. McCluskey, Ian D. Johnston, Christabel KL Tan, and Mark C. Tracey. "Fully integrated digital microfluidics platform



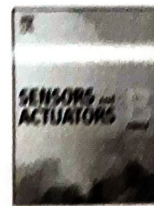
- for automated immunoassay; A versatile tool for rapid, specific detection of a wide range of pathogens." *Biosensors and Bioelectronics* 128 (2019): 52-60.
- 177 Liu, Qi, Xinlian Zhang, Xiaoxu Li, Sixiu Liu, and Guodong Sui. "A semi-quantitative method for point-of-care assessments of specific pathogenic bioaerosols using a portable microfluidics-based device." *Journal of Aerosol Science* 115 (2018): 173-180.
- 178 Lee, Chang Heon, Hyunho Seok, Woohyuk Jang, Ji Tae Kim, Geunsang Park, Hyeong-U. Kim, Jihun Rho, Taesung Kim, and Taek Dong Chung. "Bioaerosol monitoring by integrating DC impedance microfluidic cytometer with wet-cyclone air sampler." *Biosensors and Bioelectronics* 192 (2021): 113499.
- 179 Jagannath, Akshaya, Hengji Cong, Jaythoon Hassan, Gabriel Gonzalez, Michael D. Gilchrist, and Nan Zhang. "Pathogen detection on microfluidic platforms: Recent advances, challenges, and prospects." *Biosensors and Bioelectronics: X* 10 (2022): 100134.
- 180 Hunt, Thomas P., David Issadore, and Robert M. Westervelt. "Integrated circuit/microfluidic chip to programmably trap and move cells and droplets with dielectrophoresis." *Lab on a Chip* 8, no. 1 (2008): 81-87.
- 181 Dumas, Simon, Mathilde Richerd, Marco Serra, and Stéphanie Descroix. "Magnetic Microtweezers: A Tool for High-Throughput Bioseparation in Sub-Nanoliter Droplets." *Advanced Materials Technologies* 8, no. 1 (2023): 2200747.
- 182 Quynh, L. K., B. D. Tu, D. X. Dang, D. Q. Viet, L. T. Hien, DT Huong Giang, and N. H. Duc. "Detection of magnetic nanoparticles using simple AMR sensors in Wheatstone bridge." *Journal of Science: Advanced Materials and Devices* 1, no. 1 (2016): 98-102.
- 183 Probst, R., J. Lin, A. Komae, A. Nacey, Z. Cummins, and B. Shapiro. "Planar steering of a single ferrofluid drop by optimal minimum power dynamic feedback control of four electromagnets at a distance." *Journal of Magnetism and Magnetic Materials* 323, no. 7 (2011): 885-896.
- 184 Yu, Wenzhuo, Haisong Lin, Yilian Wang, Xu He, Nathan Chen, Kevin Sun, Darren Lo et al. "A ferrobatic system for automated microfluidic logistics." *Science Robotics* 5, no. 39 (2020): eaba4411.
- 185 Li, An, Huizeng Li, Zheng Li, Zhipeng Zhao, Kaixuan Li, Mingzhu Li, and Yanlin Song. "Programmable droplet manipulation by a magnetic-actuated robot." *Science advances* 6, no. 7 (2020): eaay5808.

- 186 Long, Zhicheng, Abhishek M. Shetty, Michael J. Solomon, and Ronald G. Larson. "Fundamentals of magnet-actuated droplet manipulation on an open hydrophobic surface." *Lab on a Chip*, no. 11 (2009): 1567-1575.
- 187 Seo, K. S., R. Wi, SungGap Im, and DoHyun Kim. "A superhydrophobic magnetic elastomer actuator for droplet motion control." *Polymers for Advanced Technologies* 24, no. 12 (2013): 1075-1080.
- 188 Assadsangabi, B., MS Mohamed Ali, and K. Takahata. "Bidirectional actuation of ferrofluid using micropatterned planar coils assisted by bias magnetic fields." *Sensors and Actuators A: Physical* 173, no. 1 (2012): 219-226.
- 189 Damodara, S., and A. K. Sen. "Magnetic field assisted droplet manipulation on a soot-wax coated superhydrophobic surface of a PDMS-iron particle composite substrate." *Sensors and Actuators B: Chemical* 239 (2017): 816-823.
- 190 Berthier, Jean, "Microdrops and Digital Microfluidics", *William Andrew* (2008), ISBN 978-0-8155-1544-9, page 195
- 191 Banerjee, U., and A. K. Sen. "Shape evolution and splitting of ferrofluid droplets on a hydrophobic surface in the presence of a magnetic field." *Soft Matter* 14, no. 15 (2018): 2915-2922.
- 192 Edalatpour, Mojtaba, Andrew D. Sommers, and Khalid F. Eid. "Variations of the static contact angle of ferrofluid droplets on solid horizontal surfaces in external uniform magnetic fields." *Langmuir* 36, no. 22 (2019): 6314-6322.
- 193 Dey, Ranabir, Udit Uday Ghosh, Suman Chakraborty, and Sunando DasGupta. "Dynamics of electrically modulated colloidal droplet transport." *Langmuir* 31, no. 41 (2015): 11269-11278.
- 194 Beyzavi, Ali, and Nam-Trung Nguyen. "Programmable two-dimensional actuation of ferrofluid droplet using planar microcoils." *Journal of Micromechanics and Microengineering* 20, no. 1 (2009): 015018.
- 195 Nahar, M. M., J. B. Nikapitiya, S. M. You, and H. Moon. "Droplet velocity in an electrowetting on dielectric digital microfluidic device" *Micromachines* 7 (71): 1–16." (2016).
- 196 Fan, Xinjian, Xiaoguang Dong, Alp C. Karacakol, Hui Xie, and Metin Sitti. "Reconfigurable multifunctional ferrofluid droplet robots." *Proceedings of the National Academy of Sciences* 117, no. 45 (2020): 27916-27926.
- 197 Lee, Junghoon, Hyejin Moon, Jesse Fowler, Thomas Schoellhammer, and Chang-Jin Kim. "Electrowetting and electrowetting-on-dielectric for microscale liquid handling." *Sensors and actuators a: Physical* 95, no. 2-3 (2002): 259-268.
- 198 Liu, Yi-Wei, Qing-Feng Zhan, and Run-Wei Li. "Fabrication, properties, and applications of flexible magnetic films." *Chinese Physics B* 22, no. 12 (2013): 127502.
- 199 Nguyen, Nam-Trung, Gulping Zhu, Yong-Chin Chua, Vinh-Nguyen Phan, and Say-Hwa Tan. "Magnetowetting and sliding motion of a sessile ferrofluid droplet in the presence of a permanent magnet." *Langmuir* 26, no. 15 (2010): 12553-12559.
- 200 Nguyen, Nam-Trung, Ali Beyzavi, Kon Meng Ng, and Xiaoyang Huang. "Kinematics and deformation of ferrofluid droplets under magnetic actuation." *Microfluidics and Nanofluidics* 3 (2007): 571-579.
- 201 Chen, Ge, Yi bo Gao, Mingzhong Li, Bing Ji, Rui Tong, Man-Kay Law, Weijia Wen, and Bingpu Zhou. "Rapid and flexible actuation of droplets via a low-adhesive and deformable

- magnetically functionalized membrane." *Journal of Materials Science* 53 (2018): 13253-13263.
- 202 Ganguly, Ranjan, and Ishwar K. Puri. "Microfluidic transport in magnetic MEMS and bioMEMS." *Wiley Interdisciplinary Reviews: Nanomedicine and Nanobiotechnology* 2, no. 4 (2010): 382-399.
- 203 Ramadan, Qasem, Daniel P. Poenar, and Chen Yu. "Customized trapping of magnetic particles." *Microfluidics and Nanofluidics* 6 (2009): 53-62.
- 204 Lee, Hakho, Alfreda M. Purdon, Vincent Chu, and Robert M. Westervelt. "Controlled assembly of magnetic nanoparticles from magnetotactic bacteria using microelectromagnets arrays." *Nano Letters* 4, no. 5 (2004): 995-998.
- 205 Rida, A., V. Fernandez, and M. A. M. Gijs. "Planar coil-based microsystem for the long-range transport of magnetic beads." In *TRANSDUCERS'03. 12th International Conference on Solid-State Sensors, Actuators and Microsystems. Digest of Technical Papers (Cat. No. 03TH8664)*, vol. 1, pp. 292-295. IEEE, 2003.
- 206 Lehmann, Ulrike, Maximilian Sergio, Stefano Pietrocola, Cristiano Niclass, Edoardo Charbon, and Martin AM Gijs. "A CMOS microsystem combining magnetic actuation and in-situ optical detection of microparticles." In *TRANSDUCERS 2007-2007 International Solid-State Sensors, Actuators and Microsystems Conference*, pp. 2493-2496. IEEE, 2007.
- 207 Beyzavi, Ali, and Nam-Trung Nguyen. "One-dimensional actuation of a ferrofluid droplet by planar microcoils." *Journal of Physics D: Applied Physics* 42, no. 1 (2008): 015004.
- 208 Deng, Tao, George M. Whitesides, Mala Radhakrishnan, Gary Zabow, and Mara Prentiss. "Manipulation of magnetic microbeads in suspension using micromagnetic systems fabricated with soft lithography." *Applied Physics Letters* 78, no. 12 (2001): 1775-1777.
- 209 Zheng, Yushan, Sara Bekhiche, and Mohamad Sawan. "Planar microcoils array applied to magnetic beads based lab-on-chip for high throughput applications." In *2011 IEEE International Symposium of Circuits and Systems (ISCAS)*, pp. 2345-2348. IEEE, 2011.
- 210 Fulcrand, Rémy, Aurélien Bancaud, Christophe Escriba, Qihao He, Samuel Charlot, Ali Boukabache, and Anne-Marie Gué. "On chip magnetic actuator for batch-mode dynamic manipulation of magnetic particles in compact lab-on-chip." *Sensors and Actuators B: Chemical* 160, no. 1 (2011): 1520-1528.
- 211 Nguyen, Nam-Trung, Kon Meng Ng, and Xiaoyang Huang. "Manipulation of ferrofluid droplets using planar coils." *Applied Physics Letters* 89, no. 5 (2006).
- 212 Hang Koh, Wei, Khoi Seng Lok, and Nam-Trung Nguyen. "A digital micro magnetofluidic platform for lab-on-a-chip applications." *Journal of Fluids Engineering* 135, no. 2 (2013): 021302.
- 213 Bijarchi, Mohamad Ali, Amirhossein Favakeh, Erfan Sedighi, and Mohammad Behshad Shafii. "Ferrofluid droplet manipulation using an adjustable alternating magnetic field." *Sensors and Actuators A: Physical* 301 (2020): 111753.
- 214 Kim, Jeong Ah, Moojong Kim, Sung Min Kang, Kun Taek Lim, Tae Song Kim, and Ji Yoon Kang. "Magnetic bead droplet immunoassay of oligomer amyloid  $\beta$  for the diagnosis of Alzheimer's disease using micro-pillars to enhance the stability of the oil-water interface." *Biosensors and Bioelectronics* 67 (2015): 724-732.

- 215 Shi, Xu, Chun-Hong Chen, Weimin Gao, Shih-hui Chao, and Deirdre R. Meldrum. "Parallel RNA extraction using magnetic beads and a droplet array." *Lab on a Chip* 15, no. 4 (2015): 1059-1065.
- 216 Lin, Gungun, Larysa Baraban, Luyang Han, Daniil Karnaushenko, Denys Makarov, Gianarelio Cuniberti, and Oliver G. Schmidt. "Magnetoresistive emulsion analyzer." *Scientific Reports* 3, no. 1 (2013): 2548.
- 217 Alexiou, Christoph, Wolfgang Arnold, Roswitha J. Klein, Fritz G. Parak, Peter Hulin, Christian Bergemann, Wolfgang Erhardt, Stefan Wagenpfeil, and Andreas S. Lubbe. "Locoregional cancer treatment with magnetic drug targeting." *Cancer Research* 60, no. 23 (2000): 6641-6648.
- 218 Griffiths, David J. "Introduction to Electrodynamics." *Cambridge University Press* (2005): ISBN 978-110-88-2290-9, pp 574-574.
- 219 Santra, Arunava, Niladri Chakraborty, and Ranjan Ganguly. "Analytical evaluation of magnetic field by planar micro-electromagnet spirals for MEMS applications." *Journal of Micromechanics and Microengineering* 19, no. 8 (2009): 085018.
- 220 Robert, C. O., and O. Handley. "Modern magnetic materials: principles and applications." *Ed. John Wiley & Sons, Inc., New York* (2000): 23.
- 221 Som, S. K., S. K. Dash, A. K. Mitra, and S. P. Sengupta. "Transport coefficients of an evaporating liquid drop in creeping flow." *Waerme-Stoffuebertrag.:(Germany, Federal Republic of)* 24, no. 3 (1989).
- 222 Peters, Franz, and Björn Gaertner. "Scaling parameters of bubbles and drops; interpretation and case study with air in silicon oil." *Acta Mechanica* 219 (2011): 189-202.
- 223 Sinha, Ashok, Ranjan Ganguly, Anindya K. De, and Ishwar K. Puri. "Single magnetic particle dynamics in a microchannel." *Physics of Fluids* 19, no. 11 (2007).
- 224 Daniel, Susan, and Manoj K. Chaudhury. "Rectified motion of liquid drops on gradient surfaces induced by vibration." *Langmuir* 18, no. 9 (2002): 3404-3407.
- 225 Chakraborty, Monojit, Udit Uday Ghosh, Suman Chakraborty, and Sunando DasGupta. "Thermally enhanced self-propelled droplet motion on gradient surfaces." *RSC Advances* 5, no. 56 (2015): 45266-45275.
- 226 Moumen, Nadjoua, R. Shankar Subramanian, and John B. McLaughlin. "Experiments on the motion of drops on a horizontal solid surface due to a wettability gradient." *Langmuir* 22, no. 6 (2006): 2682-2690.
- 227 Marmur, Abraham, and Eyal Bittoun. "When Wenzel and Cassie are right: reconciling local and global considerations." *Langmuir* 25, no. 3 (2009): 1277-1281.
- 228 Petrov, P., and I. Petrov. "A combined molecular-hydrodynamic approach to wetting kinetics." *Langmuir* 8, no. 7 (1992): 1762-1767.
- 229 Voinov, O. V. "Hydrodynamics of wetting." *Fluid Dynamics* 11, no. 5 (1976): 714-721.
- 230 Cox, R. G. "The dynamics of the spreading of liquids on a solid surface. Part 1. Viscous flow." *Journal of Fluid Mechanics* 168 (1986): 169-194.
- 231 Yarnold, G. D., and B. J. Mason. "A Theory of the Angle of Contact." *Proceedings of the Physical Society. Section B* 62, no. 2 (1949): 121.
- 232 Blake, T. D., and J. M. Haynes. "Kinetics of liquidliquid displacement." *Journal of Colloid and Interface Science* 30, no. 3 (1969): 421-423.
- 233 Dutta, Susovan. 2008. "Characterizing Magnetic field from Planar Spiral Electromagnets for Microfluidic Applications." ME diss. *Jadavpur University, Kolkata*

- 234 Rosensweig, R. E., S. Elborai, S-H. Lee, and M. Zahn. "Ferrofluid meniscus in a horizontal or vertical magnetic field." *Journal of Magnetism and Magnetic Materials* 289 (2005): 192-195.
- 235 Ekwebelam, C. C., and H. See. "Determining the flow curves for an inverse ferrofluid." *Korea-Australia Rheology Journal* 20, no. 1 (2008): 35-42.
- 236 Balu, Balamurali, Adam D. Berry, Dennis W. Hess, and Victor Breedveld. "Patterning of superhydrophobic paper to control the mobility of micro-liter drops for two-dimensional lab-on-paper applications." *Lab on a Chip* 9, no. 21 (2009): 3066-3075.
- 237 Podgorski, T., J-M. Flesselles, and L. Limat. "Corners, cusps, and pearls in running drops." *Physical Review Letters* 87, no. 3 (2001): 036102.
- 238 Schneemilch, Matthew, Robert A. Hayes, Jordan G. Petrov, and John Ralston. "Dynamic wetting and dewetting of a low-energy surface by pure liquids." *Langmuir* 14, no. 24 (1998): 7047-7051.
- 239 Paulssen, Dorothea, Steffen Hardt, and Pavel A. Levkin. "Droplet sorting and manipulation on patterned two-phase slippery lubricant-infused surface." *ACS Applied Materials & Interfaces* 11, no. 17 (2019): 16130-16138.
- 240 R. Karwa, Heat and Mass Transfer, Springer, ISBN 978-981-10-1556-4, pp323-333.
- 241 Alex, Ancy Smitha, R. S. Rajeev, K. Krishnaraj, N. Sreenivas, S. K. Manu, C. Gouri, and V. Sekkar. "Thermal protection characteristics of polydimethylsiloxane-organoclay nanocomposite." *Polymer Degradation and Stability* 144 (2017): 281-291.
- 242 Hu, Hongxing, David Eustace, and Christoph A. Merten. "Efficient cell pairing in droplets using dual-color sorting." *Lab on a Chip* 15, no. 20 (2015): 3989-3993.
- 243 Wu, Liang, Pu Chen, Yingsong Dong, Xiaojun Feng, and Bi-Feng Liu. "Encapsulation of single cells on a microfluidic device integrating droplet generation with fluorescence-activated droplet sorting." *Biomedical Microdevices* 15 (2013): 553-560.
- 244 Chen, Peng, Yu-Yen Huang, Kazunori Hoshino, and John XJ Zhang. "Microscale magnetic field modulation for enhanced capture and distribution of rare circulating tumor cells." *Scientific Reports* 5, no. 1 (2015): 8745.
- 245 Ghaffari, Ali, Seyed Hassan Hashemabadi, and Mansour Bazmi. "CFD simulation of equilibrium shape and coalescence of ferrofluid droplets subjected to uniform magnetic field." *Colloids and Surfaces A: Physicochemical and Engineering Aspects* 481 (2015): 186-198.
- 246 Bayley, Hagan, Brid Cronin, Andrew Heron, Matthew A. Holden, William L. Hwang, Ruhma Syeda, James Thompson, and Mark Wallace. "Droplet interface bilayers." *Molecular BioSystems* 4, no. 12 (2008): 1191-1208.
- 247 Gennes, Pierre-Gilles, Françoise Brochard-Wyart, and David Quéré. *Capillarity and wetting phenomena: drops, bubbles, pearls, waves*. Springer New York, 2004.
- 248 Nguyen, Nam-Trung, and Zhigang Wu. "Micromixers—a review." *Journal of Micromechanics and Microengineering* 15, no. 2 (2004): R1.



# Magnetically actuated transport of ferrofluid droplets over micro-coil array on a digital microfluidic platform



Debiprasad Chakrabarty, Susovan Dutta, Niladri Chakraborty, Ranjan Ganguly\*

Department of Power Engineering, Jadavpur University, Kolkata 700098, India

## ARTICLE INFO

### Article history:

Received 8 February 2016

Received in revised form 17 May 2016

Accepted 1 June 2016

Available online 2 June 2016

### Keywords:

Ferrofluid

Digital microfluidics

Droplet manipulation

Magnetic field

Micro-coil array

## ABSTRACT

Magnetic manipulation of liquid droplets in microfluidic environment offers a promising tool for sample handling in lab-on-chip devices. Biofunctionalized ferrofluid droplets can effectively carry a measured volume of analytes or reagents on a flat microfluidic platform, executing key tasks of a micrototal analysis system ( $\mu$ -TAS). However, achieving precise control using on-chip miniaturized magnetic coils is challenging and requires delicate combination of operating parameters, e.g., magnetizing current and timing of switching, fluid viscosity, droplet size, etc. Here we present a numerical analysis of magnetic manipulation of an immiscible, microliter-scale ferrofluid droplet over a thin aqueous film on a solid substrate using embedded micro-electromagnet coils. The numerical model is first validated against the experimentally observed droplet trajectory in a simple, single-coil configuration. Subsequently, two-dimensional manipulation of the ferrofluid droplets on the liquid film is predicted numerically when the magnetic field is produced by a sequentially switched array of square spiral microelectromagnets. By adjusting the operating parameters, we show that the droplet can be moved in predefined meandering path over an active substrate area. The transport is broadly classified into viscosity- and inertia-influenced regimes. Transport time of the droplet for the viscous regime is expressed in terms of a generalized group-variable involving the operating parameters. The study is important for selecting the design bases for a magnetically manipulated sample handling system for digital microfluidic platforms.

© 2016 Elsevier B.V. All rights reserved.

## 1. Introduction

Microfluidics is the enabling technology of handling fluid flow in diminutive amounts, typically ranging from nanoliters to microlitres, in micro total analysis systems ( $\mu$ -TAS). These devices are capable of performing varied bioanalytical tasks, which are normally carried out in a lab, like sample preparation, purification, separation, reaction, transport, immobilization, labeling, biosensing and detection on a chip [1]. These devices offer advantages over the conventional bioanalytical protocol through reduced biochemical reaction time, enhanced efficiency and mobility and reduced sample and reagent consumptions. Small reactor volumes are also favored where the analyze sample is available in extremely small amount, e.g., in case of a forensic detection. The key generic steps in any MEMS-(Microelectromechanical Systems) based bioanalytical device (e.g. a biosensor) involves sample handling for mixing, reaction and separation. Active microfluidics refers to the defined manipulation of the working fluid by active (micro) components

such as micropump or micro valves. There has been a recent shift of sample handling strategy from the continuous-flow to the droplet-based system, where sample droplets can be stored and manipulated in an immiscible liquid. Samples and reagents can be confined in an immiscible carrier in spherical droplets which are dispersed in another immiscible fluid that is flown through the channel. Droplet-based microfluidics is relatively free from the common problems of flow-through microfluidics like sample dilution and cross-contamination [2,3]. Several useful applications of droplet-based microfluidics, e.g., protein purification [4], biosensor [5], immunoassays [6], DNA-replication [7], cell-based assays [8], bio-molecular extraction [9] etc. have underscored the importance of on-chip droplet manipulation [10,11]. Magnetic force offers a viable alternative for the manipulation of microdroplets. Functionalized magnetic nanoparticles, either in the form of ferrofluid droplets or magnetic microspheres offer a facile tool for micromanipulation on microfluidic platform. Magnetic force is used widely for handling magnetic beads [12,13] in microchannels and capillaries in the context of active mixing [14] and immunomagnetic separation in microfluidic devices [15], or in studies related to magnetic drug targeting [16,17]. Ganguly et al. [18] provides an insight into the transport of ferrofluid and magnetic microspheres

\* Corresponding author.

E-mail addresses: [ranjan@pe.ju5l.ac.in](mailto:ranjan@pe.ju5l.ac.in), [rgangu2@yahoo.com](mailto:rgangu2@yahoo.com) (R. Ganguly).

Debiprasad Chakrabarty

## 2-Dimensional, magnetic actuation of ferrofluid droplet on an open surface-microfluidic platform

Debiprasad Chakrabarty<sup>1</sup>, Niladri Chakraborty<sup>2</sup>, Ranjan Ganguly<sup>2,\*</sup>

<sup>1</sup> Department of Electrical Engineering, College of Engineering and Management, Kolaghat, West Bengal 721171

<sup>2</sup> Department of Power Engineering, Jadavpur University, LB 8, Sector 3, Salt Lake, Kolkata 700106

### ABSTRACT

The role of non-contact manipulation of discrete droplets on surface microfluidic platforms have wide applications in development of low-cost biosensors and biomedical diagnostic systems. Magnetic digital microfluidic platforms utilize magnetic force to actuate ferrofluid droplets on open hydrophobic surface and offers distinctive benefits compared to other digital microfluidic actuation schemes. This allows droplets – containing different type of sample and reagents – to be actuated and controlled independently; this can be leveraged to achieve different bioanalytical protocols for point of care diagnosis and other different micro-total analytical systems. Here investigate, through a physically realistic model, magnetic field-actuated transport of a spherical cap ferrofluid droplet on a surface microfluidic platform. Manipulation of a microliter-volume droplet in a sequence of rectilinear paths, leading to a guided-transport is achieved through an array of double-layer, planar, square-shaped electromagnetic micro-coils embedded in the substrate. Appropriate sequence of coil energization for attaining the desired trajectory of the droplet is described. The study paves the foundation of developing more complex digital microfluidic devices for different biomicrofluidic applications.

**Keywords:** Magnetic fluid; Microfluidics; Droplets; Surface tension; Numerical model

### 1. INTRODUCTION

Digital microfluidics (DMF) is an emerging fluid handling technology, which has a wide range of significant applications in the areas of automation, miniaturization and biochemical applications. In surface-type DMF, liquid is manipulated in the form of discrete droplets containing samples and reagents on an open, integrated microfluidic platform [1,2,3,4] instead of an enclosed microchannel. Droplet-based surface-type DMF (SDMF) has many outstanding features such as portability, less sample consumption, shorter chemical reaction time and flexibility compared to the conventional flow-through microfluidics. Here each droplet can be controlled independently without complex networks of channels, pumps, valves, or mechanical mixers. Thus, numerous reaction processes can be achieved at the same time with a simple and compact design. Magnetic forced-based SDMF offer distinctive advantages where droplet filled with magnetic particles actuates under influence of magnetic force. Magnetic SDMF is easy to implement in term of fabrication and integration for point-of-care diagnostics with flexible controllability and high accuracy.

Here flat surfaces of Silica, PMMA or PDMA, coated with a low surface-energy materials such as Teflon AF (amorphous fluoropolymer) may be used to support droplets with limited spreading, and transport those using localized magnetic field gradients using miniaturized permanent magnet [5] or electromagnet coils [6] or by combination of both permanent magnet and electromagnet. Prior works on flow-through magnetic DMF [7,8] have shown the feasibility of droplet actuation using permanent magnet or electromagnetic rail based approaches, but they are limited in terms of flexibility and sans the controllability, for example, the capability of droplet operation along predefined paths. To attain two-dimensional flexible and controllable operation of ferrofluid droplets on a hydrophobic surface, planar microcoil array [9,10] or combination of planar coils coupled with bias field of permanent magnets [9] can be a more suitable substitute. Nguyen et al. [11] proposed a simple magnetic digital microfluidic device to drive ferrofluid droplet by four planar coils in combination with a pair of permanent magnets and a soft magnetic steel sheet. Manipulation of large amounts of individual droplets using a deformable magnetic membrane was achieved by Chen et al. [12]. In our previous study, we demonstrated a complex, two-dimensional manipulation of liquid droplets over a thin aqueous film on an open surface using a periodically switched array of electromagnetic micro-coils [13]. However, compatibility of the film-fluid with the droplet liquid and the stability of the film pose constraints. So to achieve more precise, flexible and wide range two-dimensional droplet manipulation, solid surface with adequate repellence to the droplet fluid is preferred. Repellence of the surface to the droplet fluid (rendering a high sessile-droplet contact angle) is a necessary condition to attain a distinct, transportable droplet as opposed to a liquid that wets, spreads and sticks to the surface. Here we present a numerical model to analyse controlled manipulation of spherical cap ferrofluid droplets on a solid substrate. Periodically switched array of electromagnetic micro-coils are used to generate a spatio-temporal distribution of magnetic field that steers the ferrofluid droplet on the surface. We use square coil with different orientation and dimension to get better packing density (minimizing the dead space between the neighbouring coils).

### 2. THEORETICAL FORMULATION

Figure 1 (a) shows the arrangement of double-layer planar square coils of two different size (six 20 mm<sup>2</sup> square coil in 1<sup>st</sup> layer and six 10 mm<sup>2</sup> square coil in 2<sup>nd</sup> layer) in a two stranded array of 12 coils (Typical dimension of a stranded array is 40 mm × 60 mm) fabricated on a flat PDMS substrate of 50 mm ×

Debiprasad Chakrabarty